DOE/CE/23810-98

LEAN FLAMMABILITY LIMIT AS A FUNDAMENTAL REFRIGERANT PROPERTY
Phase III

Final Technical Report
February, 1997 - February, 1998

William Grosshandler, Michelle Donnelly, and Carole Womeldorf

BUILDING AND FIRE RESEARCH LABORATORY
National Institute of Standards and Technology
Gaithersburg, MD 20899

August, 1998

Prepared for
The Air-Conditioning & Refrigeration Technology Institute
Under
ARTI MCLR Project Number 660-52401, Mod. 3

This program is supported, in part, by U.S. Department of Energy (Office of Building Technology) grant number DE-FG02-91CE23810: Materials Compatibility and Lubricants Research (MCLR) on CFC-Refrigerant Substitutes. Federal funding supporting this program constitutes 93.57 % of allowable costs. Funding from non-governmental sources supporting this program consists of direct cost sharing of 6.43% of allowable costs, and significant in-kind contributions from the air-conditioning and refrigeration industry.

DISCLAIMER

The U.S. Department of Energy's and the air-conditioning industry's support for the Material Compatibility and Lubricants Research (MCLR) program does not constitute an endorsement by the U.S. Department of Energy, nor by the air-conditioning and refrigeration industry, of the views expressed herein.

NOTICE

EXECUTIVE SUMMARY

Alternative refrigerants are being developed by industry to prevent the further destruction of stratospheric ozone by chlorofluorocarbons (CFCs), which had been the working fluids of choice for many air-conditioning and refrigeration machines. Hydrofluorocarbons (HFCs) are one class of compounds that are being pursued as replacements because their ozone depletion potential is zero. In general, the exchange of fluorine atoms on an HFC molecule with hydrogen atoms decreases its atmospheric lifetime, and it may also increase the efficiency of the working fluid. Both of these effects are highly desirable from environmental considerations since they act to mitigate global warming.

Unfortunately, more hydrogen on an HFC is usually associated with an increase in flammability. An accepted method for determining the flammability limits of gaseous fuels is ASTM Standard E 681. The minimum and maximum concentrations of the fuel in air for flame propagation are based upon the observed ignition and growth of a flame in a vessel filled with a quiescent fuel/air mixture. A clear distinction is sought between a non-propagating flicker and a flame, which has enough horizontal propagation to be hazardous. When applied to hydrocarbons, these tests give well-defined results. Weak fuels like many HFCs have a great sensitivity to the test conditions and provide ambiguous limits. The ignition source, vessel geometry and operator subjectivity contribute to this ambiguity.

Many of the difficulties associated with the ASTM apparatus are not present in a planar, twin-flame, counter-flow burner. With this burner, steady flames first are established under favorable conditions, and then the fraction of fuel is diminished in small increments until the flame is extinguished. The tests are repeated at progressively lower flow rates, which are inherently more capable of sustaining combustion. By plotting the fraction of fuel at extinction versus the flow rate and extrapolating to an experimentally unattainable zero-flow condition, an unambiguous limit of flammability can be attained. Unlike the ASTM apparatus, the counter-flow burner method entirely avoids issues surrounding the design of an ignition mechanism, it minimizes heat loss and wall effects, and also it is amenable to computational analysis.

The Air-Conditioning and Refrigeration Technology Institute began a program at the Building and Fire Research Laboratory of National Institute of Standards and Technology in October, 1994 to examine the potential for the counter-flow burner to accurately measure flammability limits of refrigerants. In phases I and II of this research (reported earlier), the feasibility of using the counter-flow burner to define the lower flammability limit (LFL) of R-32 (CH_2F_2) and the minimum ratio of the moles of R-125 (C_2HF_5) to moles of R-32 to render an R-125/R-32 mixture non-flammable (i.e., the critical flammability ratio, CFR) were demonstrated. Theoretical calculations were made of the structure of R-32 flames in air and in mixtures with R-125 to assist in interpretation of the results. The objectives for phase III of the study were (i) to determine the sensitivity of the measured LFL to changes in burner design, (ii) to modify the burner to operate at elevated temperatures and with liquid refrigerants (R-245ca, or $C_3H_3F_5$), and (iii) to design a simple burner that could be used by industry and other research laboratories for estimating the flammability of new refrigerants.

The most significant design variable that affects the LFL is the burner diameter. The flammability limits included in this report were obtained using a 12 mm ± 0.2 mm diameter contoured nozzle burner, with 12 mm ± 0.2 mm spacing. A 17 % increase in burner diameter makes it difficult to stabilize the R-32 flame, while a 17 % decrease in diameter results in a 20 % decrease in the LFL. The repeatability of the data for a fixed burner geometry is high, with results varying less than ± 3 of the LFL for R-32 and the CFR for R-125/R-32. The variability of the upper flammability limit for

R-32 is about ± 4 %. The greatest variation (approximately ± 10 %) is in the conditions, which lead to a flammable mixture of R-245ca and air.

The following flammability limits (in terms of mole fraction) and critical flammability ratios (moles R-125 to R-32) were found during the course of this research, all with air at a pressure of 98 kPa ± 2 kPa:

R-32, lower limits	R-32, upper limit
0.14 ± 0.004 (dry, 30 °C)	0.27 ± 0.01 (8.5 $mg_{water}/g_{dry\ air}$, 100 °C)
0.13 ± 0.004 (8.5 $mg_{water}/g_{dry\ air}$,100 °C)	
R-125/R-32, CFR	**R-245ca, flammable range**
17.6/82.4 to 18.4/81.6 (dry, 30 °C)	0.10 to 0.12 (8.5 $mg_{water}/g_{dry\ air}$, 100 °C)
21.6/78.4 to 22.4/77.6 (8.5 $mg_{water}/g_{dry\ air}$, 100 °C)	nonflammable (8.5 $mg_{water}/g_{dry\ air}$, 50 °C)
	nonflammable (dry, 100 °C)

The absolute accuracy of the measured limits is three to four times more uncertain than the repeatability, due to the sensitivity to burner diameter. Additional experiments with finer control on the burner spacing and with more flexible velocity profiles are needed to unravel the relation between the LFL and the flow field/heat transfer in the burner. A two-dimensional numerical model of the burner, with the ability to vary the geometry and inlet conditions, is also necessary to properly interpret the results. Unlike for the ASTM apparatus (for which the absolute accuracy has never been established for hydrofluorocarbons), a reliable model can be developed for the counter-flow burner with a reasonable amount of effort.

The research burner operates easily at 100 °C with a controlled humidity. It is estimated to take less than eight hours and 500 mg of each refrigerant to determine the LFL and CFR of materials with properties similar to R-32 and R-125. About three times the material and time is expected for low flammability liquid refrigerants similar to R-245ca. A design is proposed for an industrial burner, which is simpler to fabricate and maintain.

This report reviews the past work done on premixed, counter-flowing flames, describes the current counter-flow burner facility and operating procedures, presents the experimental results with the analysis that yields the above flammability limits, and recommends further activities that could lead to a science-based methodology for assessing the risk of fire from refrigeration machine working fluids.

ACKNOWLEDGMENT

Support for this work was provided by the U.S. Department of Energy and the air-conditioning industry through the Material Compatibility and Lubricants Research program, as administered by the Air-Conditioning & Refrigeration Technology Institute. The assistance of the ARTI program manager, Steven R. Szymurski, is gratefully acknowledged. The Advanced Technology Program of NIST provided support for the flame velocity measurements and much of the modeling effort. Special thanks go to Carolyn White and Richard Harris for their contributions to the experimental measurements. The assistance of William Rinkinen for the design of the burner and of Jaeson Howze for the initial flame calculations are also appreciated.

TABLE OF CONTENTS

LEAN FLAMMABILITY LIMIT AS A FUNDAMENTAL REFRIGERANT PROPERTY
Phase III

INTRODUCTION

Background

Chlorofluorocarbons (CFCs) have been phased out of production for use as refrigerants because of chlorine's destructive effect on stratospheric ozone. Alternative chemical compounds are being adopted in which the chlorine atoms are replaced with fluorine and/or hydrogen atoms; however, replacing halogen atoms in the molecule with hydrogen atoms can transform a nonflammable CFC into a potentially flammable material. An example is the nonflammable R-12 (CCl_2F_2) and flammable R-32 (CH_2F_2). The efficiency and flammability of R-32 and other alternative refrigerants must be carefully balanced in mixtures to provide safe (nonflammable) and environmentally friendly (energy efficient and reduced or zero ozone depleting potential) refrigerants.

The safety of refrigerants used by the air-conditioning and refrigeration industry is classified according to rules set in ANSI/ASHRAE Standard 34-1997 [1], which specifically refers to ASTM Standard E 681-1994 [2] for determining the minimum concentration of a gas in air necessary to sustain a flame. There are three classes of flammability. A Class 1 refrigerant shows no ability to propagate a flame when mixed with air at 101 kPa and 21 °C. A Class 2 refrigerant can propagate a flame when mixed with air at 101 kPa and 21 °C, but only at concentrations greater than 0.10 kg/m^3. It also must have a heat of combustion less than 19 MJ/kg. A Class 3 flammability rating applies to a refrigerant with a higher heat of combustion, or with the ability to propagate a flame when mixed in concentrations less than 0.10 kg /m^3. The determination of the minimum concentration for flame propagation, or lean flammability limit (LFL), is based upon the observed ignition and growth of a flame in a 5 L to 12 L vessel filled with a quiescent fuel/air mixture at a specified uniform temperature and pressure. The standard test attempts to draw a clear distinction between a mixture, which creates a non-propagating flicker and a flame which has enough horizontal propagation to be hazardous. When applied to fuels like methane or propane, these tests give well-defined results. Weak fuels like R-32, however, have a greater sensitivity to the test conditions and provide ambiguous limits. The ignition source (spark, match-head, heated wire) and energy level, the complex geometry of the flame, and wall effects all contribute to this ambiguity.

Many of the difficulties associated with the ASTM measurements of the LFL are not present in the approach suggested by Law, et al. [3] They used a planar, twin-flame, counter-flow arrangement to determine the volume flow rate at which burning CH_4/air and C_3H_8 /air mixtures are extinguished. By repeating the experiments at diminishing fuel concentrations, it is possible to plot the concentration versus the flow rate, and to extrapolate the results to identify the concentration corresponding to an experimentally unattainable zero-flow condition, which is an equivalent definition of the LFL. Unlike the ASTM apparatus, the counter-flow burner method entirely avoids issues surrounding the design of an ignition mechanism, it minimizes heat loss and wall effects, and also it is amenable to computational analysis.

In the previous and current phases of the work described in this report, a twin-flame counter-flow burner, similar to that used in reference [3], was selected to examine the behavior of refrigerant/air mixtures. Figure 1 is a photograph of flames stabilized about the stagnation region of two identical, vertically-aligned, counter-flowing jets of premixed R-32 and air under different sets of

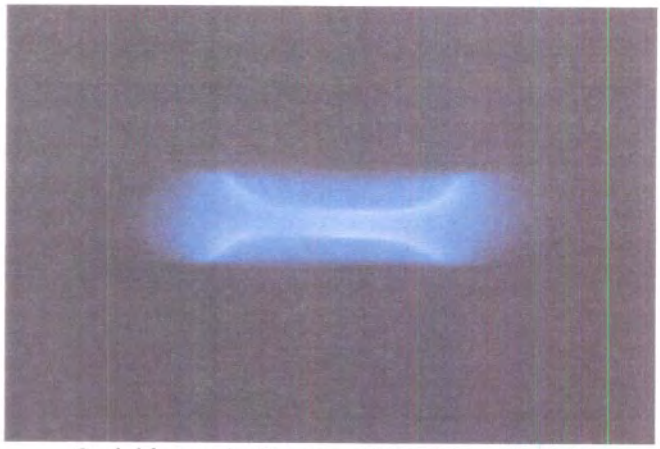

Stoichiometric Flame Velocity = 42 cm/s

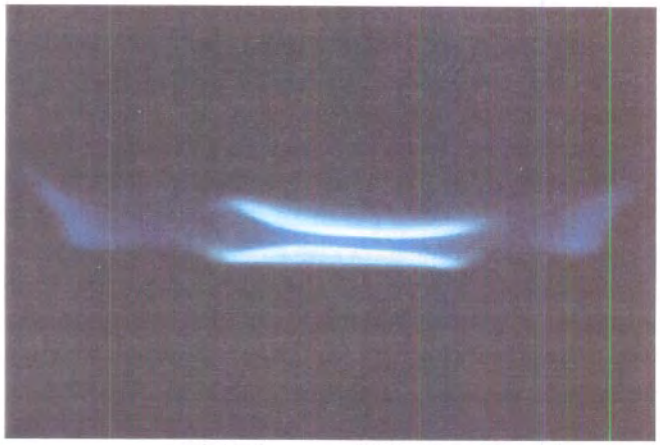

Rich Flame Velocity = 24 cm/s

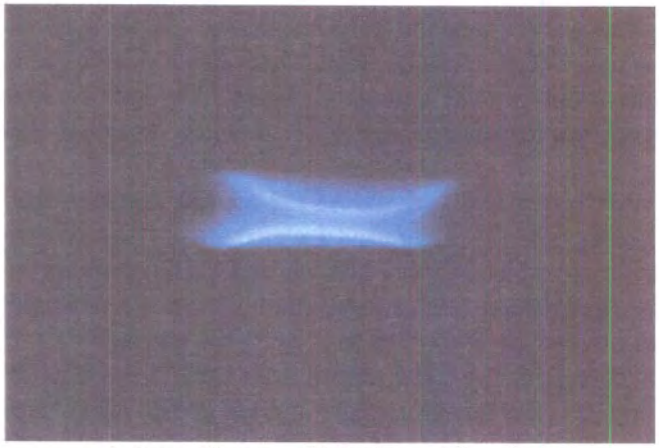

Lean Flame Velocity = 18 cm/s

Figure 1. Photographs of opposed-flow burner with twin flames from an R-32/air mixture, showing impact of varying flow velocity and equivalence ratio

conditions. The flames can be extinguished in one of two ways: by reducing the rate of chemical reaction to increase the time required for combustion to occur, or by increasing the flow velocity to decrease the residence time in the reaction zone. When the spacing between the burner jets and the exit velocity is fixed, decreasing the concentration of fuel reduces the rate of chemical reaction. At the limiting lean mixture, the reaction rate is slowed to the point that the residence time in the flame (which is maintained about constant since the velocity and spacing are fixed) is insufficient for complete combustion to occur, leading to flame extinction. On the other hand, when a fixed concentration of the fuel is maintained, increasing the jet velocity forces the flames towards the stagnation plane lying equidistant between the two burner jet outlets. At a sufficiently high velocity the time through the reaction zone becomes so short that the reactants pass through faster than they can burn, decreasing the combustion efficiency to a point that not enough heat is released to propagate the flame. Again, extinction follows. The residence time in the burner can also be controlled by changing the distance between the jets. A lesser distance for a fixed jet outlet velocity produces a higher velocity at the flame front, leading to a decrease in time available for the combustion reaction to occur.

The effect of jet velocity and spacing can be combined into a single parameter called the global stretch rate, K_g, defined as the average velocity at the exit of the burner jet divided by the distance between the exit plane and the stagnation plane (i.e., half the nozzle separation). The concentration (or mole fraction) of refrigerant at extinction can be plotted against diminishing values of K_g, and linear extrapolation used to determine the minimum concentration of fuel required to propagate a flame under the most favorable (or least stretched, i.e., $K_g = 0\ s^{-1}$) flow conditions. This is the LFL for the refrigerant for the given initial conditions (ambient temperature, pressure and relative humidity).

The extrapolation to a zero-stretch condition approach had been used prior to the current study to determine the flammability limits of highly flammable fuels such as hydrocarbons. The LFL of slightly flammable fuels, including many proposed refrigerants, previously had not been measured in a flowing arrangement. The feasibility of using an opposed-flow burner to measure the limiting lean mixture for a weakly flammable refrigerant gas in air at standard conditions was evaluated in Phase I of this project [4]. Phase I additionally proved the feasibility of using an opposed-flow burner arrangement for determining the critical flammability ratio (CFR) of R-125/32 mixtures, where the CFR is the minimum mole fraction necessary of the non-flammable component to render a binary refrigerant mixture non-flammable.

Phase II of the refrigerant flammability project [5] was devoted to designing and evaluating an improved version of the concept developed in Phase I. A new opposed-flow burner test facility was built to provide repeatable, precisely described flames and extinction conditions. Analysis of the experiments indicated that it is possible to determine the lower flammability limit of R-32 repeatable to better than 1 % of the limit value. The absolute uncertainty reported, 5 %, includes a conservative assessment of the impact of the uncertainty in the flow system calibration.

Objectives

The ultimate goal of this research program is to provide industry with an accurate, repeatable method for measuring flammability limits. Phases I and II produced the design of a measurement method that is a radical departure from ASTM E 681-1994, utilizing an opposed-flow burner. Experimental data taken in the earlier phases demonstrated that the lower flammability limit of R-32/air mixtures and the critical flammability ratio of R-32/R-125/air mixtures could be determined accurately, resulting in data consistent with those measured with the ASTM E 681-1994 apparatus, and with a high degree of repeatability. The following are significant questions, which remained about the opposed-flow burner apparatus, the answers to which are the objectives of Phase III:

- Is the absolute value of the LFL sensitive to small changes in burner design?

- Can the burner operate and produce flame limits and critical flammability ratios at elevated temperatures [e.g., Elevated Temperature Flammability Limit at 100 °C ($ETFL_{100}$) and CFR @ 100 °C], or with marginally flammable refrigerants (i.e., ASHRAE class 2 refrigerants and class 1/2 refrigerant blends)?

- How might one simplify the burner design and economize its operation for use by industry, and what are the tradeoffs between designs?

The research has been organized around three distinct tasks to answer these questions.

Sensitivity of LFL to burner design: The theory states that the extinction stretch rate can be approached either by increasing the velocity for a fixed nozzle spacing, or by decreasing the spacing for a fixed exit velocity. The first approach was used in Phase II, with the nozzle spacing fixed at 12 mm. In Phase III, the burner spacing has been set at different values to determine the effect on the zero-stretch limit. Ideally, the absolute value of the LFL should not change, but associated perturbations in buoyancy and heat transfer can influence the results. Additional experiments have been conducted with the diameter of the burner changed, and the LFL measurement repeated.

The shape of the nozzle determines the velocity profile. This geometric parameter also has been examined, with the converging nozzle replaced with a straight tube.

Burner operation at elevated temperature and with less flammable fuel: Current industry safety standards require the measurement of elevated temperature flame limits (ETFL) at 100 ° C. The opposed flow burner has been modified to operate at inlet gas temperatures up to this level. The air and refrigerant mixture are heated in the burner, the lower portion with heating tapes and the upper portion with water previously passed through a small boiler to elevate the temperature above 100 °C. Thermocouples located in the burner monitor the outlet temperature. The operation has been evaluated at atmospheric pressure with R-32/humid air mixtures at 100 °C.

Most measurements to date in the NIST burner have had R-32 as one of the components in the fuel/air mixture. While R-32 is an order of magnitude less flammable than a hydrocarbon like propane, it is not the least flammable "slightly-flammable refrigerant" being considered by the air-conditioning and refrigeration industry. Operation of the opposed-flow burner presupposes that, if a refrigerant is reactive enough, a flame can be stabilized under close-to-stoichiometric conditions. When this is not the case, a different operating procedure is required. The refrigerant R-245ca has been reported to have a finite, but small, flammability range. However, a steady flame cannot be obtained when R-245ca is the sole fuel. R-32 has been mixed in to increase the ease of ignition. By decreasing the concentration of R-32 for a fixed flow of R-245ca, extinction occurs for a particular stretch-rate/equivalence ratio condition. This procedure is repeated and the results extrapolated to identify the minimum amount of R-32 required to have a stable flame under ideal (i.e., zero stretch and close-to-stoichiometric mixture) conditions. Measurements have been made of the $ETFL_{100}$ of R-245ca with air containing 0.0086 g water vapor per g dry air (i.e., 50 % relative humidity at 23 °C). Measurements of the CFR of an R-125/32 blend at ambient temperature and 100 °C with air containing 0.0086 g water vapor per g dry air are also included in this report.

Simplifying burner design and operation: Great care has gone into the design of the NIST facility. The nozzles are specifically contoured to produce a flat velocity profile at the exit. The

Table 1. Thermophysical properties of refrigerants examined

Name	Formula	Molec. Wt. g/mole	[a]Boiling Pt. @ 101.3 kPa	[a]Sat. Press. @ 25 °C	[b]Enthalpy of Combustion MJ/kg_{fuel}	[a]Viscosity, kg/m-s (25 °C)	[a]Thermal cond., W/m-°C (25 °C)	[a]Specific Heat (C_p), kJ/kg-°C (25 °C)
R-32	CH_2F_2	52.0	-51.7 °C	1691 kPa	-9.35	12.18	0.01407	0.8430
R-125	CHF_2CF_3	120	-48.1 °C	1377 kPa	-3.92[c] to -4.12[d]	13.11	0.01394	0.7964
R-245ca	CHF_2-CF_2CH_2F	134	25.2 °C	100.5 kPa	-8.79[c,e] to -9.72[d,e]	513.6 (liq) 10.4 (gas)	0.09012 (l) 0.0124(g)	1.304 (l) 0.9185 (g)

[a] Huber et al. [36] [b]Burgess et al. [7] [c]COF_2 in products [d]no COF_2 in products [e]estimate

burner is designed to operate over a wide range of inlet velocities and stretch rates. Computer operated mass flow controllers are used to maintain and monitor the flow. While these procedures are necessary for a NIST standard facility, a number of constraints on the design and operating conditions may be relaxed without compromising too much the accuracy of the results. For example, replacing the contoured nozzles with straight pipe sections with the same internal diameter (12 mm) greatly simplifies the construction and maintenance of the burner. It also facilitates the control of temperature for the refrigerant air mixture.

An advantage of the opposed-flow burner approach is that some systematic errors in flow measurement are canceled when the data are reduced. For example, an error in estimating the total volume flow to the burner propagates in a linear fashion to the estimated extinction stretch rate. But because the LFL is found by extrapolating to the zero stretch condition, the intercept is unaffected by a change in slope caused by a systematic error in determining flow rate. Similarly, if the same method were used to calibrate the air and refrigerant flow meters, the calibration of one can be checked against the other, minimizing the impact of systematic errors on the absolute value of the volume fraction of refrigerant in the mixture. Thus, a simplified (and less expensive) flow control system may be suitable for an industrial-grade unit.

An operating procedure has been provided along with estimates of the total amount of chemical required and the time involved to measure the LFL of a pure refrigerant and the CFR of a binary mixture (at 100 °C, 101 kPa, and 50% relative humidity). Drawings of the burner are provided for those who wish to build their own test apparatus. In addition, a design for a new burner and flow control system is proposed to reduce the cost of the facility and increase ease of operation.

Thermochemical Properties of Refrigerants

The flammability limits of gaseous mixture are determined by the heat released during the combustion reaction, the heat absorbed by the materials intimately involved, and the minimum temperature required to overcome an activation energy. Thermodynamic properties (see Table 1) control the first and second quantities, while chemical kinetics dictates the third. The kinetics are discussed later in the analysis section; the equilibrium reactions are discussed below.

The complete, stoichiometric combustion of R-32 in dry air is given by the following expression:

$$CH_2F_2 + (O_2 + 3.76\ N_2) \rightarrow CO_2 + 2\ HF + 3.76\ N_2 \qquad \{R1\}$$

The equivalence ratio, Φ, for an arbitrary mixture is defined as the actual R-32/air mole ratio divided by the stoichiometric ratio, 1/4.76; the mole fraction, $X_{R\text{-}32}$, is defined as the moles of R-32 divided by the total moles in the mixture, which, for a flowing system like the counter-flow burner is equivalent to the volume flow of R-32 divided by the total volume flow. Thus, $X_{R\text{-}32,stoich} = 1/5.76 = 0.1736$ is the stoichiometric mole fraction of R-32 in dry air.

A stoichiometric oxidation reaction can be written for any refrigerant, regardless of whether or not it is flammable. For R-125 and R-245ca, the high F/H ratios in the fuel lead to varying amounts of two additional products of combustion: COF_2 (carbonyl fluoride) and CF_4 (tetrafluoromethane). (Note that if moisture is present, COF_2 quickly converts to CO_2 and HF.) Unlike R-32, the assumed product composition is sensitive to the final temperature. Stoichiometric reactions under dry, adiabatic conditions lead to high temperatures that maximize the amount of COF_2; i.e.,

$$CHF_2CF_3 + (O_2 + 3.76\ N_2) \rightarrow 0.5\ CO_2 + HF + COF_2 + 0.5\ CF_4 + 3.76\ N_2, \qquad \{R2\}$$

and

$$CHF_2CF_2CH_2F + 2.5\ (O_2 + 3.76\ N_2) \rightarrow 2\ CO_2 + 3HF + COF_2 + 9.40\ N_2. \qquad \{R3\}$$

At temperatures well below the adiabatic condition, dry carbonyl fluoride decomposes to equal amounts of CO_2 and CF_4. All three compounds are of equal concentration at equilibrium when the temperature is about 1000 °C. COF_2 levels become inconsequential at room temperature, leading to the following alternative complete combustion reactions:

$$CHF_2CF_3 + (O_2 + 3.76\ N_2) \rightarrow CO_2 + HF + CF_4 + 3.76\ N_2, \qquad \{R2'\}$$

and

$$CHF_2CF_2CH_2F + 2.5\ (O_2 + 3.76\ N_2) \rightarrow 2.5\ CO_2 + 3HF + 0.5\ CF_4 + 9.40\ N_2. \qquad \{R3'\}$$

In either case, the stoichiometric amount of air remains fixed.

The mole fraction of the less (or non-) flammable component in a binary refrigerant mixture is given the symbol x. The stoichiometric, adiabatic combustion of R-125 or R-245ca with R-32 is written as

$$\chi CHF_2CF_3 + (1\text{-}\chi)CH_2F_2 + (O_2 + 3.76\ N_2) \rightarrow$$

$$(1\text{-}.5\chi)CO_2 + (2\text{-}\chi)HF + \chi COF_2 + .5\chi CF_4 + 3.76\ N_2, \qquad \{R4\}$$

or

$$\chi CHF_2CF_2CH_2F + (1\text{-}\chi)CH_2F_2 + (1 + 1.5\chi)(O_2 + 3.76\ N_2) \rightarrow$$

$$(1+\chi)CO_2 + (2+\chi)HF + \chi COF_2 + (3.76 + 5.64\chi)N_2. \qquad \{R5\}$$

As with the pure refrigerants, the COF_2 in the products reduces to 50 % CO_2 and 50 % CF_4 when the final temperature drops below about 200 °C.

The actual temperature and products of combustion in a flame are controlled by the chemical kinetics of the reactants and strongly influenced by heat loss to the surrounding environment.

However, it is convenient to first examine what temperature and species concentrations would result from idealized adiabatic, equilibrium conditions. These can be determined for different values of equivalence ratio using the NASA chemical equilibrium computer code [6]. Figure 2 shows the results for R-32/dry air mixtures, initially at 25 °C and 101 kPa. The peak temperature, 1940 °C, occurs when $\Phi = 1.05$. At around the same Φ the CO_2 reaches a peak mole fraction of about 0.13. The mole fraction of HF at stoichiometric conditions is close to 0.30, and it continues to increase with Φ. The mole fraction of H_2O is over two orders-of-magnitude less than the mole fraction of CO_2.

Figure 3 is a similar plot for R-125/dry air mixtures. The maximum temperature is 400 °C less than in the R-32 flame, and the mole fraction of COF_2 is second only to HF, with CF_4 becoming more dominant in rich mixtures. CO_2 is present but at much lower values than in R-32/air mixtures, and water vapor exists only in parts per million.

The adiabatic equilibrium temperature is directly dependent upon the enthalpy of formation of the reactants. For R-245ca, no specific data on the enthalpy of formation could be located; however, by examining the compilation by Burgess et al. [7], it is possible to estimate the contribution of the different CH_xF_y groups to the enthalpy of formation of the parent compound. A value of $\Delta H_f = 7580$ kJ/kg ± 380 kJ/kg was used for the calculations shown in Figure 4. The peak adiabatic temperature varies between 1775 °C and 1843 °C, depending upon which extreme in ΔH_f is used in the calculation. As with R-32, HF is the dominant product, followed by CO_2, and neither mole fraction is much effected by the choice of ΔH_f. No appreciable H_2O is formed. The higher temperatures favor smaller molecules, which explains the significant difference in mole fraction of F-atom with different enthalpies of combustion.

RESEARCH FACILITY DESIGN

The experimental facility consists of a number of subsystems as shown schematically in Figure 5. Central to the design is the research counter-flow burner. The inlet flow control system maintains the proper mixture and amount of incoming materials to the burner, including the air, gaseous and liquid refrigerants, water vapor, and nitrogen. The exhaust treatment system scrubs the acid gases formed during combustion from the effluent before it is released into a chemical hood. The burner operation and data acquisition are controlled with a personal computer and custom software. Most of the subsystems were described in the Phase II report [5]; however, additional discussion is provided below to document changes in the system or where it is necessary to improve understanding.

Counter-flow Burner

The counter-flow burner, shown in Figure 6, is approximately cylindrical, about 100 mm in diameter and 450 mm high. It rests on a 12 mm thick aluminum base plate 300 mm in diameter. There are upper and lower sections to the burner, both of which are identical in design. The sections are connected by four rods to center the jets and maintain their axes parallel. Ignition is provided manually with a retractable butane lighter. When the fuel concentration is within flammable limits, a symmetric twin flame is formed on either side of the mid-plane, as can be seen in the photograph in Figure 1. The critical dimensions are the nozzle separation and the nozzle diameter, both of which are fixed at 12.0 mm ± 0.2 mm for the majority of the experiments. Air premixed with the fuel enters the upper and lower sections through 9.5 mm tubes. The flow is uniformly distributed and straightened with an 80 mm inner diameter by 100 mm long tube containing a 35 mm long piece of 4 mm cell size honeycomb and fine mesh screens to break up large eddies. The converging nozzle is designed from two matched cubic contours following the criteria of Morel [8], with an area contraction ratio of 44:1.

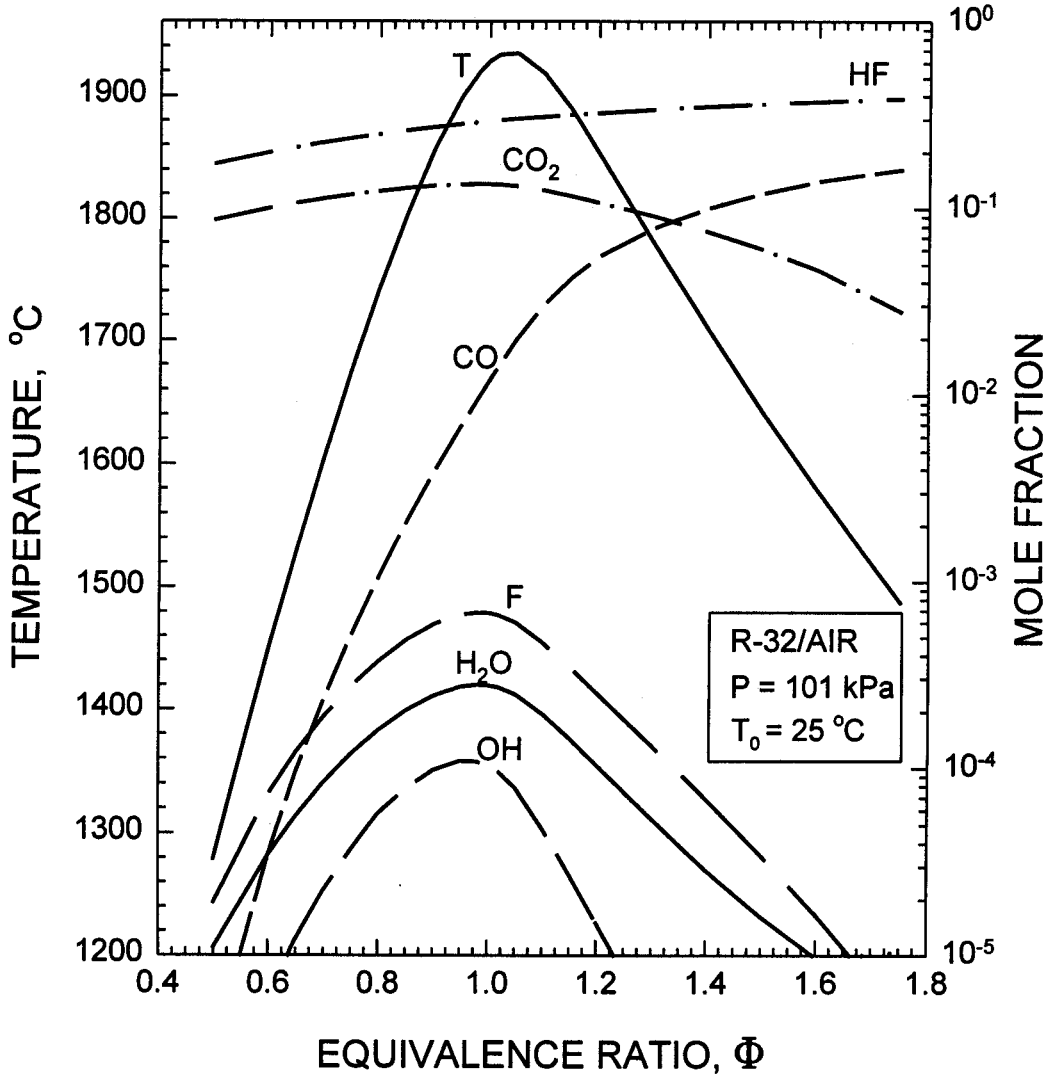

Figure 2. Calculated equilibrium composition and temperature of R-32/dry air mixtures

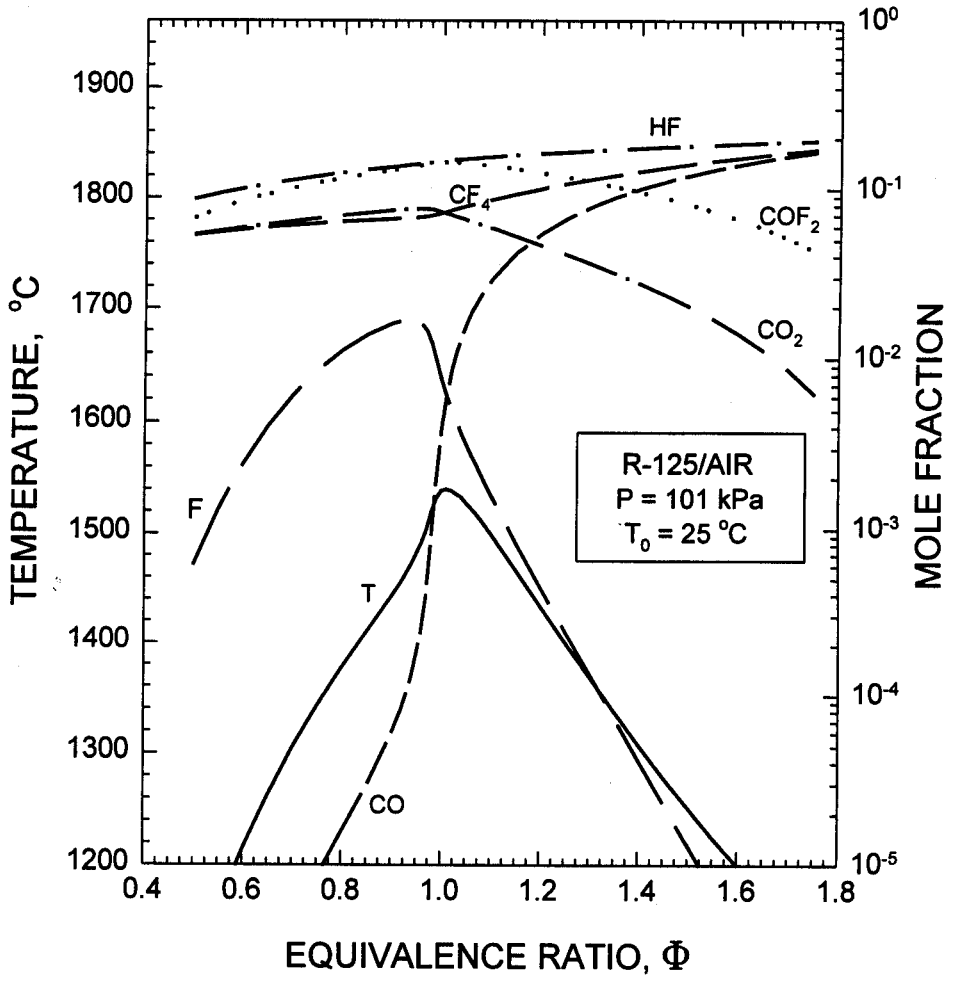

Figure 3. Calculated equilibrium composition and temperature of R-125/dry air mixtures

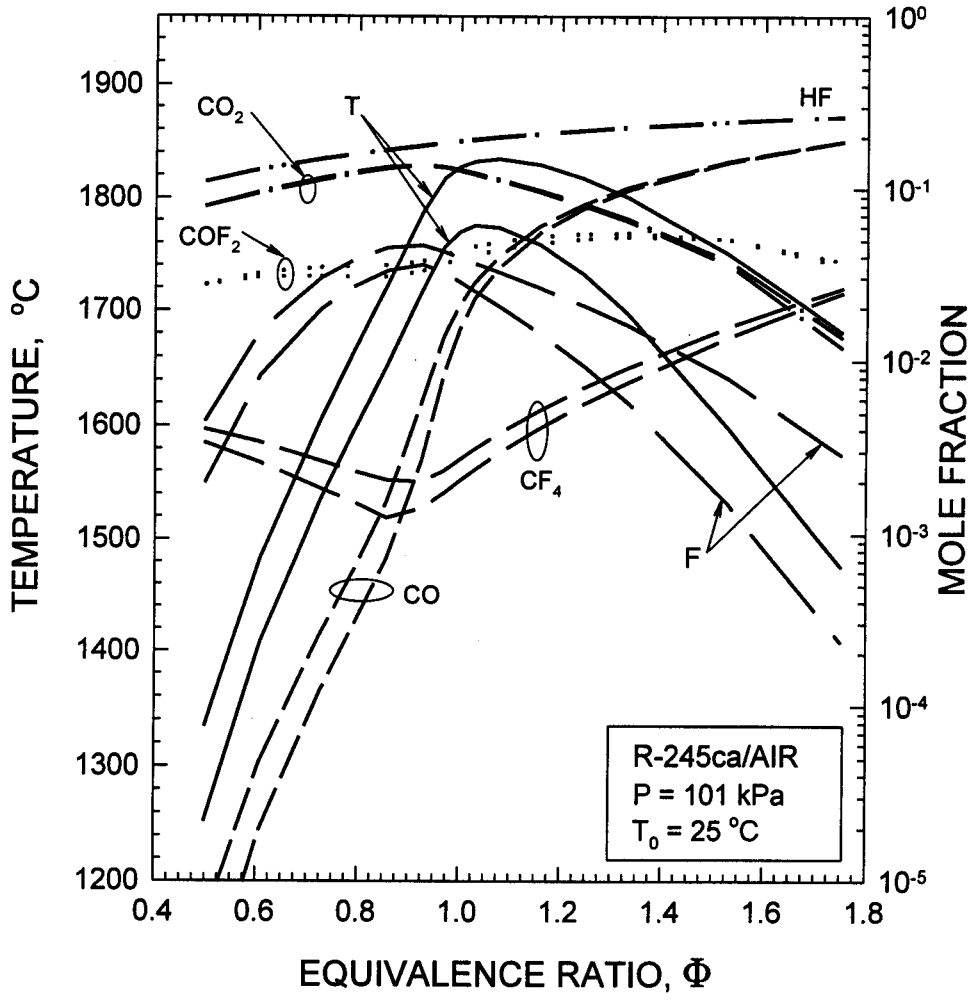

Figure 4. Calculated equilibrium composition and temperature of R-245ca/dry air mixtures, showing impact of ΔH_f

The purpose of the straightener and contraction is to produce a more uniform velocity profile with low turbulence intensity at the exit. Nitrogen flows in a 1.0 mm thick concentric annulus to quench the reactants as they escape from the flame, to prevent the flame from stabilizing on the nozzle rim, and to reduce entrainment of air. To eliminate unwanted air currents around the burner and direct the exhaust gases upward, the entire burner is enclosed within a 300 mm inside diameter, 6 mm thick Plexiglas tube. Drawings of the critical burner components are included in the Appendix F.

The burner flanges directly exposed to the flames are water-cooled to maintain their integrity and to minimize heat transfer back into the nozzle. Water flows through a copper tube coiled around the upper chamber of the burner to prevent the exhaust gases from preheating the upper section. Thermocouples are located on the centerline just upstream of the contraction nozzles to monitor the incoming mixture temperatures. Flammability measurements at temperatures above the ambient are conducted by heating the air/refrigerant mixture and controlling the temperatures of the upper and lower burner sections. Water is passed through a 600 W electrical heat exchanger to boost the temperature at the inlet of the upper cooling coil to about 110 °C. The temperature of the reactants in the lower section of the burner is maintained at about 100 °C by using heating tapes wrapped around the main body. (Note that heating tapes cannot be used on the upper section of the burner because the high HF levels in the exhaust quickly degrade fiberglass insulation.) Fine control of the reactant temperatures is accomplished by adjusting the flow of water through the upper and lower nozzle outlets. (A side benefit of keeping the temperature of the flanges close to 100 °C is that it significantly reduces corrosion of the stainless steel by preventing HF from condensing.)

Flow Control Systems

Reactant supply: The facility is designed to accurately control the flow of the combustion air, gaseous refrigerants (e.g., R-32 and R-125), liquid refrigerants (e.g., R-245ca), gaseous hydrocarbons (e.g., CH_4 and C_3H_8), liquid hydrocarbons (e.g., C_5H_{12}), and nitrogen. The gases are stored in individual cylinders at their respective room temperature vapor pressures. The air is certified to have a mole fraction of O_2 equal to 0.2110 ± 0.0002, with water and hydrocarbon levels below 10^{-6}. The remaining components (N_2, Ar, and CO_2) are as taken from the atmosphere. The R-32 is claimed by the manufacturer to contain mass fractions of water and non-volatile residues of less than 10^{-5} and noncondensable contaminates of less than 1.5 % by volume. The R-32 is stored as a liquid at room temperature and 1.6 MPa. The R-125 contains a minimum mole fraction of 0.995 C_2HF_5 and is stored at 1.4 MPa and room temperature. Air and ethane are the largest contaminants in the CH_4 but the minimum purity is 0.9995 mole fraction. Table 2 summarizes the chemical compounds used in the study, their purity, and the suppliers.

Gas flow controllers: The flow of the individual gas streams is controlled through an MKS, Inc.,[1] Multi Gas Controller type 647B. This instrument powers, reads and controls the mass flow controllers (MFCs) listed in Table 3. The resolution of the gas controller was increased from 0.1 % to 0.01 % of the full scale for each controller by modifications to the software. All flow controllers are calibrated to ± 2 % of value with the gas used during testing. The calibration reference is a digital bubble meter. This flow meter was tested using the NIST standard piston prover and has been shown [9] to be accurate to within ± 1 % over its entire range, 0.1 L/m to 25 L/min.

[1]Certain trade names and company products are mentioned in the text or identified in an illustration in order to specify adequately the experimental procedure and equipment used. In no case does such identification imply recommendation or endorsement by the National Institute of Standards and Technology, nor does it imply that the products are necessarily the best available for the purpose.

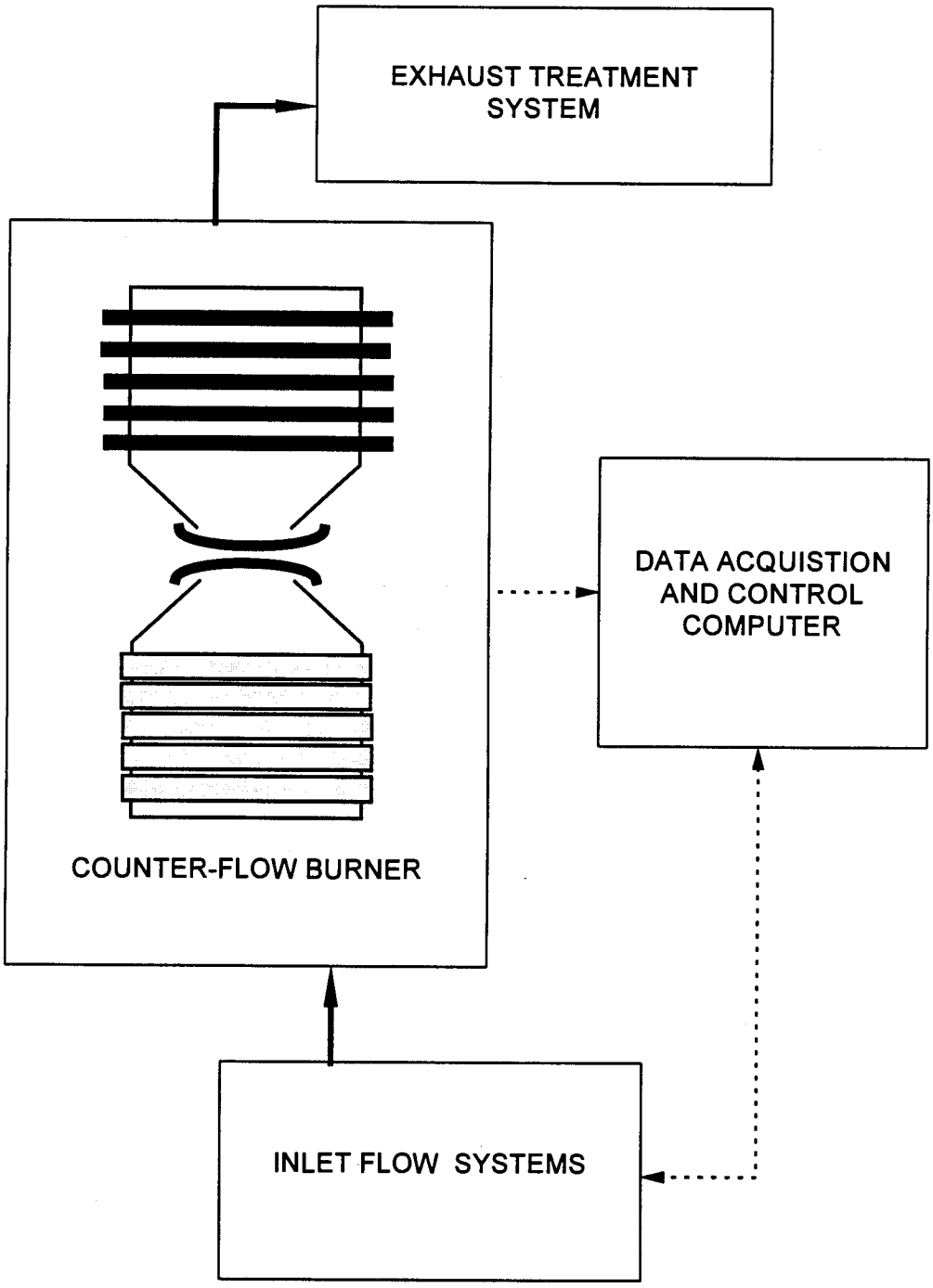

Figure 5. Block diagram of experimental facility

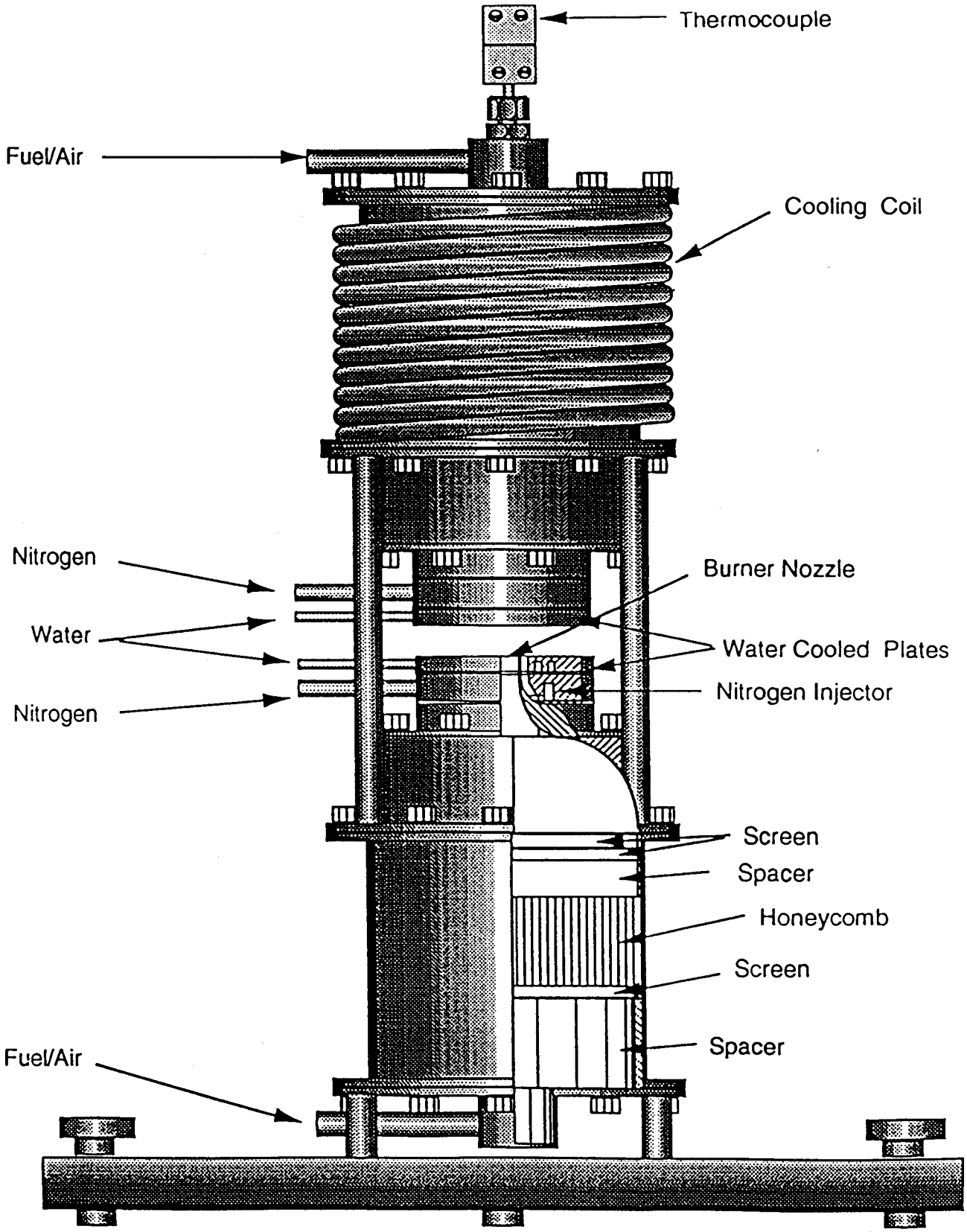

Figure 6. Overall view of counter-flow burner

Table 2. Chemical compounds used in study

Common Name	Chemical Formula	Minimum Purity, mole fraction	Supplier
air	O_2, N_2, Ar, CO_2	0.2110 ± 0.0002 O_2	Matheson
R-32	CH_2F_2	0.998	Allied Signal
R-125	C_2HF_5	0.995	Allied Signal
R-245ca	$CHF_2CF_2CH_2F$	unspecified	Allied Signal
R-245ca	$CHF_2CF_2CH_2F$	0.98	Lancaster Synthesis
methane	CH_4	0.9995	Matheson
propane	C_3H_8	0.95	Air Products
isopentane	C_5H_{12}	0.95	Fluka
nitrogen	N_2	0.99998	MG Industries

Table 3. Mass flow controllers

MFC #	Calibrated Gas	Approximate Range, L/m	Uncertainty, L/m	MKS Model Number
1	Air (top)	5.0	± 0.05	1159B-05000-SN
2	R-32 (top)	2.5	± 0.012	1359C-05000-SN
3	R-125 (top)	0.15	± 0.0008	1359C-00500-SN
4	R-125 (bottom)	0.30	± 0.0015	1359C-01000-SN
5	R-32 (bottom)	1.0	± 0.005	1359C-02000-SN
6	Air (bottom)	10.0	± 0.05	1359C-10000-SN

Gas pressures at the inlet of the controllers are regulated at 140 kPa ± 3 kPa to standardize initial flow conditions and validate the gas calibrations. (The R-32 supply bottle is connected to a lower pressure expansion tank to minimize pulsations in the flow of gas.) Teflon tubing, 6.4 mm in diameter, is used to transport the gases. The more and less flammable refrigerants are mixed just after leaving the flow controllers. The air is routed through a humidity system prior to reaching the burner. At the burner inlet, the air and the refrigerant mixture are combined and delivered to the upper and lower sections of the burner through 9.5 mm stainless steel tubes. Figure 7 is an overall schematic of the flow control subsystem showing how the gas supply is connected to the burner.

Humidity control: The initial design for adding water vapor to the air stream was to bubble the outlet of the mass flow controller through two glass bubblers operating in series. Each bubbler was filled with 0.50 L of de-ionized water in which 1.25 kg of $Mg(NO_3)_2$ salt had been dissolved. (The magnesium nitrate was supplied by Fisher Scientific with an assay value greater than 99.9 %.) Greenspan [10] has shown that at 25 °C and 101 kPa, this salt solution equilibrates at a relative humidity of 52.9 % ± 0.2 %. The bubblers were placed in a room temperature water bath and the humid air at the outlet passed through a particle trap to ensure no water drops remained suspended in the air stream.

The method described by Greenspan is for a closed system in which equilibrium easily can be obtained. However, in the open system used here, the continuous introduction of dry air carries with it a small but constant amount of CO_2. The purity of the solution decreases as the H_2O and CO_2 react to form H_2CO_3, dropping the equilibrium relative humidity. During the first several minutes the humidity [as measured within 2 % using a fast response digital hygrometer (Fisherbrand Instant Hygrometer #11-661-7B)] drops by 0.25 % per minute. This decline continued throughout testing, making a continual replenishment of the salt solution necessary.

To reduce the variability in the relative humidity and eliminate the need to refresh the solutions, an alternative design was chosen that is more appropriate for a flowing system. A relative humidity of 50 % at 23 °C and standard pressure corresponds to a humidity ratio of 0.0086 $g_{water}/g_{dry\ air}$. This same humidity ratio is reached when air is saturated at 12 °C. Saturation is achieved by bubbling air through pure de-ionized water that is cooled in a refrigerated bath. A single 2.5 liter bubbler with 0.6 L of water is used for each air stream. The outlet flow of cooled, humidified air passes through a Teflon condenser tube 9.5 mm in diameter and about 1.5 m long maintained at the same temperature to trap water droplets that might be carried through the bubblers. A ± 0.7 °C swing in temperature causes the equilibrium humidity ratio to vary ± 0.0004 $g_{water}/g_{dry\ air}$. Thus, the humidity ratio can be increased or decreased by increasing or decreasing the temperature of the bath, even though the air stream may not be fully equilibrated with moisture. The temperature in the bubbler is measured with a mercury thermometer to within 0.2 °C, and the humidity is checked prior to each test with the hygrometer at the inlet to the burner. A sketch of the humidifier is shown in Figure 8.

Liquid refrigerant flow control: Liquid fuels and refrigerants with boiling points near room temperature can be either pre-vaporized and metered as a gas or pre-cooled and metered as a liquid. The latter technique was chosen for the R-245ca. Two 100 ml stainless steel syringes with silicon rubber O-ring seals are used to store the refrigerant. The syringes are encased in copper cooling coils to prevent the refrigerant from boiling. (Pyrex glass syringes with Teflon seals and a steel body were found to be unsatisfactory because uneven thermal expansion caused them to leak profusely at temperatures below 15 °C.) A Harvard Apparatus model 975 syringe drive depresses the plungers to deliver between 0.1 and 2.0 ml/min to within ± 0.01 ml/min. The temperature as measured with a thermocouple on the outside of the syringe is controlled to between 4 °C and 7 °C by circulating water from an Endocal RTE-100 chiller through the copper coils.

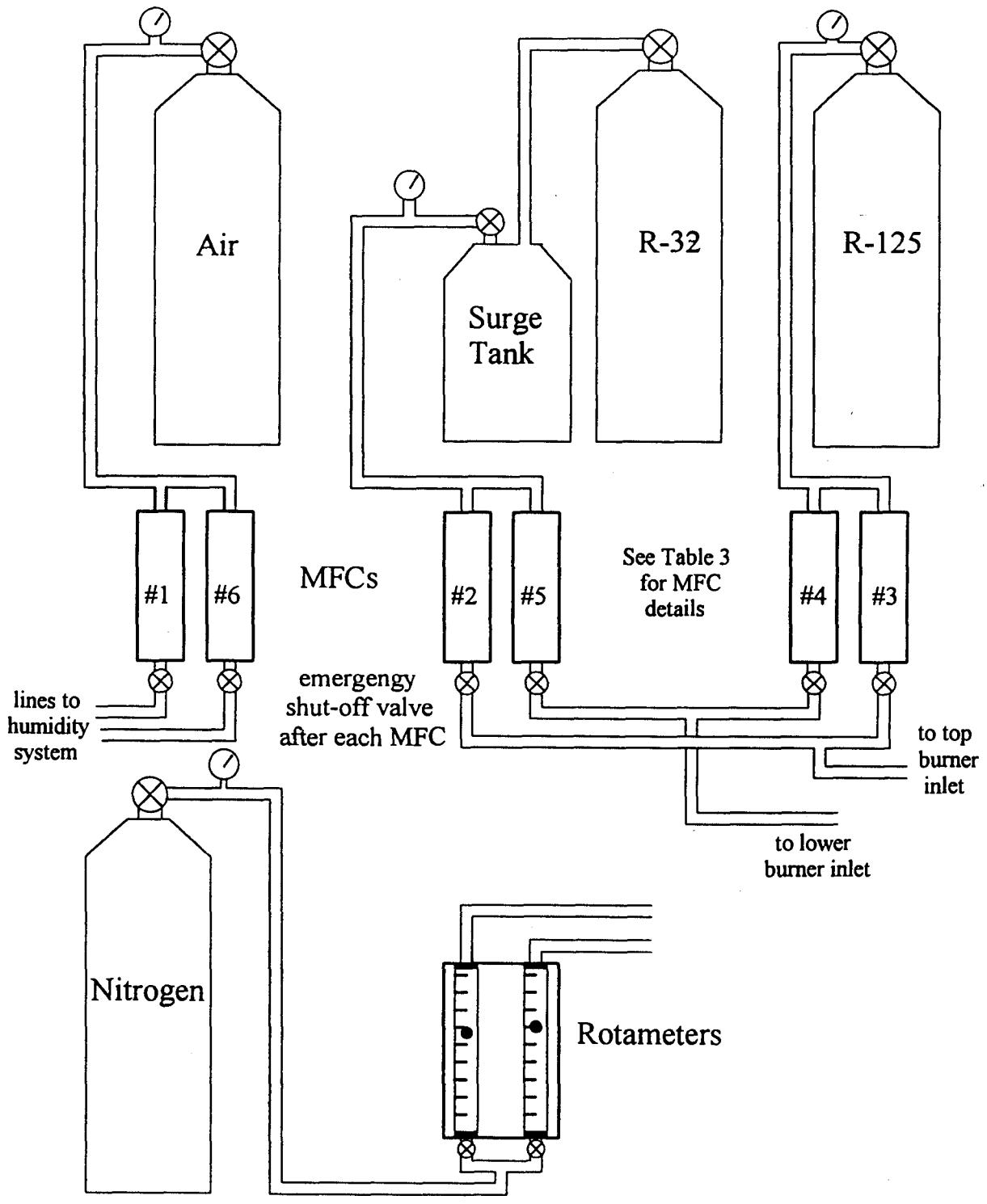

Figure 7. Schematic of gas supply and flow controls for flammability measurements

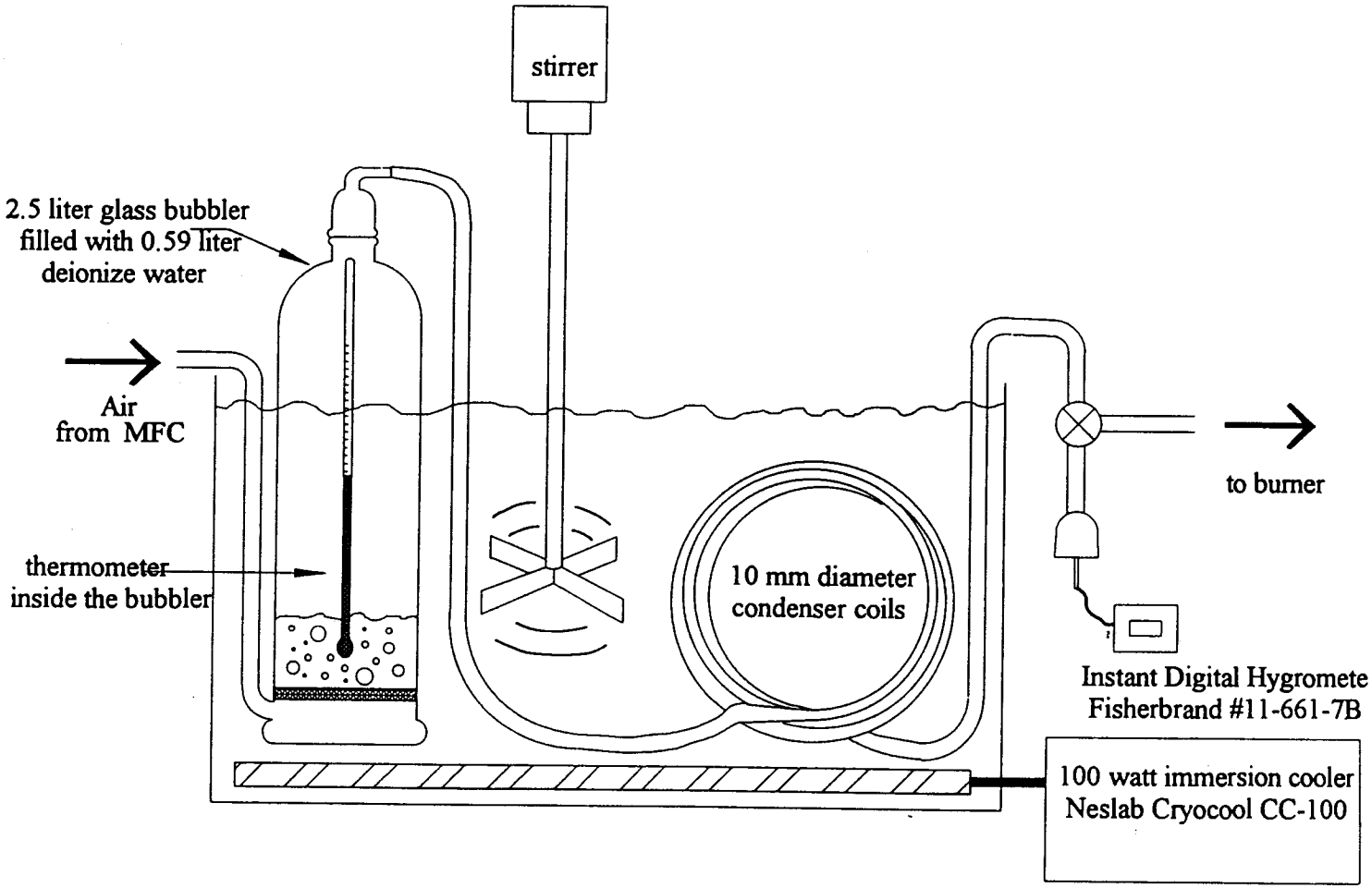

Figure 8. Components of air humidifier

The liquid refrigerant flows from the syringe in a 3 mm stainless steel tube directly to a 13 mm diameter, 150 mm long stainless steel tube filled with glass beads and wrapped with a 200 W heating tape. The temperature inside the tube is heated to approximately 80 °C to fully vaporize the liquid. The refrigerant is then transported into the burner through 6.4 mm Teflon tubing, maintained above 45 °C to prevent the refrigerant from condensing in the lines prior to injection into the combustion air flow. A ball valve at the outlet of the syringe allows the syringe to be filled from the refrigerant supply tank, as shown in Figure 9.

R-245ca is currently available only in limited research quantities at correspondingly high prices. Because of this, isopentane, with a normal boiling point close to R-245ca, was chosen as a surrogate to test that the syringe drive and boiler operated in a steady manner. Even though isopentane is much more flammable than R-245ca, the steadiness of the isopentane flame was a direct indication that the R-245ca could be delivered precisely and continuously during the performance of a flammability measurement.

The syringe drive was also tested with decafluoropentane ($C_5H_2F_{10}$), a non-flammable solvent made by DuPont that has a normal boiling point of 50 °C. An R-32/air flame was first established at the desired stretch rate and equivalence ratio. The syringe drive was then started and the R-32 flow was slowly decreased until the flame was extinguished at the critical flammability ratio.

Exhaust gas cleanup: Hydrofluoric acid makes up 30 % of the exhaust stream from stoichiometric combustion of R-32/air mixtures. Much of the HF is removed using a water spray scrubber. The components of the exhaust gas clean-up system are shown in Figure 10. A polypropylene, corrosion resistant blower (Dayton model 5C089) draws the combustion products through polypropylene pipe (diameters between 90 mm and 140 mm) and routes the cleaned gases to the exhaust vent in a chemical hood. A damper at the entrance to the exhaust pipe meters dilution air to reduce the temperature of the gases and minimize disturbances to the flame caused by excessive exhaust vacuum. A second damper placed just ahead of the blower provides additional control on the exhaust flow. A nozzle (BETE 80° spray angle fog nozzle) is used to spray laboratory water at a rate of approximately 550 ml/min at 69 kPa (gauge) counter to the upward traveling exhaust gas. The acidic water is collected at the bottom of the pipe and drained by gravity into a vented, four liter polyethylene jar. About 90 % removal efficiency can be achieved under normal operating conditions. To achieve closer to complete removal, a second scrubber in series with the first is recommended. After one or two flame extinction measurements, the water spray is stopped, the jar is removed and the effluent is neutralized with NaOH to a pH of 7 ± 1 before being disposed of in the laboratory sink. Extreme care must be exercised to safeguard the operator from contact with the hydrofluoric acid solution. The addition of NaOH to the collection jar prior to operation may be a safer procedure.

Operating Procedure and Data Acquisition

Overall experimental control is provided by a 486, 33 MHz personal computer with 12 MB RAM. National Instruments LabVIEW 3.1.1, operating with Microsoft Windows 3.1, is used to communicate with the mass flow controllers over an IEEE Standard 488 GPIB talker/listener interface. A special modification to the communication EPROM of the 647B mufti gas controller increases the resolution of the communication from 0.1 % to 0.01 % of the full scale of flow of each MFC. This combined with the high accuracy of the calibrated MFCs allows the operator control over each gas flowing into the burner to better than ± 2 % of the reading. A 12 bit National Instrument Data Acquisition Card (AT-MIO-16E-10) collects readings from various thermocouples, a cold junction terminal block and a barometer. The thermocouple cold junction terminal block (NI, SC-2070) provides the ambient temperature reading, ± 0.5 °C. The atmospheric pressure near the flame is

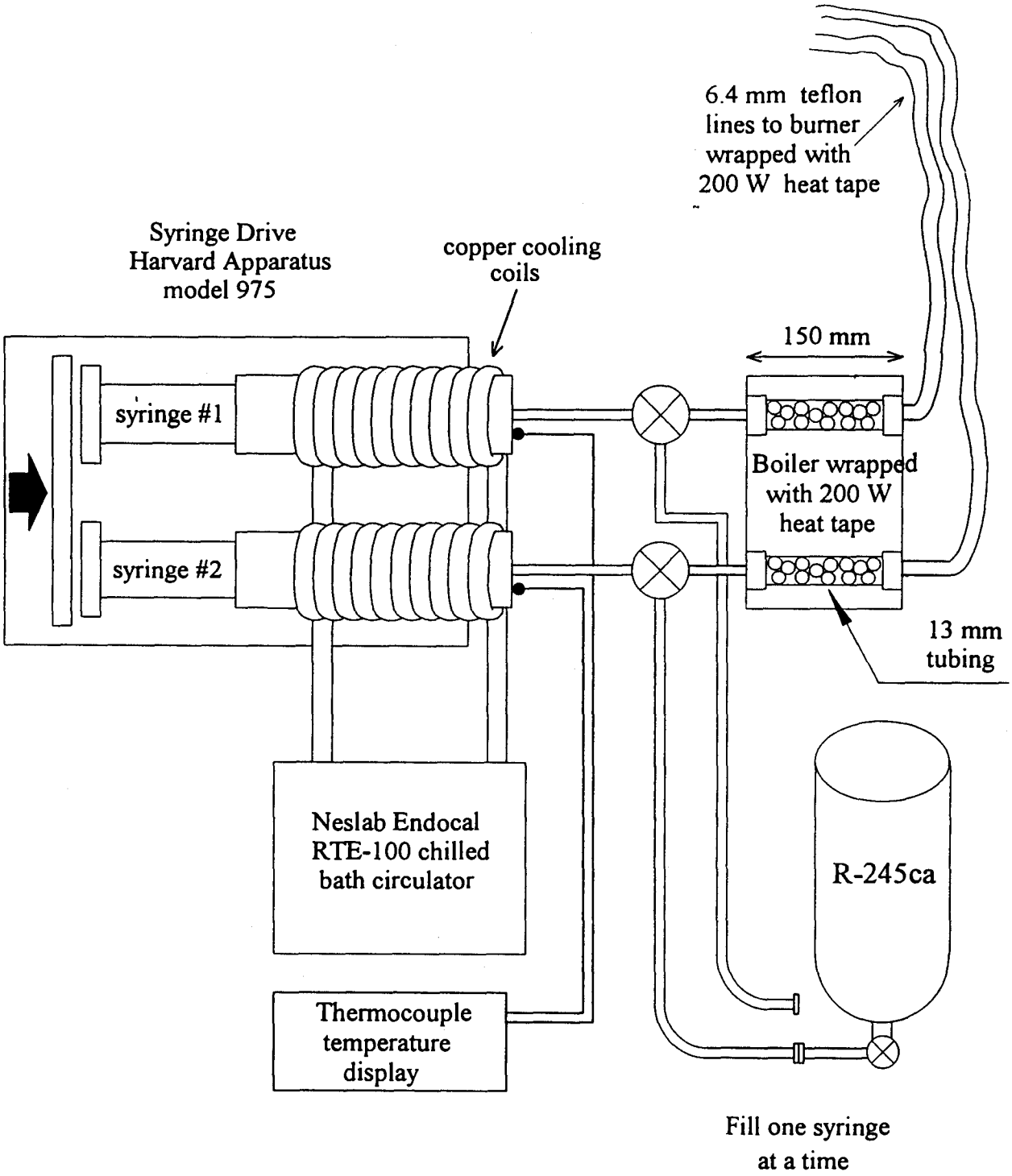

Figure 9. Components of liquid refrigerant injector

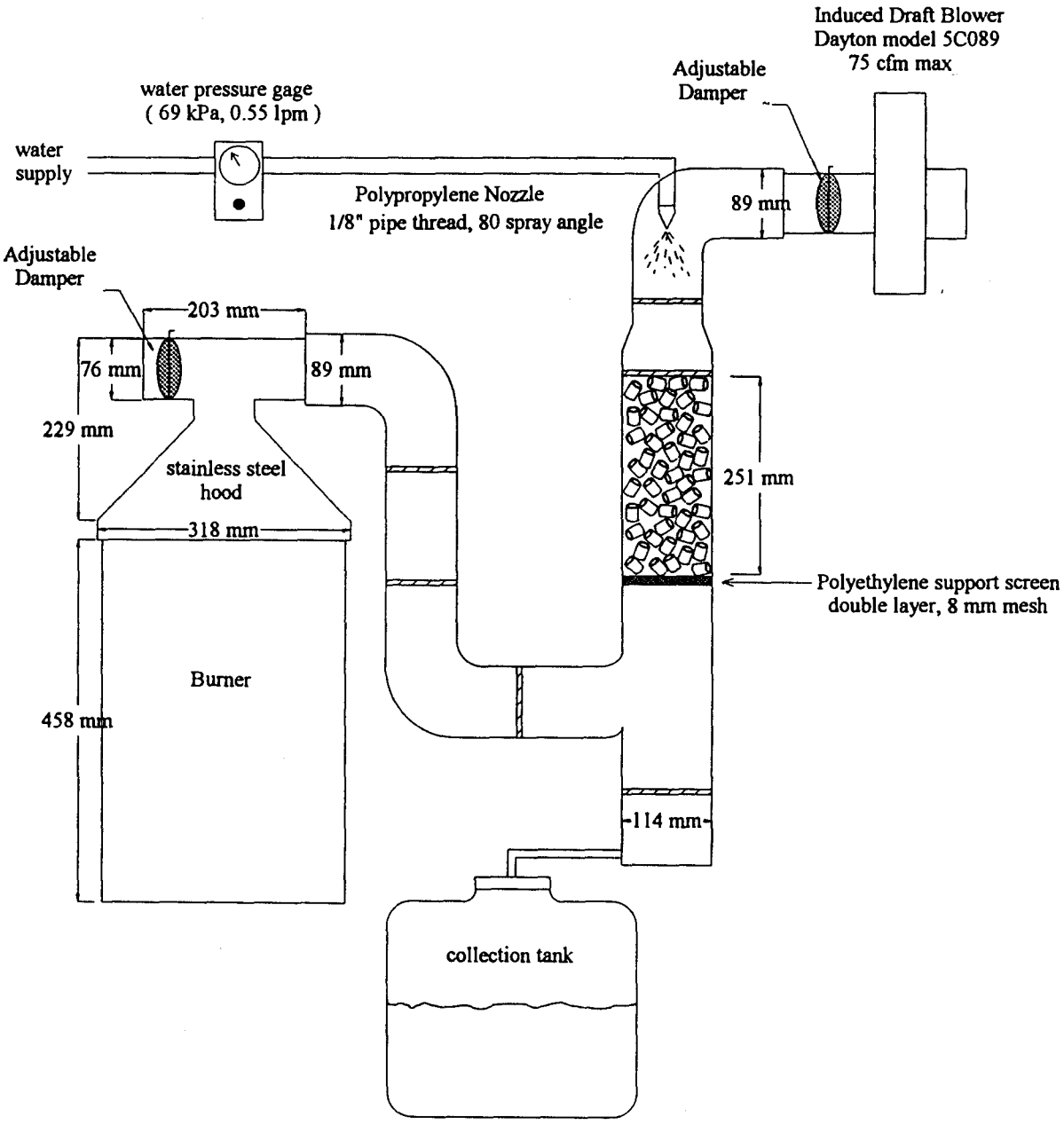

Figure 10. Schematic of exhaust gas scrubber

continuously measured (± 15 Pa) with a Druck 145 DPI Digital Barometer. The computer controls the settings and monitors ambient, burner, and flow conditions through a custom programmed virtual instrument (VI) called TWINFLAM. Programming is in visual C and is specifically for running these tests. Given a desired flame condition, TWINFLAM calculates the appropriate gas flow values, corrects for ambient conditions, and sends signals via the 647B to the mass flow controllers. Refer to Appendix C for more information about the data acquisition program.

For a given burner geometry and fuel/refrigerant, either the equivalence ratio, Φ, or the global stretch rate, K_g, can be chosen as the independent experimental variable. The other of the two then becomes the dependent parameter. K_g is defined as the nominal velocity at the exit plane of the nozzle divided by the distance from the exit to the stagnation plane (or half the nozzle separation). The exit velocity is calculated from the total volumetric flow through the nozzle (corrected for the water vapor added to humidify the air and the ambient pressure and temperature at the burner outlet) divided by the exit area. The mole fraction of less flammable refrigerant is calculated as its volume flow divided by the total flow of the less and more flammable refrigerant mixture. When testing pure fuels, this value is set to zero.

Appendix A lists the step-by-step operating procedure to measure the LFL and CFR. Before beginning an experiment, the burner is pre-heated and measurements of the air humidity are taken. An initial lighting condition is chosen that is robust enough for easy ignition, but has a flow velocity greater than the flame speed to prevent flashback into the burner. The required flows for a given K_g and Φ are determined by TWINFLAM and converted to GPIB signals which are sent to the MFCs. The flame is ignited with a butane lighter (Olympian GM3X). Depending on the conditions, the luminescent region is 10 mm to 20 mm in diameter and the gap between the flames is about 4 mm or less. After the initial flows are set, the program goes into a monitoring loop. While in this mode, current temperature, pressure and flows conditions are read and the updated values of K_g and Φ are recalculated over an average of seven readings. During the test, the burner temperature is maintained by adjusting the speed of the water flow surrounding the nozzle outlets.

Once the flame has stabilized, the settings can then be changed to alter the flame composition and bring it closer to extinction. This is done by initiating a "data read" which ends the monitoring loop and appends the current flame conditions to a data file. One or more of the input parameters (K_g, Φ, % less flammable component) may then be changed and the new MFC signals sent to move the flame toward extinction. The flammability limits for a pure gas are found by either increasing K_g or decreasing Φ to find the lean limit (increase Φ for rich limits). To determine the critical flammability ratio of gas mixtures, the percent of less flammable refrigerant is increased throughout the test. At each step-change, the flames move closer together and then re-stabilize until the merged flames extinguish. When the flame has reached the extinction point, the data at this condition is written to the end of the test file. The gases are then shut off and preparations are made for the next test. An estimate of the amount of material and time required to conduct the tests is given in Appendix B.

EXPERIMENTAL RESULTS

A series of experiments were conducted to compare the LFL of R-32 and the CFR of R-125/32 measured in humidified air at 100 °C, to the previous measurements of these quantities in dry air at room temperature. In the process, a complete flammability curve for R-32 in humidified air at 100 °C as a function of the flame stretch rate has been generated, permitting an estimate of the rich flammability limit as well. Results of the counter-flow burner experiments with R-245ca are also discussed. Prior to giving the flammability results, however, the investigation into the sensitivity of the measurements to changes in burner geometry is presented.

Impact of Geometric Variables and Operating Procedure

The flammability limits determined with the ASTM apparatus are known to vary with the size of the vessel and the ignitor geometry, as well as with the details of the operating procedure. The counter-flow burner does not depend upon a particular ignitor design, but the spacing between the nozzle outlets and the size and shape of the nozzle affect the results. The sensitivity of the results to changes in operating procedure has been evaluated. The base-line geometry had the contoured nozzles with outlet diameters of 12 mm, spaced 12 mm apart. This was the standard condition for all the earlier measurements, as well.

Effect of nozzle shape: The contoured nozzle is designed to produce a close to flat velocity profile at the exit of an unopposed jet discharging into a large, quiescent volume. Measurements of the velocity profile 2 mm downstream of the nozzle exits were made in a non-reacting flow using a TSI IFA 300 hot wire anemometer and signal processor. When the two jets are aligned in opposition (in contrast to discharging individually into a large quiescent volume) the centerline speed is found to be well below the nominal value estimated from the total volume flow and the cross-sectional area. This can be seen in Figure 11. Towards the edge of the jet, the flow accelerates to a value greater than the nominal value, indicated by the dotted line. This general shape has been observed by others studying the dynamics of opposed flow jets [11]. The upper and lower flows were not independently controlled. Based upon this result, the flow control system was modified and all subsequent experiments were run with independent control of the upper and lower jet velocities.

The profile in a fully-developed laminar pipe flow is parabolic, producing a centerline speed that is twice the average. If a constant area nozzle is used, the gas speed at the center of the outlet will be somewhat less than twice the nominal, depending upon the length of the nozzle. The effect on the measured LFL for CH_4 (in dry air at room temperature) of varying the nozzle design from a contoured to a constant-area geometry was studied with the diameter held constant at 12 mm. The spacing was 14 mm for the contoured nozzle and 14.6 mm for the straight nozzle. The straight nozzle design increased the LFL to 0.051, which is beyond the 95 % confidence interval of 0.049 ± 0.001 for the contoured nozzles spaced 12 mm apart and greater than the value of 0.048 reported by Ishizuka and Law [27].

An experiment was run with screens inserted into the straight nozzles to see if this might improve the results. While the screens appeared to allow the burner to be operated at a slightly lower stretch rate, they led to an increase in extrapolated LFL for CH_4/air to more than 0.053. It is uncertain why this occurred, but if turbulence were generated by the screens the flame may have been destabilized.

Effect of nozzle spacing: Two 1 mm thick washers were placed on each of the four support posts separating the upper and lower nozzles so that the distance between the two increased to 14 mm. The extrapolated lower flammability limit of CH_4 in dry air at room temperature increased to a mole fraction of 0.0497, which is within the upper limit of the 95 % confidence interval determined when the spacing was 12 mm. The scatter in data is slightly higher at the larger spacing.

Effect of nozzle diameter: The effect of nozzle opening was examined with three different diameter (10 mm, 12 mm, and 14 mm) straight nozzles. A constant area design was used (rather than the contoured design) for ease of fabrication. With CH_4/air mixtures, increasing the diameter from 12 mm to 14 mm (with the spacing kept constant at 14.6 mm) has no statistically significant effect on the LFL. For the R-32/air mixture, no stable flame could be maintained when the diameter was increased from 12 mm to 14 mm (at a spacing of 14.6 mm), and this did not change when screens were inserted

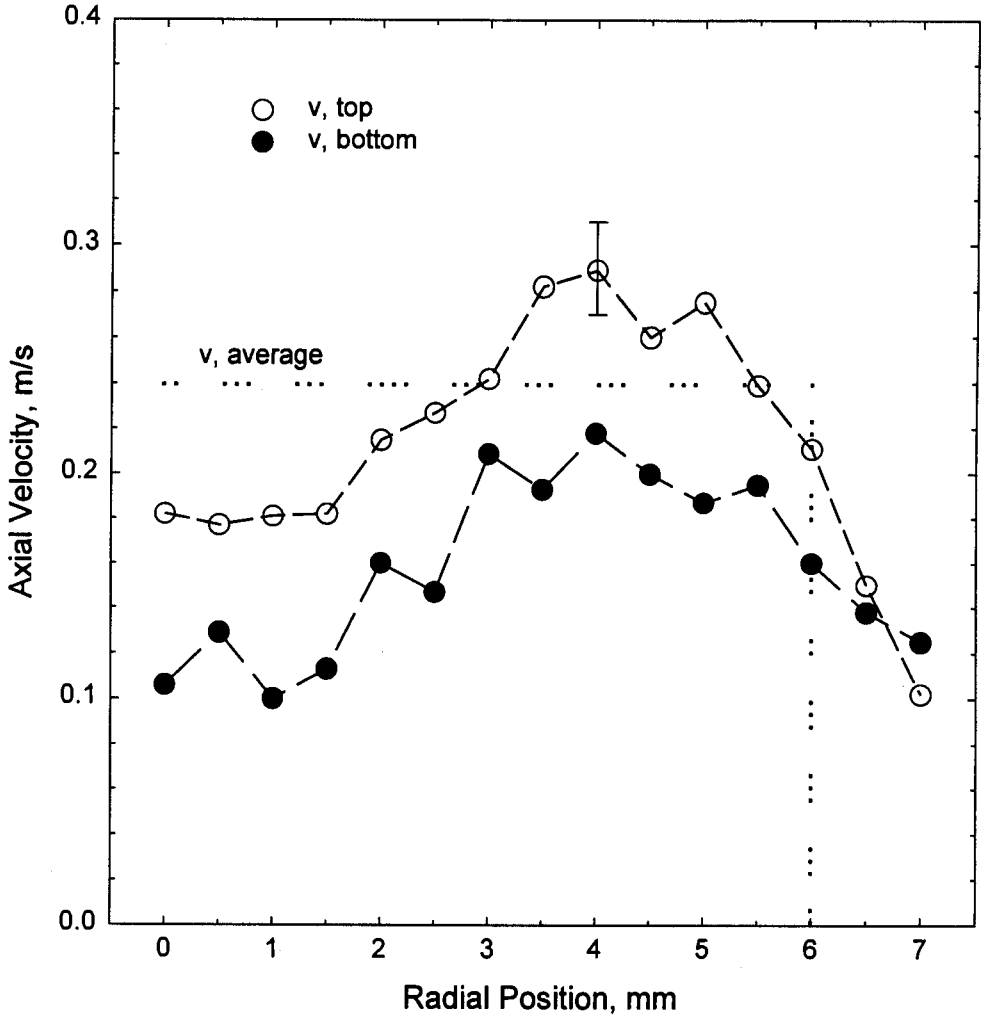

Figure 11. Outlet velocity measured in non-reacting, counter-flow jets from contoured nozzles without independent control. The maximum fluctuation is indicated with the error bar. Dotted line represents profile assuming uniform average velocity from total volume flow.

into the straight nozzle outlets.

Decreasing the nozzle diameter to 10 mm (with a nozzle spacing of 12.7 mm) led to significantly more stable flames. The extrapolated LFL for CH_4/air decreased to about 0.046, and the LFL for R-32/air (dry and at room temperature) dropped dramatically from 0.14 to near 0.11. The general trend was unaffected by the presence or absence of screens at the nozzle outlet.

Conclusions from parametric study of geometry: The important conclusions that are drawn from the parametric study are the following:

- The contoured nozzles produce a slightly lower value of LFL than the constant area nozzles.
- There is no advantage to adding straightening screens at the outlet of the nozzle.
- A spacing of about 12 mm gives consistent results for LFL for both a hydrocarbon and a hydrofluorocarbon.
- R-32/air flames are much more sensitive to burner diameter than CH_4/air flames, with diameters as large as 14 mm having a destabilizing affect, and diameters as small as 10 mm having a stabilizing effect.

The decrease in measured LFL with nozzle diameter is problematic since it is this sort of ambiguity that the counter-flow burner is meant to overcome. Additional experiments with finer control on the burner spacing and with more flexible velocity profiles are needed to unravel the relation between the LFL and the flow field/heat transfer in the burner. A two-dimensional numerical model of the burner, with the ability to vary the geometry and inlet conditions, is also necessary to properly interpret the results. Unlike for the ASTM apparatus, a reliable model can be developed for the counter-flow burner with a reasonable amount of effort. Pending further studies, one must attribute a measured LFL to a specific burner geometry. The 12 mm diameter contoured nozzle, with 12 mm spacing, is recommended for yielding the most consistent and reliable values for flammability, with an expected accuracy for that particular geometry of ± 3 % of the measured mole fraction. In the absolute sense, however, the uncertainty will remain three to four times higher until additional research is conducted.

Sensitivity to operating procedure: The impact on the LFL of the initial conditions, the approach to extinction and the operation of the exhaust scrubber were examined. Ignition can be difficult if the initial mixture ratio and stretch rate are outside of a limited range. Flash back is only a problem for highly flammable fuels like methane. It was not found to be a concern for R-32. The act of removing the ignitor from the lit flame can extinguish the flame before the measurement even begins. Likewise, if the draw on the exhaust is too great, the flame can be extinguished when the fan is turned on. Once the flame has reach a steady condition with the ignitor removed and the exhaust operating properly, there is no memory of the ignition process, so that the measured extinction value is totally divorced from how ignition was accomplished.

Buoyancy dominates the flow at low inlet velocities. A global stretch rate of 30 s^{-1} appears to be a practical lower limit for producing an undistorted flame, although some flames can be stabilized at a stretch rate as low as 25 s^{-1}. When determining the LFL by extrapolation, there is no need to run tests at stretch rates greater than 70 s^{-1}.

The mole fraction of refrigerant at which a flame is extinguished for a fixed global stretch rate is increased by external disturbances to the flame. Excessive exhaust flow, unintended leaks into the Plexiglas burner chamber, and the flowing nitrogen shield can stretch the flame beyond the nominal value. All of these effects become more important at the lower stretch rates. A systematic study was performed with variable flow in the nitrogen shield, and it was found that if the average velocity of the nitrogen gas was greater than 30 % of the outlet velocity of the fuel/air mixture, then the LFL was

measurably increased. Experiments run with zero nitrogen flow gave consistent average results, but the standard deviation was slightly higher for the lowest stretch rates.

Flammability Measurements of R-32

Experiments were conducted in R-32/air mixtures maintained at 100 °C ± 5 °C. The measurements were all taken using the 12 mm diameter contoured nozzles, spaced 12 mm apart, with the nitrogen shield gas flowing at a velocity about 30 % of the reactant jet velocity. Experiments were run with dry air and with the dew point maintained between 11.6 °C and 13.4 °C. A dew point of 12.0 °C corresponds to a relative humidity of 50 % at standard pressure and 23 °C.

Figure 12 is a plot of the extinction R-32 mole fraction as a function of the global stretch rate. The data points are represented by the open and solid circles, corresponding to dry and humidified air, respectively. The solid line is a linear fit through the moist air data for global stretch rates between 30 s^{-1} and 70 s^{-1}. An extrapolation of the line to a zero stretch condition yields a lean flammability limit mole fraction ($ETFL_{100}$) of 0.131 ± .001. Also plotted in Figure 12 are the data and linear fits of the room temperature measurements taken from the Phase II report [5] for dry air (open diamonds, dashed line) and air with a relative humidity at standard conditions of 43 % ± 2 % (solid diamonds, dotted line). Both the previous and current work indicate that the variation in LFL (at a fixed temperature) for differing humidity is less than the experimental uncertainty. However, the temperature can be seen to have a significant impact on the LFL, decreasing the lean limit from about 0.14 for temperatures under 35 °C to about 0.13 for temperatures near 100 °C. While the intercepts change with the temperature, the curves remain almost parallel. The slope of the extinction mole fraction versus stretch rate curves lie between 0.00046 s and 0.00048 s.

The equivalence ratio that leads to the maximum extinction stretch rate changes with the properties of the fuel. For example, Law et al. [3] found that for methane/air mixtures, the highest extinction stretch rate occurs for $\Phi = 0.95$, while for propane/air mixtures, the most robust mixture is associated with an equivalence ratio near 1.20. To determine the mixture of R-32 in air that leads to the most difficult flame to extinguish, additional experiments were performed for stoichiometric and rich conditions.

Figure 13 is a plot of the extinction mole fraction for rich and lean R-32 flames versus global stretch rate, with the reactants initially at a nominal temperature of 100 °C and dew point of 12 °C. The lower portion of the curve, for K_g less than 70 s^{-1}, includes the same data as shown in Figure 12. The horizontal line corresponds to $\Phi = 1.0$ ($X_{R\text{-}32}$= 0.1736). It is evident that the stoichiometric condition is nowhere near the most difficult to extinguish. Operating at an R-32 mole fraction of 0.202 increases the extinction stretch rate to 156 s^{-1}, compared to 102 s^{-1} for a stoichiometric flame. The peak mole fraction corresponds to an equivalence ratio of about 1.20, which is similar to the behavior of propane/air flames.

The structure of rich flames is more complex than flames in lean mixtures because recombination reactions lead to multi-carbon species and soot, and preferential diffusion of the H-atom is enhanced among the field of larger hydrofluorocarbon molecules. Even so, inspection of the upper branch of the flammability curve in Figure 13 suggests that a linear extrapolation to a zero-stretch condition can yield an easily identifiable upper limit. A straight-line fit through the data with $X_{R\text{-}32} \geq 0.24$ has a y-intercept of 0.271; excluding data with stretch rates greater than 60 s^{-1} produces a slightly lower value, 0.263. These values are less than most of those reported in the literature, which range for ambient initial conditions from 0.269 using a flame tube and fuse wire [12] to 0.334 measured in the ASTM E-ASTM E 681-1994 apparatus with a match ignitor [13].

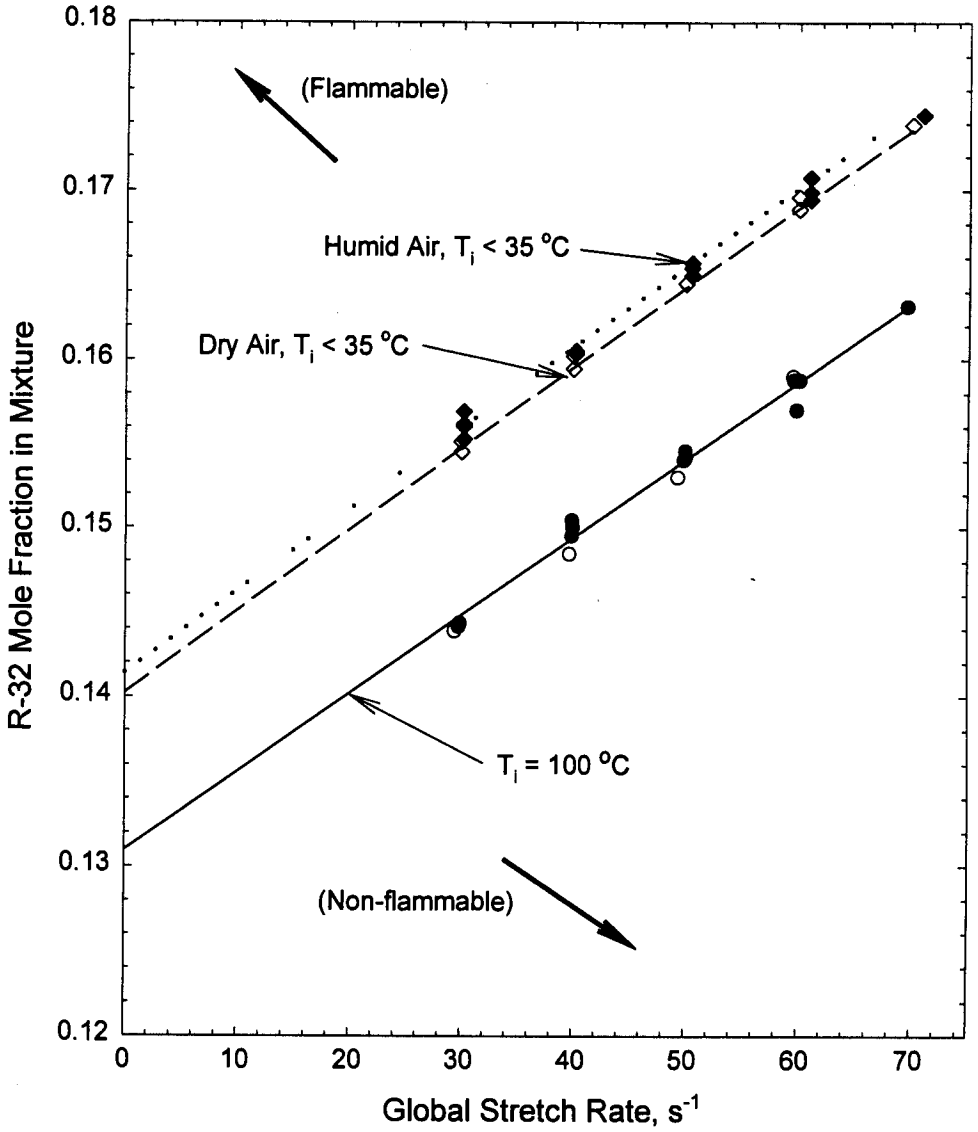

Figure 12. Extinction mole fraction of R-32/air mixtures as a function of flame stretch, showing impact of initial temperature and humidity. Solid symbols: T_{dewpt}=12 °C; open symbols: dry air.

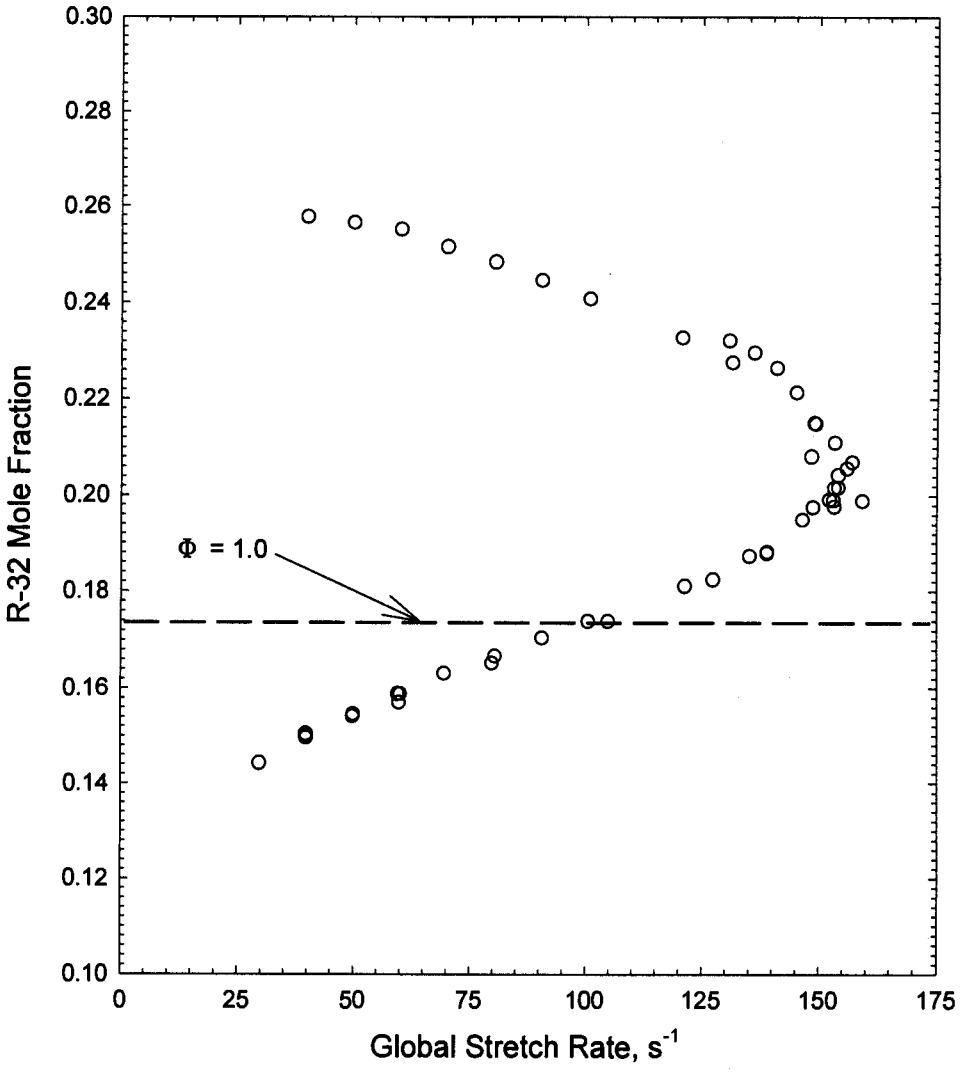

Figure 13. Full flammability curve for R-32/air mixtures at 100 °C and a 50 % relative humidity (at 23 °C).

CFR of R-125/32

The complete combustion at stoichiometric conditions of a mole fraction of R-125, $x_{R\text{-}125}$, in an R-125/32 refrigerant mixture is shown in reaction {R4} in the background section. The total equivalence ratio (i.e., assuming both refrigerants contribute to the fuel) is defined as

$$\Phi = 4.76\,(V'_{R\text{-}125} + V'_{R\text{-}32})/V'_{air} \qquad (1)$$

where V' is the volume flow of the respective gases.

The critical flammability ratio, CFR, is the value of x required to render the refrigerant/air mixture non-flammable under the most conservative (i.e., zero stretch) conditions. The CFR was measured during Phase I of this research [4] using an earlier version of the counter-flow burner. The value of the CFR for R-125/32 in dry air (at a temperature which was not recorded) was estimated to be 0.185 ± 0.008. These experiments were repeated using the redesigned research burner.

Figure 14 is a plot of the global stretch rate at flame extinction as a function of total equivalence ratio for different mole fractions of R-125 in the refrigerant mixture at about 30 °C. When no R-125 is present, the maximum occurs around Φ =1.25. The extinction stretch rate is not a strong function of equivalence ratio in this region (for fixed x), but the peak in the curve shifts downward from when x=0 to $\Phi_{peak} < 1.15$ when x= 0.120. The mole fraction of R-125 is plotted in Figure 15 (filled circles) as a function of the corresponding maximum extinction stretch rate from Figure 14. If a straight line is fit to all the data (the dotted line), it intersects the ordinate when $x(0) \equiv x_0 = 0.149$. If the zero stretch condition is identified by extrapolating data restricted to less than 48 s^{-1} (the solid line), then x_0 is about 0.170, which can be taken as a conservative estimate of the CFR for R-125/32 mixtures in dry air at 30 °C ± 5°C and 99.4 kPa ± 0.8 kPa.

The data from the room temperature measurements of the CFR of R-125/32 showed little sensitivity to the exact value of the equivalence ratio, but that the most robust flames occurred between an overall equivalence ratio of 1.15 and 1.25. To streamline the process of obtaining the CFR for elevated temperatures and humidity, the operating procedure was modified to permit $x_{R\text{-}125}$ to be increased in small increments while maintaining the overall equivalence ratio and the global stretch rate constant. Three values were chosen for Φ: 1.15, 1.18, and 1.20. The 12 mm diameter contoured nozzles with 12 mm spacing were used in the burner.

The mole fraction of R-125 at which the flame extinguished is shown in Figure 16, plotted versus the global stretch rate. The filled squares are for Φ = 1.15, the open circles for Φ = 1.18, and the open triangles represent the data from the Φ = 1.20 tests. The reactant temperature for this series was set to 100 °C ± 5 °C, and the dew point was kept between 12.2 °C and 13.2 °C. Comparing Figure 16 to Figure 15, the stabilizing effect of the higher temperature and humid conditions is easily seen. The importance of temperature on flame stabilization is known from theoretical considerations, and was also demonstrated in the R-32 LFL tests. The R-32 experiments showed no sensitivity to relative humidity, but it is possible that the water vapor becomes more significant in CFR measurements at the higher values of $x_{R\text{-}125}$, where the H/F ratio becomes small. A separate test series is required to ascertain the relative importance of humidity compared to the temperature for enhancing the combustion as the mixture approaches the CFR.

For stretch rates less than 30 s^{-1}, the value of the R-125 extinction mole fraction falls off quickly, a result that was not noted with the dry air, room temperature measurements. The flame was observed to operate in an erratic way at these low values of flame stretch, probably due to the high buoyancy forces and interactions with the hotter nozzle surface. Additional disturbances might also be associated with the bubbling action of the humidifier, which was not present in the room temperature CFR study.

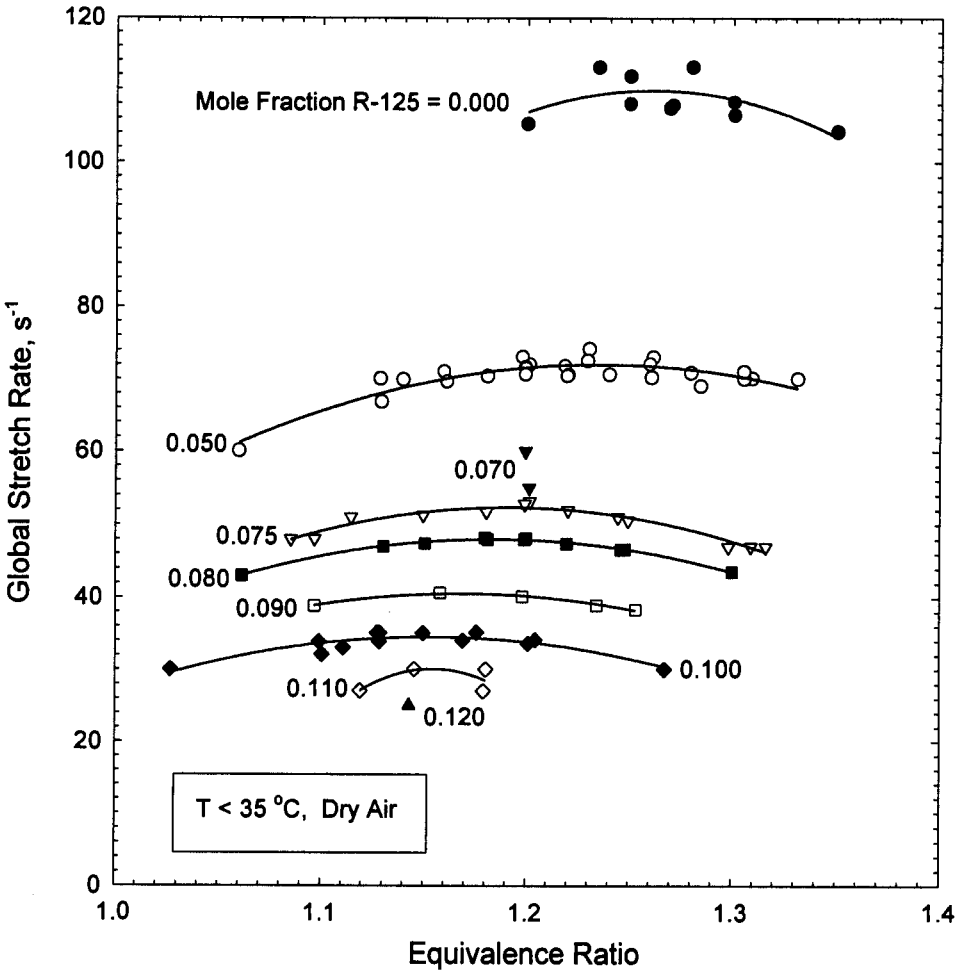

Figure 14. Extinction stretch rates for fixed values of x as a function of total equivalence ratio

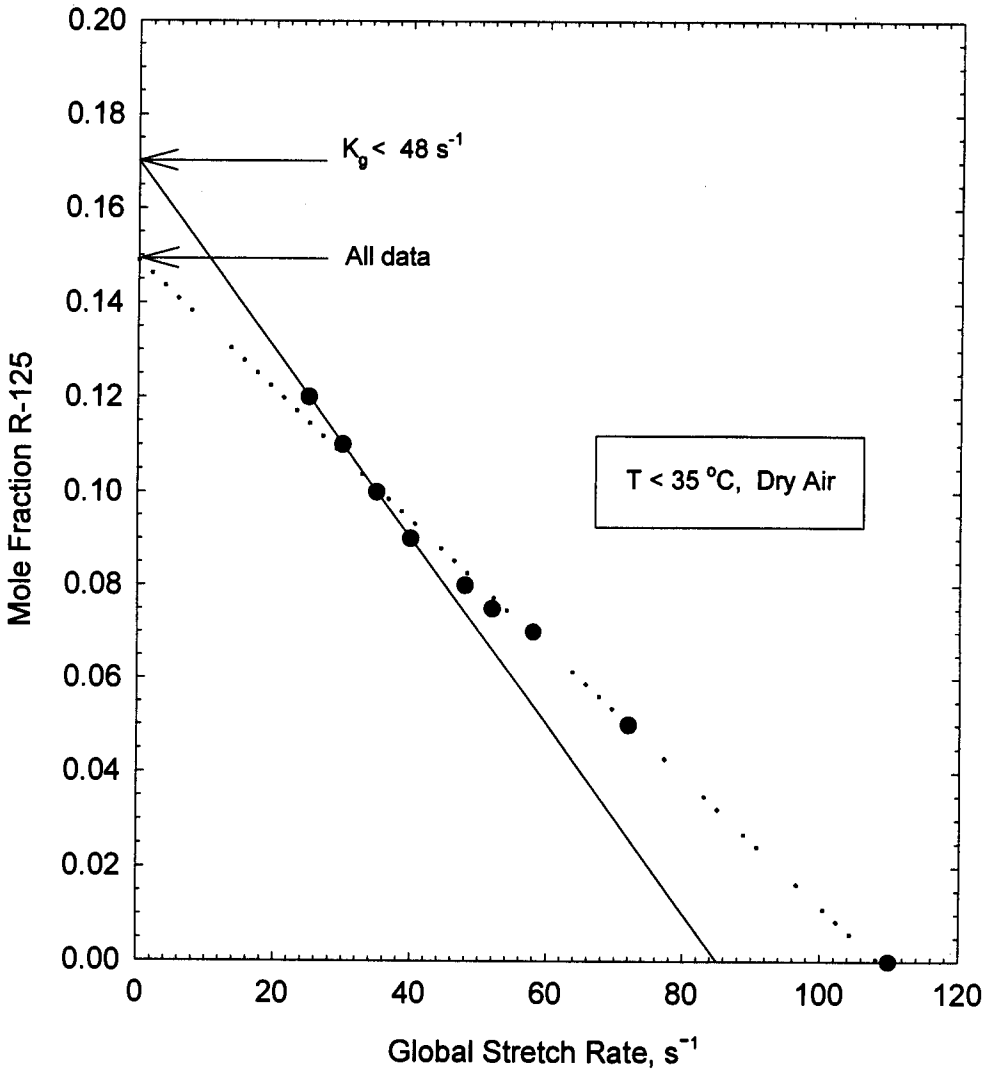

Figure 15. Values of x required to render R-32/125/air mixtures non-flammable as a function of flame stretch

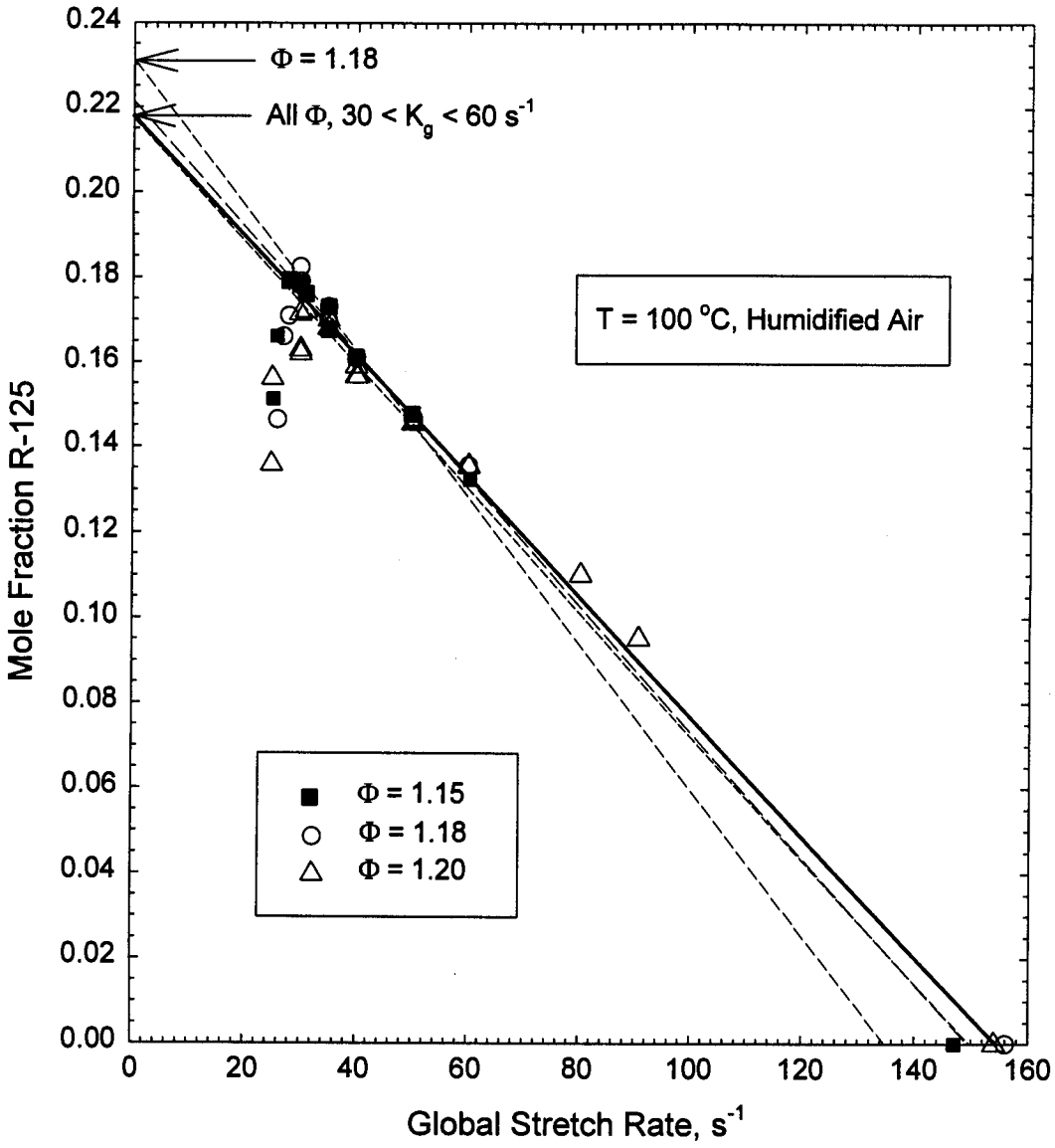

Figure 16. Mole fraction of R-125 at extinction as function of global stretch rate for reactants at 100 °C and dew point of 12 °C. The dashed curves are best fits through data, excluding high and low values of K_g, corresponding to three values of Φ. The solid line is best fit without regard to Φ.

Straight-line extrapolations to the zero stretch condition were performed independently for each of the three values of overall equivalence ratio. The extinction values of $x_{R\text{-}125}$ for K_g less than about 30 s^{-1} and greater than around 60 s^{-1} were not considered in arriving at the dotted lines shown in Figure 16. The values of x_0 resulting from the $\Phi = 1.15$ and $\Phi = 1.20$ tests are close to each other; at an equivalence ratio of 1.18, x_0 reaches its maximum value, 0.230. The solid line in Figure 16 is the best fit when all values of Φ are lumped together, yielding an intercept of $x_0 = 0.217$. The most conservative value for the CFR at 100 °C and a 50 % relative humidity (corrected to 23 °C) is 0.23.

Flammability Measurements of R-245ca/R-32 Mixtures

R-245ca has a boiling point close to room temperature, which necessitates using an alternative fluid metering system and operating procedure. Liquid refrigerant is drawn into two, 100 ml, cooled, stainless steel syringes. The syringes are placed onto a motorized drive unit that is equipped with cooling coils to maintain the refrigerant in a liquid state, at a temperature below 7.5 °C. The speed of the syringe drive is adjustable in discrete increments only. Because R-245ca is much less flammable than R-32, it is necessary to add a more flammable component to the reactant stream to enable ignition.

The procedure adopted to determine the flammability limits of R-245ca/air mixtures is to first ignite the flame with the syringe drive engaged but with a preponderance of R-32 present, at an overall equivalence ratio around 1.3 and a stretch rate between 50 s^{-1} and 100 s^{-1}. Once the flame is stabilized, the mole fraction of R-32 is reduced, while either the overall equivalence ratio or the stretch rate is maintained constant. The fraction of R-32 in the refrigerant mixture and the stretch rate at the point of extinction are noted, and the test is repeated for a different initial stretch rate. By plotting the mole fraction of R-245ca in the refrigerant mixture as a function of the extinction stretch rate, a graph similar to Figure 15 is obtained.

The solid circles plotted in Figure 17 show the results for an initial reactant temperature of 100 °C and a room temperature relative humidity of 50 %. The data exhibit a sharp break at a mole fraction of R-245ca equal to about 0.24. For smaller values of $x_{R\text{-}245}$, the refrigerant acts in a manner similar to R-125, inhibiting the R-32/air reaction due to its high molecular weight and lower reactivity. A straight line extrapolation from these low values of $x_{R\text{-}245}$ (solid line in Figure 17) would suggest that R-245ca is non-flammable, with a CFR in R-32 of about 0.34. On the other hand, the zero stretch limit based upon $x_{R\text{-}245} > 0.24$ (or $K_g < 60$ s^{-1}) leads to the conclusion that R-245ca/air mixtures can sustain a flame under idealized conditions since a straight line intersects the y-axis at a value of $x_{R\text{-}245}$ greater than unity. The data used for extrapolation represent overall equivalence ratios between 1.26 and 1.35.

The effects of initial reactant temperature and relative humidity on the extinction mole fraction of R-245ca can also be seen in Figure 17. The open diamonds represent tests done with the initial temperature reduced to 50 °C and the relative humidity held constant at 50 %, and the squares with dots show what occurs if the air is not humidified and the temperature is maintained at 100 °C. Both reducing the temperature and the relative humidity lead to lower values of extinction mole fraction. The limited data taken at these conditions suggest that either change is sufficient to cause the extrapolated straight line to intersect the y-axis below unity ($x_{R\text{-}245,0} < 1.0$), implying that R-245ca is non-flammable under these conditions. If a single correlation is derived using all data for stretch rates less than 60 s^{-1}, the dotted line in Figure 17 is the result.

Figure 18 shows how the extinction stretch rate is affected by the overall equivalence ratio. The data are grouped according to the value of $x_{R\text{-}245}$. The scatter within each grouping is associated with the variations in the initial temperature, the relative humidity and the exact value of $x_{R\text{-}245}$. The open hexagon symbols represent the data for pure R-32 ($x_{R\text{-}245} = 0$). The strong influence of $x_{R\text{-}245}$ on the extinction stretch rate is the most obvious feature of the figure. A sensitivity of K_g to overall

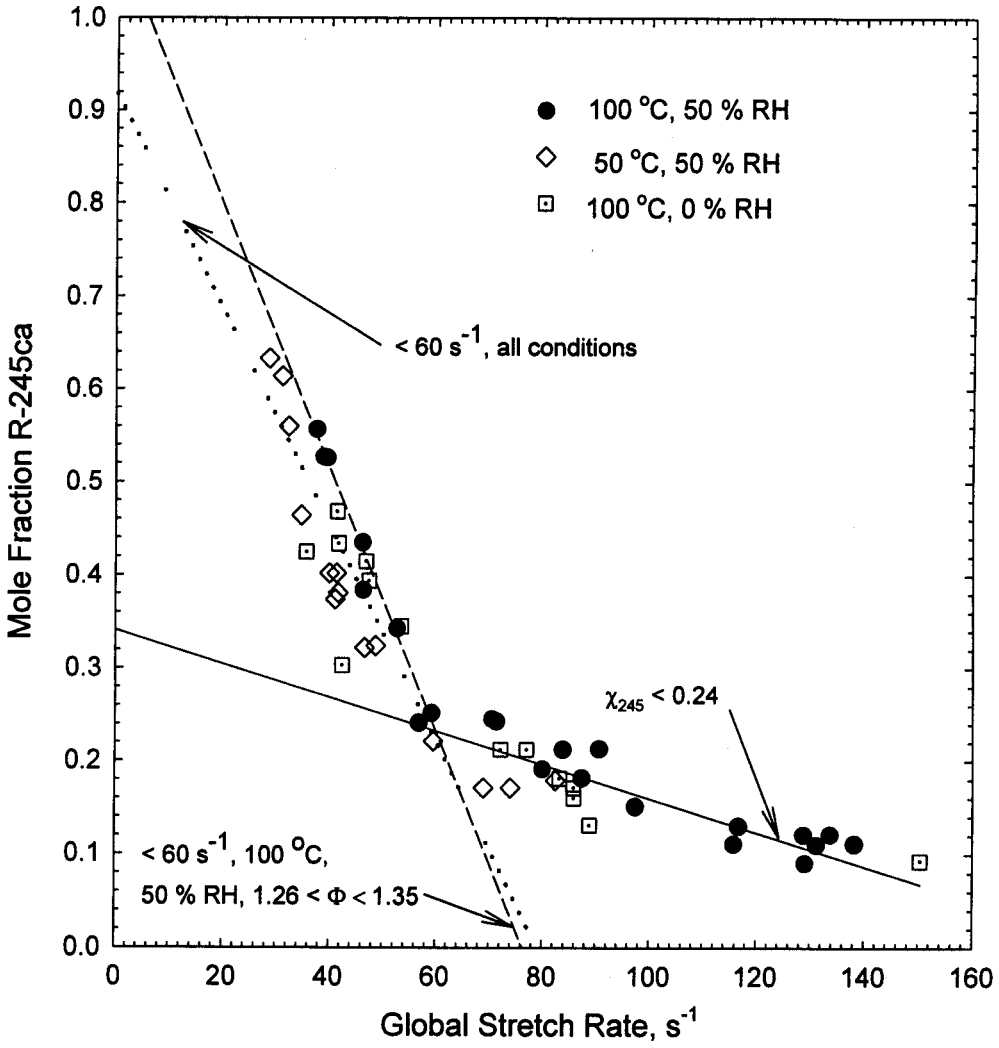

Figure 17. Mole fraction of R-245ca mixed with R-32 as a function of extinction stretch rate. Solid circles: 100 °C, 50 % relative humidity; diamonds: 50 °C, 50 % relative humidity; squares: 100 °C, 0% relative humidity.

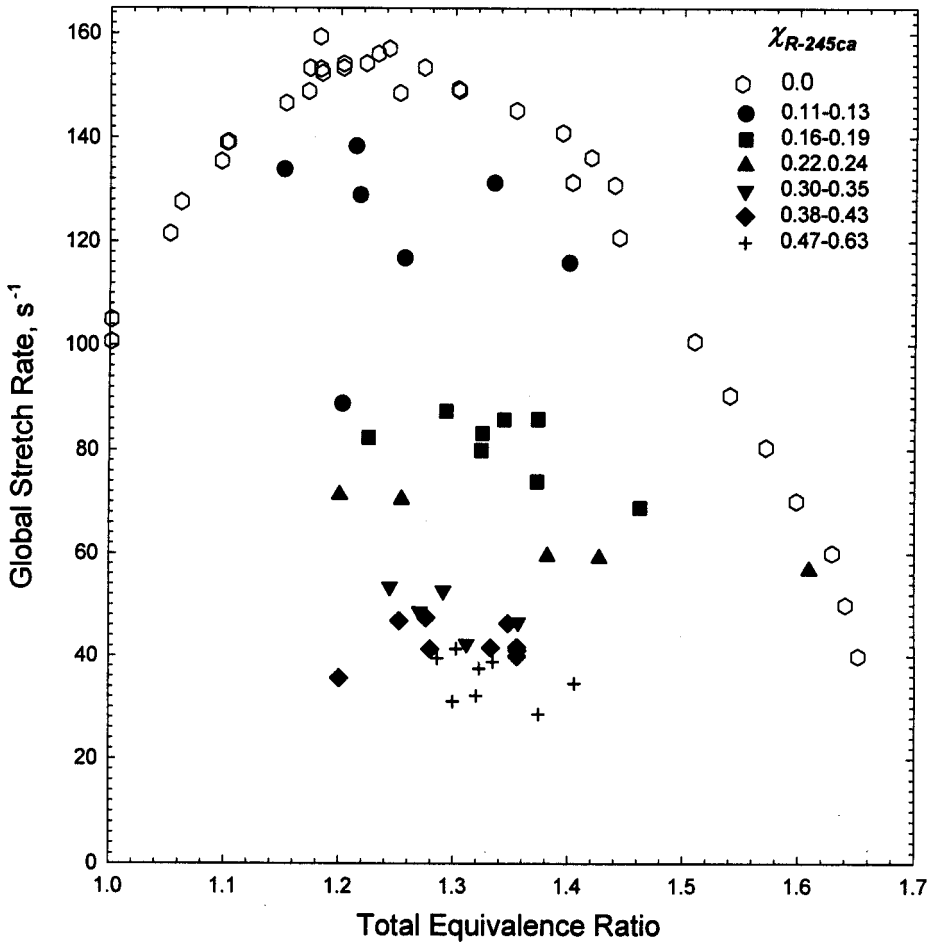

Figure 18. Dependence of extinction stretch rate on total equivalence ratio for ranges of x_{R245}

equivalence ratio is not observed, although a slight shift in the peak to higher Φ_{tot} with increasing $X_{R\text{-}245}$ can be imagined.

Table 4 summarizes the intercept values ($X_{R\text{-}245,0}$) and correlation coefficients found by trying to separate out the effects of humidity, temperature and equivalence ratio. Correlation coefficients less than 0.90 result when the data are scattered or not well correlated by a straight line. Intercepts greater than unity imply pure R-245ca/air mixtures are flammable; extinction stretch rates less than zero imply that the R-245ca/air mixtures are non-flammable at the conditions stated. Additional measurements are required to better quantify the precise boundaries of flammability for R-245ca, but clearly they are sensitive to the initial conditions, with equivalence ratios around 1.32, higher temperatures, and moister air increasing the chance of flammability. (The same conclusions regarding equivalence ratio and humidity were reached by Smith, et al. [37], using the ASTM E 681-1994 apparatus.) It is also important to keep the strict definition of "flammable" in perspective, since under no conditions obtainable in the laboratory counter-flow burner could a pure R-245ca/air flame be stabilized.

Table 4. Intercept values for R-245ca/air flames found using the tests conditions indicated

Stretch rate s^{-1}	Temperature °C	Relative Humidity @ 23 °C	Φ_{total}	$X_{R\text{-}245,0}$	Correlation Coefficient	$K_{g,0}$, s^{-1}
30 - 60	50 - 100	0 % - 50 %	1.1 - 1.6	0.92	0.77	< 0
30 - 60	100 ± 5	50 % ± 4 %	1.26 - 1.35	> 1.0	0.96	6.0
30 - 60	50 ± 5	50 % ± 4 %	1.27 - 1.41	0.98	0.91	< 0
30 - 60	100 ± 5	0 %	1.20 - 1.36	0.58	0.17	< 0
30 - 60	50 - 100	0 % - 50 %	1.26 ± 0.02	0.91	0.66	< 0
30 - 60	50 - 100	0 % - 50 %	1.32 ± 0.02	> 1.0	0.70	12
30 - 60	50 - 100	0 % - 50 %	1.37 ± 0.02	> 1.0	0.89	3.8

ANALYSIS AND DISCUSSION

Uncertainty Analysis

The LFL and CFR reported in the previous sections are subject to uncertainties from several sources, including errors in flow measurements; variations in temperature, pressure and composition; the rate at which the extinction point is approached; changes in burner geometry; and non-linear effects near the zero stretch rate condition. Flow calibration and measurement uncertainties were examined and described in detail for the R-32/air LFL measurements in the Phase II report [5]. An uncertainty in mole fraction of ± 0.008, with a 95 % confidence interval, was estimated based upon the assumed linear relation between the LFL and stretch rate, and the dependence of each on the uncertainty in measured flows. In the Phase III work, additional mass flow controllers (MFCs) have been added which are sized to operate close to the middle of their dynamic range during most of the experiments. The additional MFCs also allow independent control of the upper and lower burner sections, to ensure that the flows are balanced equally.

The impact on the uncertainty of the results caused by variations in humidity, unknown concentrations of trace species in the reactants, and variations in inlet temperature can not be expressed in a simple mathematical expression because of the complex relationships between these parameters and the flame chemistry. The uncertainty in dew point is about ± 1 °C, which, based upon the measurements with and without any moisture added, is estimated to be an insignificant source of uncertainty for the $ETFL_{100}$ of R-32; the error in the CFR@100 °C of R-125/32 and the $ETFL_{100}$ of R-245ca could be larger, but is still likely to be smaller than the uncertainty from the flow. The average temperature of the reactants as they enter the burner nozzle varies less than 10 °C, and the maximum difference in temperature between the upper and lower sections is approximately the same. Higher temperatures are known to stabilize the flame, but since the actual temperature at extinction varies in the experiment in a non-systematic way, the uncertainty in LFL and CFR caused by variations in reactant temperature can be reduced by replication. The high degree of repeatability of the extinction conditions indicate that such random errors are smaller than the uncertainty in flow. The impact of the barometric pressure, which ranges between about 98 kPa and 100 kPa, is even less than that of the initial temperature since combustion theory predicts almost no change in flame stability for such a small change in pressure.

The extinction process is dynamic and the response time of the MFCs and burner are non-zero. This means that the exact conditions at the nozzle exit and in the flame during the precise point of extinction are not measured. The uncertainty due to this behavior is reduced by ensuring that changes in flow conditions occur at a rate slower than the response time of the burner and control system, which is about 10 s. The conditions at extinction are taken to be the readings just after the change in flow setting. Thus, the uncertainty can be taken as one half the increment between the previous and final step. This value varies among tests, but is usually less than 0.5 % of the recorded stretch rate or mole fraction.

Intentionally changing the burner geometry significantly affected the measured LFL, as was discussed in the results section. This is distinct from small changes due to imperfections in the burner or misalignments in assembly. The burner was disassembled for cleaning a number of times and physically relocated from one laboratory to another. No extraordinary care was taken to reassemble the nozzles precisely in the same manner each time. It is estimated that the nozzle spacing and centerline alignment could have varied by as much as 0.5 mm. As long as an entire test sequence was conducted without disassembling the burner, no additional uncertainty in LFL was found distinct from the random errors associated with run-to-run variations.

The variations in flammability limit (> 8 % of the LFL for methane, more for R-32) caused by gross changes in the burner geometry (± 20 % in spacing and diameter, straight nozzles versus contoured nozzles) are associated with non-idealities in the flame structure. The theory is premised on the following:

- that the flame is axisymmetric;
- that the radial gradients of scalar quantities are much less than the axial gradients;
- that all chemical species diffuse at equal rates, and at about the same rate as the diffusion of heat and momentum; and
- that the system is adiabatic.

The first two assumptions increase in validity as burner diameter and spacing become large, and when the initial velocity profile is flat. The diffusion coefficients vary among the individual species by an order of magnitude, but are not affected directly by geometry. Likewise, the gradients in the primary reaction zone which drive diffusion are established by the chemistry and not the exact geometry. However, the rate of diffusion of all species in the radial direction is lessened as the flame becomes more one dimensional.

Heat transfer to the burner walls by conduction and to the surrounding environment by radiation causes the flame to be non-adiabatic. Conduction losses are small, in general, and are lessened as the distance between the flame and the burner are increased, either by increasing the nozzle diameter or the spacing.

Radiation losses are also small in absolute terms, but increase directly with the mean-beam-length of the high temperature flame zone. Thus, radiation losses are enhanced as the size of the burner is increased, which is the trend opposite from the first three assumptions above and the conduction losses. It is possible that the dichotomy in behavior related to scale is responsible for the complicated relationship between gross changes in burner geometry and the measured flammability limits.

Fortunately, the LFL of methane measured in the current study with nozzle diameter and spacing near 12 mm is consistent with that of other researchers using different counter-flow burner designs in normal and microgravity experiments. There are no other reported measurements of the LFL for R-32 using counter-flow burners of any design, but the value determined in the current 12 mm burner is consistent with those measured using the ASTM apparatus by numerous people.

Comparison to Chemical Kinetics Flame Model

The extinction of dual, one-dimensional, counter-flow hydrocarbon/air flames has been numerically modeled with some success by a number of researchers [14,15]. The addition of fluorine to the hydrocarbon kinetics scheme greatly expands the number of molecular species that need to be tracked in the calculations. The computational penalty associated with including a complete chemical kinetics mechanism such as the one developed by Burgess, et al. [7], in a two-dimensional computation that accounts for the non-ideal nozzle flow is impractical, and may be unnecessary to explain the qualitative behavior observed in the experimental methane and R-32 flames.

As a more tractable alternative, the flames were assumed to be one-dimensional, freely propagating, and adiabatic. The structure of such a flame can be calculated in a straightforward manner using the PREMIX code [16] developed by Sandia National Laboratories with the chemical kinetics package CHEMKIN [17]. The methane/air chemistry was based upon the GRI mechanism [18], while the F/C/H/O mechanism developed by Burgess et al. [7] was used to model the detailed

fluorine chemistry with reactions up through C_2. A total of 780 chemical reactions were assumed to take place among 83 species, as listed in Appendix D.

The PREMIX flame code has a number of options which control the calculation procedure and can impact the predicted species mole fractions, temperature profile, and flame speed. In the current study the secondary effect of the temperature gradient on mass diffusion (Soret effect) was included. Upwind differencing was used for the convective term, and the flame was assumed to be anchored at the location where the temperature reached 127 °C. The parameters GRAD and CURV control the development of the grid spacing, with small values of each restraining the maximum first and second derivatives in the species profiles that will be tolerated. The former was set at 0.1 and the latter at 0.3. The absolute and relative tolerances placed on convergence of the Newton iteration were 1.0×10^{-9} and 1.0×10^{-4}, respectively.

The required number of grid points across the flame in a converged solution ranged between 126 for a stoichiometric CH_4/air flame to 238 for an R-32/air flame approaching its lean flammability limit. The computational domain extended from - 50 mm to + 1000 mm. The numerical program as received from Sandia National Laboratory was designed to run on a work-station, but the code was modified for the current effort to be compatible with the NIST Convex C3820 vector machine. Depending upon the initial conditions in the problem and the accuracy of the first guess for the temperature profile, it took from 1000 s to 40,000 s of CPU time to reach a converged solution.

Stoichiometric methane and R-32 mixtures: The complete combustion of a mixture of methane and R-32 at an overall equivalence ratio of unity is given by the following expression:

$$\chi CH_2F_2 + (1-\chi)\,CH_4 + (2-\chi)(O_2 + 3.76\,N_2) \rightarrow CO_2 + 2\chi HF + 2(1-\chi)H_2O + 3.76(2-\chi)N_2 \qquad \{R6\}$$

where χ is the mole fraction of R-32 in the binary fuel. Computations were performed, first, in the limiting cases of $\chi = 1$ and $\chi = 0$ to compare the structure of a pure R-32/air flame to that of a methane/air flame.

The upper graph in Figure 19 is a plot of the temperature in the two flames. The initial temperature at the left is 25 °C. In the methane flame, the temperature rises steeply within the first millimeter and reaches 1960 °C by the end of the computational domain. The temperature in the R-32 flame builds up more slowly but eventually reaches almost the same value (1930 °C). By transforming the distance scale to a time scale, the temperature-time gradient can be used to accentuate the difference in temperature build up within each of the two stoichiometric flames, as seen in Figure 20. The magnitude of the methane/air peak is 25-fold greater than the magnitude of the R-32/air peak, and the methane peak occurs almost an order-of-magnitude earlier in time.

The lower portion of the graph in Figure 19 compares the mole fractions of CO, OH and CH_2 (ground-state) in the CH_4 and CH_2F_2 flames. The carbon monoxide begins to form earlier in the R-32 flame, but the rate of formation of CO in the CH_4 flame accelerates and reaches its maximum mole fraction sooner, followed by a decay to the final equilibrium value. The peak CO mole fraction is about the same in both flames. The OH mole fraction is indicative of the size of the chain-propagating radical pool, and is shown to peak in the R-32 flame beyond the CO. The level of OH is about an order-of-magnitude smaller than the OH in the CH_4 flame. The ground-state triplet methylene (CH_2) behaves in a way representative of other small hydrocarbon radicals (e.g., CH_3, CH). It reaches a peak at a location close to that of the CO, and then practically disappears shortly beyond the OH maximum for both fuels. The mole fraction of CH_2 in the R-32 flame is over ten times lower than in the methane flame.

When the R-32 and methane are combined into a single flame, the calculated normal flame

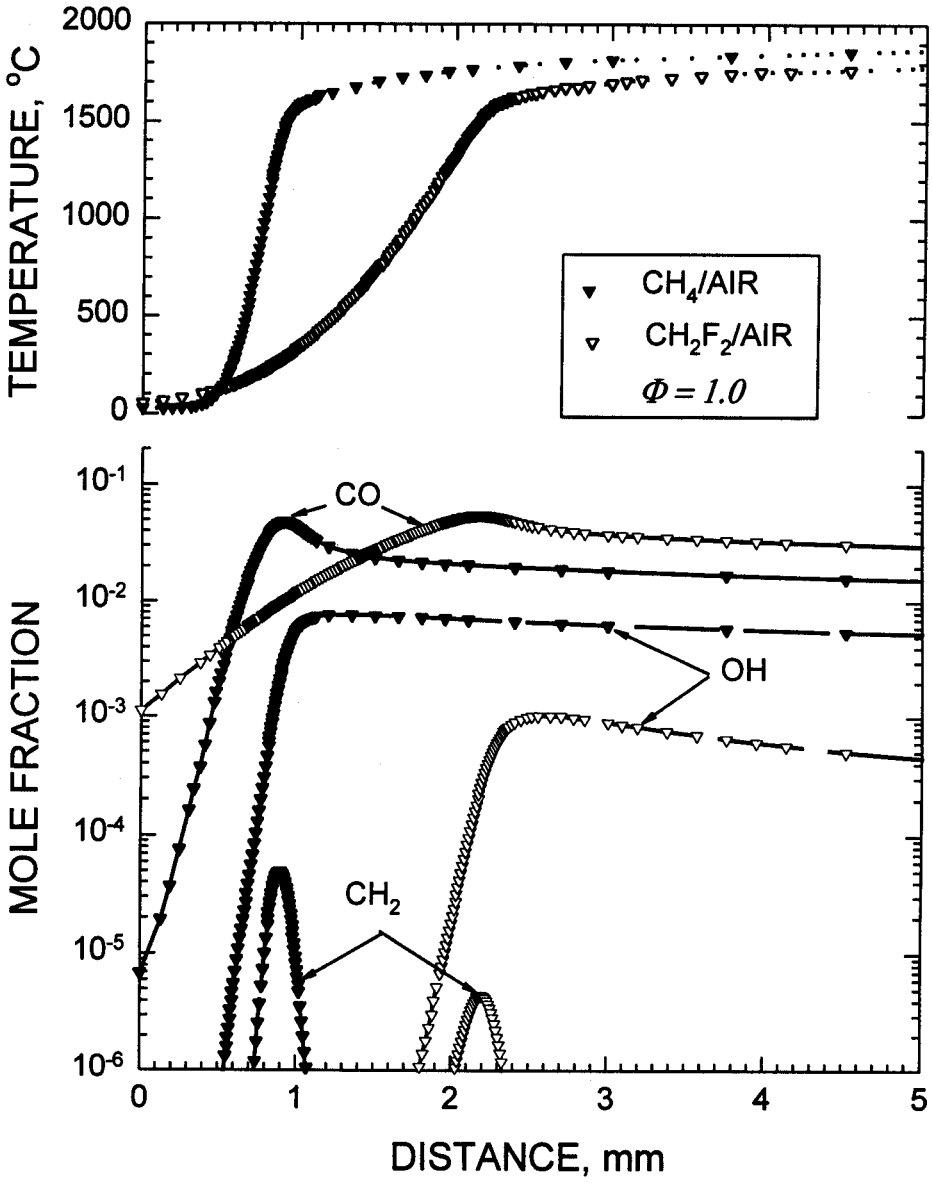

Figure 19. Computed temperature and species profiles through one-dimensional methane/air and R-32/air flames

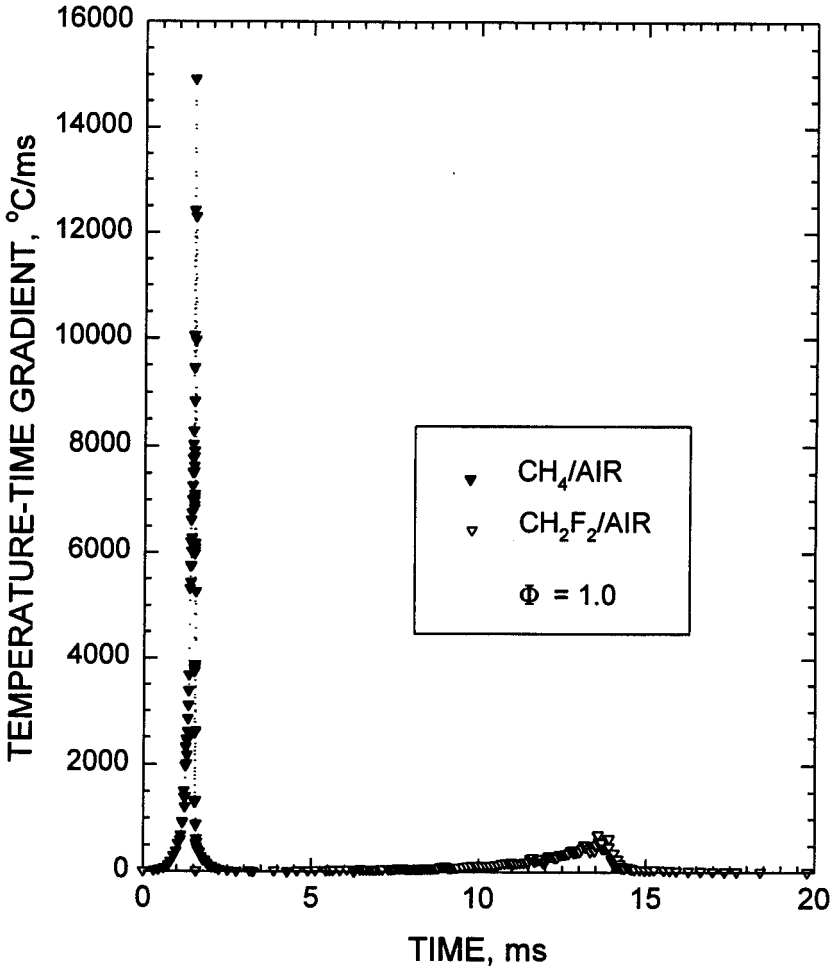

Figure 20. Computed rate-of-temperature increase across one-dimensional flame, comparing R-32/air and methane/air mixtures

speed, v_0, for a stoichiometric mixture decreases from 407 mm/s to 67 mm/s as the mole fraction of refrigerant is increased from 0 to 1.0. The calculated flame speeds are shown in Figure 21, along with the final flame temperatures and maximum OH and H mole fractions. The flame temperature varies only slightly with the fraction of R-32, whereas the OH and H drop monotonically to less than 15 % of their initial value as x is increased from 0 to 1.

The calculated flame speed for pure methane/air is in agreement with measurements by Linteris and Truett [19], the lone experimental study identified in which the speed of an R-32/methane/air flame has been explicitly determined. They used a premixed, laminar nozzle burner in which increasing amounts of R-32 were added to an initially lean, stoichiometric or rich methane/air flame. The flame speed was determined from Schlieren photographs of the flame cone angle. The solid diamonds plotted in Figure 21 are their data. The measured flame speeds at x = 0 and x= 0.18 are within the uncertainty of those predicted by the PREMIX model. (The numerical uncertainty for lean flames is estimated to be ± 20 mm/s based upon repeated calculations using different initial temperature profiles and grid control parameters.) For the highest mole fraction of R-32 studied in the experimental flame (x = 0.46), the overall equivalence ratio was about 1.2 (even though Φ based upon the methane/air ratio was 0.9). The difference in equivalence ratios between the measurements of Linteris and Truett and the PREMIX prediction (in which Φ=1.0) may account for the 45 mm/s discrepancy in flame speed. This was not confirmed with PREMIX because the fluorine mechanism is uncertain in rich mixtures.

Lean R-32/air mixtures: The impact of equivalence ratio on the structure of the pure R-32/air flame also has been examined numerically, and compared to the impact of Φ on the methane/air flame. Figure 22 is a plot of the final temperatures and peak OH and H mole fractions as a function of Φ. As one would expect, the temperature of the refrigerant flame decreases continuously with decreasing Φ. It is noteworthy, however, that the final temperature in the R-32 flame exceeds that of the methane flame when the equivalence ratio is leaner than 0.90. Of great significance is the difference in behavior of the peak OH mole fraction for the two fuels. For the R-32/air flame, not only is the level of the OH much less, but also the shape of the curve is qualitatively different. The calculated OH mole fraction in the methane/air flame drops by a factor of ten as Φ changes from 1.0 to 0.5, and H-atom by a factor of 100. In the R-32/air flame the OH mole fraction actually increases slightly as the flame moves from stoichiometric to Φ = 0.8, but remains close to 0.001 over the entire range of equivalence ratios examined. The H-atom mole fraction decreases monotonically with Φ, but not as steeply as calculated for the methane/air flame. The slower change in OH and H-atom mole fractions with decreasing equivalence ratio contributes to the ambiguity in the defining a precise flammability limit for R-32/air flames.

Figure 22 compares the propagation speeds for the two flames at different values of Φ. The normal flame speed drops slowly with decreasing equivalence ratio in the R-32 flame, eventually attaining a value of 36.7 mm/s for Φ = 0.68. The numerical model computes a value of 29 mm/s for an unstretched, adiabatic methane/air flame at an equivalence ratio of 0.48.

R-125/32: The chemistry of two-carbon hydrofluorocarbon oxidation is included in the kinetics scheme of Burgess et al. [7], which allowed the flame speed of R-125/32 mixtures to be estimated in the Phase II report [5]. Figure 23 is a reprint of those results. The flame temperature, velocity, and OH concentration for the stoichiometric R-32/air flame are used to normalize the parameters as the mole fraction of R-125 in the fuel mixture is increased from 0 to 0.14. The overall equivalence ratio is kept at 1.0 based upon the definition in Equation (1) (see p. 28). The temperature drops only slightly as the R-125 fraction is increased. However, the OH decreases dramatically, dropping to about 5 % of the pure R-32

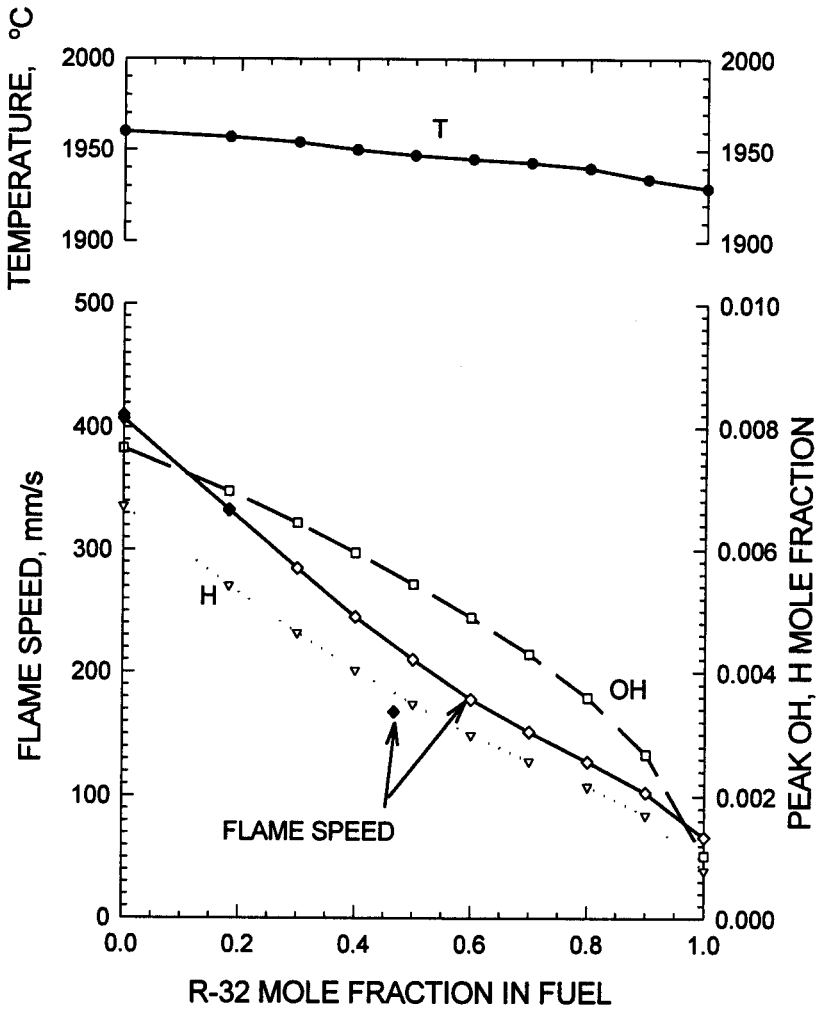

Figure 21. Effect of replacing methane with R-32 on stoichiometric flame speed (open diamonds), equilibrium temperature (circles), and peak mole fractions of H (triangles) and OH (squares). Experimental flame speeds [17]: filled diamonds.

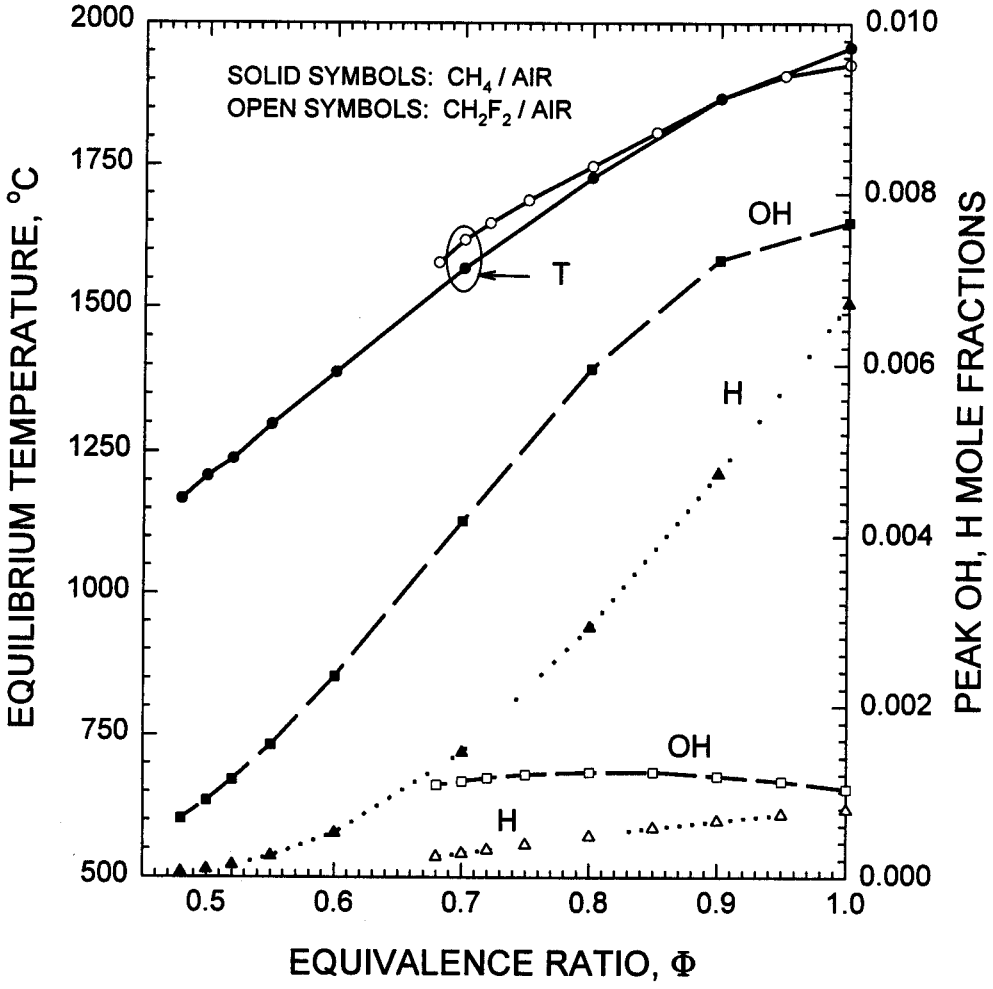

Figure 22. Computed equilibrium temperature and peak OH and H radical mole fractions as a function of equivalence ratio, comparing methane/air to R-32/air flames.

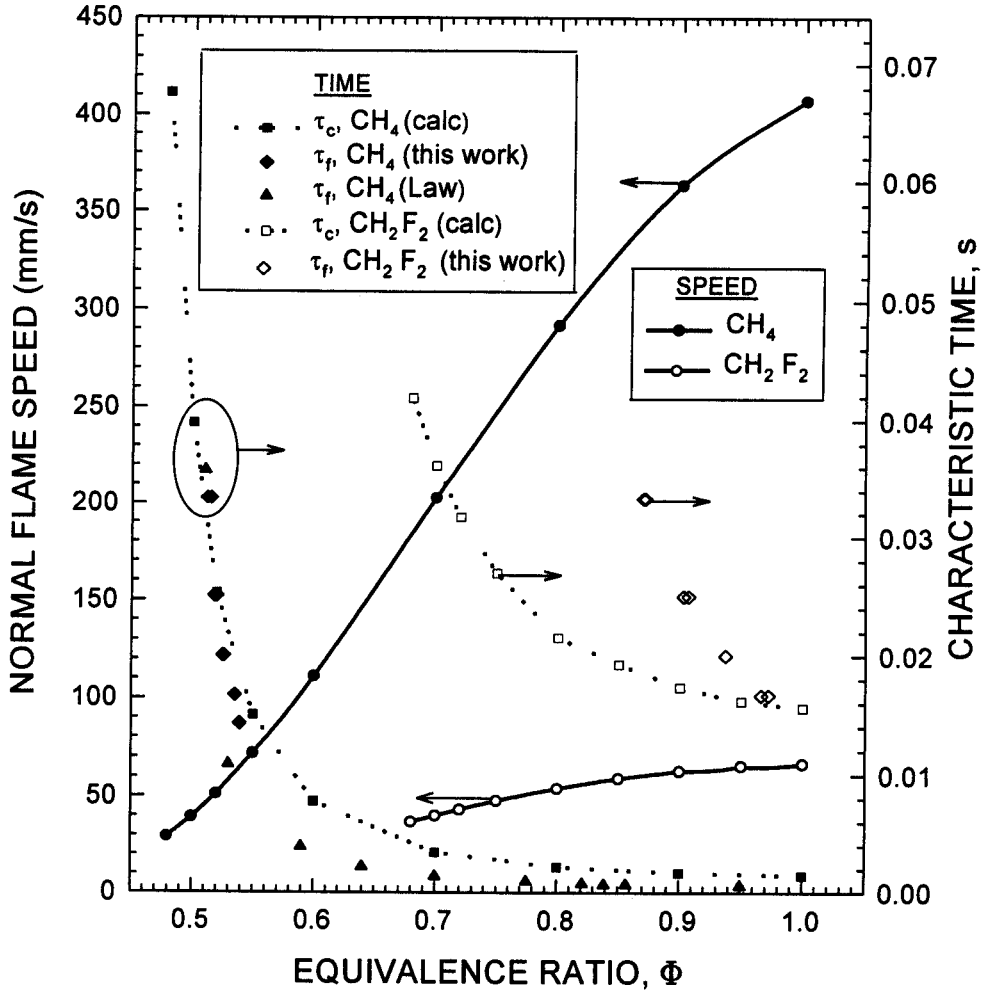

Figure 23. Effect of equivalence ratio on computed flame speed and characteristic time for chemical reaction, compared to estimated residence time in experimental flames at extinction

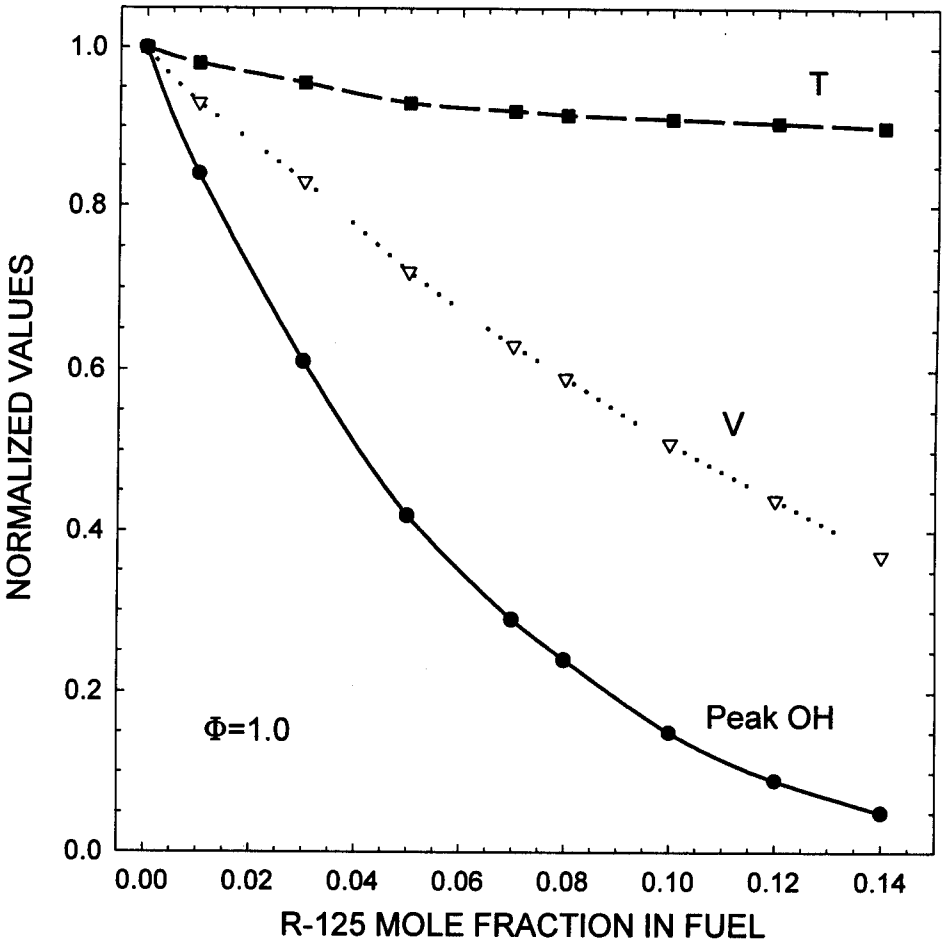

Figure 24. Calculated flame parameters as a function of the amount of R-125 on a stoichiometric R-125/32/dry air flame initially at 25 °C

flame when the R-125 fraction is 0.14. The flame speed at this R-125 level is less than 40% of the pure R-32 flame.

Impact of relative humidity and initial temperature: All of the flame calculations presented so far have taken the air to be dry. Figure 25 demonstrates what happens when moisture is added to the air. The saturation pressure of water at 25 °C is 3.17 kPa. This means that when the air pressure is atmospheric (101 kPa) the mole fraction of water at 100 % relative humidity is 0.031. The actual mole fraction of water used in the calculations is reduced by a factor equal to the mole fraction of air in the dry air plus fuel mixture. The upper graph in Figure 25 is for a stoichiometric 10 % R-125/90 % R-32 flame, and the lower graph is for a lean ($\Phi = 0.70$) R-32/air flame. The final temperature is not much affected by the moisture, but the peak OH mole fraction increases almost four-fold in the R-125/32 flame. Interestingly, the normalized flame speed is enhanced with added moisture in the R-125/32 flame, while it is reduced in the R-32/air flame. This seeming inconsistency can be explained by comparing the H-atom to F-atom ratio in the two flames. The pure R-32/air flame has an H/F ratio of 1:1 independent of the stoichiometry. This means that there is no excess of fluorine atoms to tie up the H-atoms critical to the flame propagation. When R-125 is added to the fuel, the H/F ratio drops below 1:1 (0.826 for the 10% R-125 flame). Hence, the water brings the OH and H levels above the threshold vital to maintaining the combustion reaction.

The final parameter investigated was the initial temperature. Figure 26 (reprinted from the Phase II report [5]) shows how the velocity, OH level and final temperature are impacted as the initial mixture temperature is increased. The system is a stoichiometric 10% R-125/90% R-32/dry air flame, with the values at 25 °C used to normalize the parameters. An initial temperature of 65 °C has an imperceptible effect on the final normalized temperature and a small positive effect on the OH mole fraction. The velocity of the flame increases by about 25 % . By comparing the impact of the temperature change to the impact of changing the mole fraction of R-125, one can estimate that an increase in initial mixture temperature of 10 °C would produce an absolute increase in the CFR of approximately 0.5 % for this particular flame system.

The Importance of Flame Speed and Damköhler Number as Measures of Flammability

The counter-flow burner experimental results cannot be predicted directly from the PREMIX/CHEMKIN calculations since flame stretch, heat loss and buoyancy have been excluded. Because these natural quenching processes are absent, the numerical code predicts a non-zero flame propagation rate for mixtures leaner than the experimental flammability limit. Westbrook [20] suggested that mixtures with one-dimensional, adiabatic flame speeds predicted to be less than 50 mm/s are beyond the flammability limit from a practical standpoint. Bui-Pham et al. [21] considered a similar criterion for identifying the rich flammability limit of a methanol/CO/air mixture, and found it to correspond to the condition where the rate of the primary chain branching reaction ($H + O_2 \rightarrow OH + O$) is equal to the rate of the primary chain terminating reaction ($H + HO_2 \rightarrow H_2 + O_2$), a suggestion originally put forth by Law and Egolfopoulos [22]. Using 50 mm/s as a qualitative measure of the flammability boundary, then, the current numerical study predicts (see Figure 23) a practical lean flammability limit of 0.53 for CH_4/air and 0.77 for R-32/air. These values for LFL are not far from some of those measured in various experimental studies, as summarized in Tables 5 and 6.

Chung et al. [23] demonstrated that extinction is likely when τ_f, the fluid mechanical residence time in the flame, is less than the characteristic chemical reaction time, τ_c. The Damköhler number is the ratio of these two values, $\mathbf{D} \equiv \tau_f / \tau_c$, so that a value less then one suggests that extinction is likely. A characteristic fluid residence time can be estimated from the conditions in the experimental burner

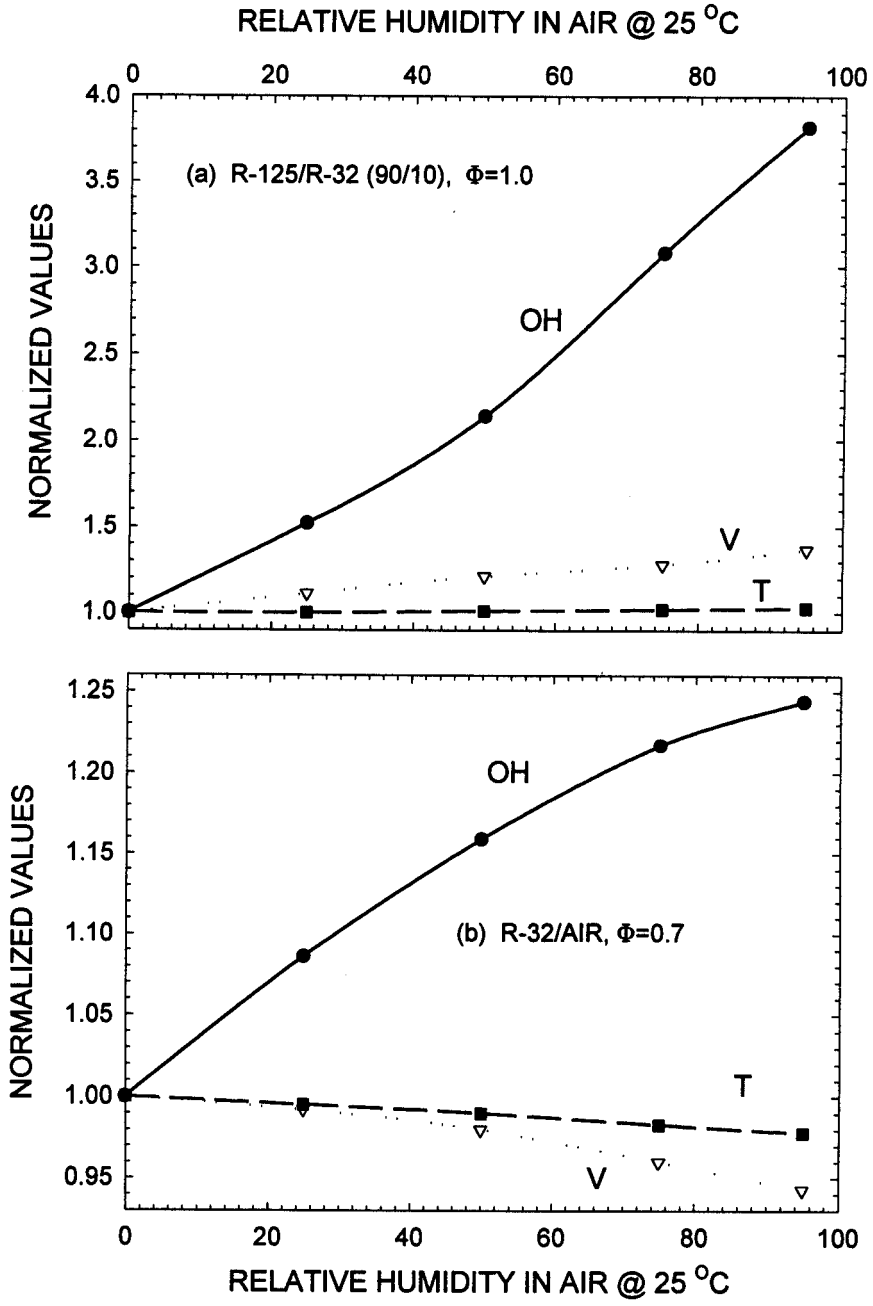

Figure 25. Effect of relative humidity on (a) 10 % R-125/90 % R-32/air flame (Φ=1), and (b) R-32/air flame (Φ=0.7)

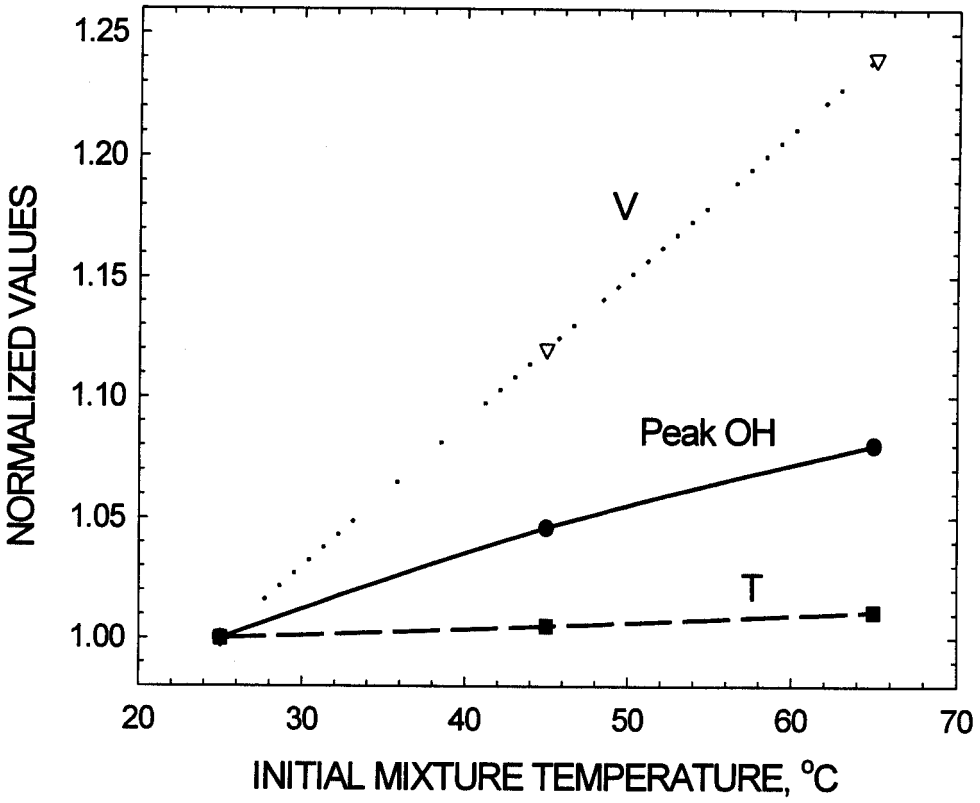

Figure 26. Effect of initial temperature on 10 % R-125/90 % R-32/dry air flame ($\Phi = 1$)

Table 5. Lean flammability limits of CH_4/air (≈ 25 °C) using different experimental methods

Author(s)	Method	Conditions	CH_4/air Lean Limit, Φ_0
Richard and Shankland [13]	ASTM E 681	5 liter, match	0.51
Zabetakis [26]	propagating flame tube	extinction	0.50
this work	counterflow, twin flame	linear extrapolation	0.49 ± 0.01
Richard and Shankland [13]	ASTM E 681	5 liter, match	0.48
Ishizuka and Law [27]	counterflow, twin flame	linear extrapolation	0.48
Yamaoka and Tsuji [28]	Tsuji burner	flame location	0.47
Maruta et al. [24]	counterflow, twin flame, μg	turning point	0.47
Sorenson et al [29]	coaxial (tent) flame	flame angle	0.40

Table 6. Lean flammability limits of R-32/air (≈ 25 °C) using different experimental methods

Author(s)	Method	Conditions	CH_2F_2/air Lean Limit, Φ_0
Dekleva et al. [12]	5 cm tube (ICI)	hot wire	1.11
Richard and Shankland [13]	4 liter tube	match	0.84
Dekleva et al. [12]	ASTM E 681, 5 liter	hot wire	0.81
Grob, D. [30]	ASTM E 681, 12 liter	hot wire	0.81
Richard and Shankland [13]	ASTM E 681, 5 liter	hot wire	0.79
this work	counterflow, twin flame	linear extrapolation	0.78 ± 0.04
Dekleva et al. [12]	ASTM E 681, 5 liter	hot wire	0.77
Dekleva et al. [12]	ASTM E 681, 12 liter	match	0.77
Dekleva et al. [12]	Autoclave, 8 liter	hot wire	0.75
Richard and Shankland [13]	ASTM E 681, 5 liter	spark	0.74
Ohnishi, H. [31]	ASTM E 681, 5 liter	paper match	0.71
Richard and Shankland [13]	ASTM E 681, 5 liter	match	0.69

and compared to the characteristic time for chemical reaction as estimated from the numerical simulation. The characteristic fluid residence time scales with the distance between the burner outlet and the stagnation plane, divided by the outlet velocity (i.e., the inverse of the global stretch rate, $1/K_g$). The residence time at the extinction limit as measured in the current study is plotted in Figure 23. The open diamond symbols correspond to the R-32/air flame and the filled diamonds refer to the methane/air flame. Also plotted in Figure 23 (solid triangles) is the inverse of the stretch rate near extinction which was determined by Law et al. in their counter-flow, premixed methane/air burner, using the slope of the local velocity on the center line in the preheat zone [3]. The two methane flame data sets are in reasonable agreement, suggesting that the *global* stretch rate at extinction may reasonably approximate the *local* stretch rate at extinction for the lean conditions examined in the current study, a conclusion also reached by Maruta et al. [24] based upon the work of Kobayshi and Kitano [25].

The dotted lines shown in Figure 23 are drawn through the characteristic reaction times, τ_c, determined from the PREMIX/CHEMKIN results (symbolized by the open and filled squares for R-32 and methane flames, respectively). The reaction time is approximated by the transit time between the location of the flame anchoring temperature, 127 °C (as suggested in [17]), and the position of the peak H mole fraction. The peak in H was selected as a marker for reaction time because of the importance of H-atom to flame propagation, and because the peak was found at a location close to the maximum levels of OH, a radical critical to the burn-out of CO.

By comparing the numerically calculated τ_c, to the experimentally determined τ_f, one can see that extinction in the actual stretched methane/air flame is predicted reasonably well by the PREMIX model when the two characteristic times are about equal to each other; i.e., $\mathbf{D} \approx 1$. The same cannot be said of the R-32/air flame. The numerical calculations suggest that, for all equivalence ratios leaner than 0.9, the flame should be more robust than the experimental data indicate. This discrepancy may be explained three possible ways.

A first possibility is that the radiative and conductive heat losses, which are not included in model, are more significant (and therefore more detrimental) to the refrigerant flame than to the hydrocarbon flame. While radiation heat loss has been included by others in PREMIX models of hydrocarbon flames [32], an estimate of the relative importance of the radiation in the two flames studied here can be made by following the approach of Hertzberg [33]. As discussed in the phase II report [5], the heat loss due to radiation leads to a limiting flame speed of $\sigma k_p l_r T_f^3 / c_p \rho$, where σ is the Stefan Boltzmann constant, k_p is the gray gas absorption coefficient, l_r is the radiation length scale, T_f is the flame temperature in Kelvin, c_p is the specific heat of the flame, and ρ is the gas density. This limiting flame speed can be compared for each of the fuels at $K_g = 40\ s^{-1}$, corresponding to an extinction equivalence ratio of 0.90 for the R-32/air flame, and $\Phi = 0.52$ for methane. At these conditions, the calculated flame thickness is approximately the same, but the flame temperature varies significantly: 2140 K for R-32/air and 1510 K for methane/air. While there is some difference in k_p between the two fuels, it about cancels with the change in density due to temperature. As a result, the radiation flame speeds scale with T_f^3, whence the effect of radiant heat loss is almost three times greater in the refrigerant flame than in the methane flame. The higher temperature in the R-32/air flame also leads to greater heat loss to the cooled burner due to conduction, which scales with $\lambda \Delta T / l_c$ and can be significant due to the low gas velocities. The conduction length scale l_c is the same in each flame, but the product of the thermal conductivity, λ, and the temperature difference between the flame and the burner, ΔT, is just nearly twice as high in the refrigerant flame. The impact of heat loss on extinction prediction is, thus, more significant in the R-32 /air flame, and adiabatic calculations of flame speed near the lean limit are more likely to over predict flame speeds when R-32 is the fuel.

A second explanation is that the inverse of the global stretch rate is a not a good indicator of

the fluid residence time in an R-32/air flame. However, it is not necessary for the absolute value of the global stretch rate to be precise, only that it vary from the true local stretch rate by a multiplicative constant. The validity of this assumption is supported by the agreement between the LFL measured with the counter-flow burner and previously reported values, and by the work done in [25]. Local velocity and temperature measurements through the flame would provide a more appropriate measurement of the fluid residence time, but may not be possible under conditions approaching extinction.

A final consideration is that the chemical kinetics mechanism is incomplete or contains incorrect rate coefficients for the fluorine-containing reactions. Linteris and Truett [19] found the same mechanism adequate to predict the flame speeds in their premixed R-32/methane/air burner, but did not attempt to model the system with a hydrogen/fluorine ratio less than 3:1. Considering the paucity of flame data under high fluorine loads like those modeled here, a large measure of uncertainty remains in the chemical kinetic scheme.

Non-linear Extrapolation to the Zero-Stretch Condition

The basis for assuming that the fundamental LFL can be obtained by a linear extrapolation of the extinction mole fraction to a global zero-stretch condition is the satisfactory agreement between the experimental measurements and a straight-line fit (e.g., Figures 12 and 15). An identical approach was used effectively by Wang et al. [34] for pre-vaporized benzene/air mixtures. Although a strong correlation is undeniable from a statistical analysis over stretch rates between about 30 s^{-1} and 60 s^{-1}, the critical lower stretch conditions necessary to confirm linearity are unattainable in the burner due to the dominance of buoyancy. Recent micro-gravity experiments have shown conclusively that the extinction mole fraction of methane does not vary in a linear fashion as the stretch rate approaches zero [24]. A more detailed analysis of the reactions is necessary to better understand the behavior of the flame at lower stretch rates.

The inverse of the chemical reaction time, τ_c, is a measure of the rate of chemical reaction in the burner. At extinction, the Damköhler number is close to unity; hence, the rate of reaction is of the order of $1/\tau_f$, which is to say K_g at extinction. If an Arhenius expression is assumed for the rate coefficient, and the reaction rate is taken to be first order in fuel and oxygen concentration, then the following empirical expression can be used to model the extinction stretch rate:

$$\text{reaction rate} \propto 1/\tau_c \approx 1/\tau_f \approx K_g = C_1 [\text{fuel}] [O_2] \exp(-C_2/T_f), \qquad (2)$$

where C_1, is a proportionality constant, C_2 is the activation temperature, T_f is the flame temperature, and the brackets indicate concentration in moles per unit volume.

If no heat losses occur, the equilibrium temperature (in Kelvin) of one mole of R-32 in air can be written in terms of the adiabatic, stoichiometric equilibrium temperature, T_{ad}, the initial temperature, T_i, and the equivalence ratio, assuming the excess air acts as a heat sink and the specific heat of the mixture per unit mass is unchanged:

$$T_f = T_i + (T_{ad} - T_i)\,\Phi / [\Phi + 0.726\,(1-\Phi)] \qquad (3)$$

The mole fractions of R-32 and oxygen are equal to $\Phi/(\Phi + 4.76)$ and $1/(\Phi + 4.76)$, respectively. The concentration of the R-32 and oxygen are proportional to their respective mole fractions and the molar density, which decreases with increasing temperature. Thus,

$$[\text{R-32}]\,[O_2] \propto \Phi / (\Phi + 4.76)^2 / T_i^2. \qquad (4)$$

For this flame, T_{ad} at $\Phi = 1.0$ is calculated from reference [6] to be 2211 K. The empirical constants are found by matching the experiment at 30 s^{-1} and 102 s^{-1}. The relation between the extinction stretch rate and the equivalence ratio becomes

$$K_g(\Phi) = 7.17 \times 10^{11} \; [\Phi / (\Phi + 4.76)^2 / T_i^2] \exp(-16\,200/T_f) \;, \; s^{-1}, \qquad (5)$$

with

$$T_f = 373 + 1838\,\Phi / [\Phi + 0.726\,(1-\Phi)], \; K. \qquad (6)$$

The equivalence ratio can be written in terms of the mole fraction of R-32 in the mixture; i.e., $\Phi = 4.76\,X_{R\text{-}32}/(1- X_{R\text{-}32})$. The dash-dot line in Figure 27 is a plot of Equation (5), indicating a far from straight region for stretch rates below 30 s^{-1}. The circles in Figure 26 are a re-plot of the lean portion of the R-32/air experimental data. For comparison, the solid line is the linear fit through the experimental data with stretch rates of 70 s^{-1} and less. The linear extrapolation yields a zero stretch mole fraction of 0.131, while the non-linear extrapolation predicts a zero mole fraction lower limit for R-32 at a zero stretch condition.

Equation (5) may be physically based, but it provides no useful estimate of the practical lower limit because it does not account for the heat loss due to radiation. Theoretical analysis of the flame structure allows one to identify a radiation limit that comes into play at very low stretch rates [35]. The radiation loss, Q_{rad}, in Joules per kilogram of R-32, from a disk shaped flame can be estimated

$$Q_{rad} = 3\tau_f \sigma k_p T_f^4 \,(RT_i/P)\,(2\Phi + 4.76)/(0.052\Phi), \qquad (7)$$

where k_p, is the absorption coefficient , σ is the Stefan-Boltzmann constant and P is the pressure. Equation (7) indicates that the radiation loss increases in an unbounded fashion directly with the flow time; hence, as K_g ($\approx 1/\tau_f$) approaches zero, the chemical reaction will be quenched.

Equation (5) still holds when the system is non-adiabatic, but the flame temperature is reduced by the absolute value of the ratio of Q_{rad} to the enthalpy of combustion of the fuel, or

$$T_{f,\,rad} = T_i + (1 - \left| \; Q_{rad}/\Delta H_c \right|)\,\{(T_{ad,\Phi=1} - T_i)\,\Phi / [\Phi + 0.726\,(1-\Phi)]\}. \qquad (8)$$

The absorption coefficient was estimated in [5] to be about 0.8 m^{-1}, ΔH_c = -9.35 $MJ/kg_{R\text{-}32}$, the initial temperature is 373 K, and P is 101 kPa. The flame temperature accounting for radiative loss is, thus,

$$T_{f,\,rad} = 373 + [1 - 4.46\times10^{-16}\,(T_{f,\,rad}^4/K_g)\,(2\Phi + 4.76)/(0.052\Phi)]\{1838\,\Phi / [\Phi + 0.726\,(1-\Phi)]\}. \qquad (8')$$

The constants in Equation (5) can be recalculated based upon the radiation-corrected temperature, yielding $C_1 = 7.35\times10^{13}$ $K^2 s^{-1}$ and C_2 = 18 300 K. Equations (5) and (8') can be solved iteratively to find the extinction equivalence ratio (or $X_{R\text{-}32}$) as a function of K_g for a flame with radiative heat loss. The dashed line in Figure 27 shows the result. Accounting for radiative heat loss does two things; first, it shifts the extinction mole fraction curve upward, and second, it demonstrates a true lower limit, as indicated by the * in Figure 27. No solutions are mathematically obtainable for $X_{R\text{-}32} < 0.118$. The non-adiabatic, non-linear theory predicts a lower value for LFL than the simple linear extrapolation; however, other affects such as conduction losses, preferential diffusion, and two-dimensional flow act to move the practical LFL upward.

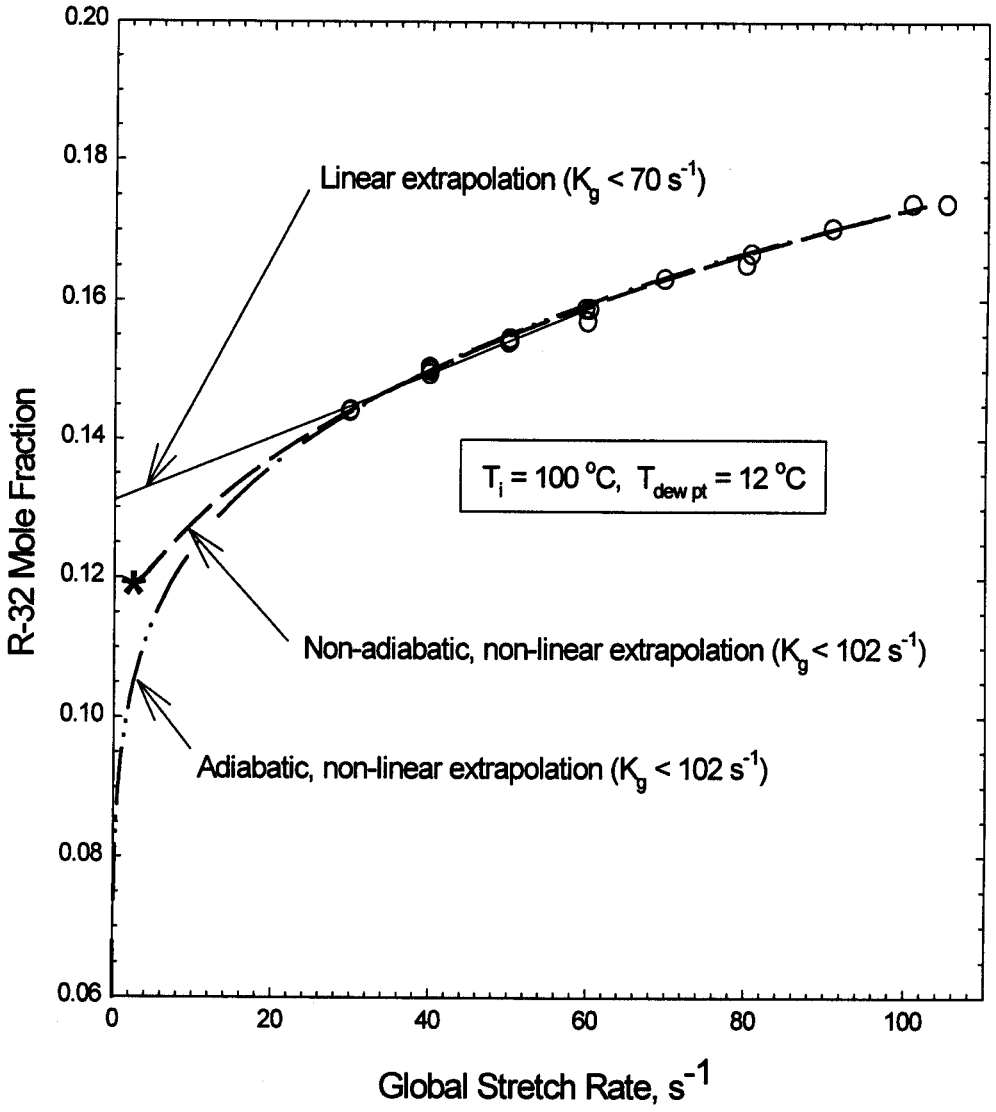

Figure 27. Comparison of non-linear and linear extrapolations to the zero stretch condition for R-32/air mixtures initially at 100 °C

A similar, non-linear analysis can be applied to the Critical Flammability Ratio calculation. For simplicity, we have examined the behavior of an R-32/N_2 mixture first. Assume that the air/R-32 ratio is constant and equal to the most robust condition (Φ=1.18) as an increasing amount of nitrogen is added. The mole fraction of the nitrogen in the R-32 plus N_2 mixture is x. The concentrations of the R-32 and oxygen are diluted by the N_2 such that they can be expressed as

$$[\text{R-32}]\,[O_2] \propto [(1-\chi)/(5.03-4.03\chi)]^2 / T_f^2 \qquad (9)$$

The nitrogen acts as a heat sink to reduce the adiabatic flame temperature according to the relation

$$T_f = T_i + (T_{ad} - T_i)\,[6.19(1-\chi)/(6.19-5.19\chi)]. \qquad (10)$$

The adiabatic temperature increase, (T_{ad} - T_i), is reduced from 1838 K to 1732 K based upon the equilibrium value computed with reference [6] for Φ=1.18 when x=0. The radiative loss can be calculated if it is assumed that the absorption coefficient remains about constant. Then,

$$Q_{rad} = 3\tau_f \sigma k_p T_f^4\,(RT_i/P)\,(6.19-5.16\chi)/[0.052(1-\chi)]; \qquad (11)$$

and, since the N_2 does not affect the enthalpy of combustion,

$$T_{f,\,rad} = 373 +$$

$$\{1- 4.46\text{x}10^{-16}\,(T_{f,\,rad}^4/K_g)\,(6.19-5.19\chi)/[0.052(1-\chi)]\}\{1732[6.19(1-\chi)/(6.19-5.19\chi)]\},\ \text{K}. \qquad (12)$$

Figure 28 is a plot of the extinction stretch rate measured with nitrogen added to the R-32. The open circles are the experimental data, taken with the temperature equal to 100 °C and a relative humidity of 50 % (referenced to 23 °C). The measured extinction values for x drop for stretch rates below 30 s^{-1}, a phenomena also observed with R-125/R-32 mixtures (Figure 16). This is due to buoyant distortions in the flame at low stretch rates. The values for C_1 and C_2 for R-32/N_2 mixtures can be recalculated from the measured extinction stretch rate for x equal zero and for x close to the maximum attainable. The extinction stretch rate becomes

$$K_g(\chi) = 5.32\text{x}10^{14}\{[(1-\chi)/(5.03-4.03\chi)]^2 / T_{f,rad}^2\}\exp(-21\,600/T_{f,rad}),\ s^{-1}. \qquad (13)$$

Equation (13) is plotted as the dashed line in Figure 28. The equation predicts extinction for $x \approx 0.64$ (indicated by the asterisk), which is a little greater than the value of 0.603 obtained by a linear fit (dotted line) of all the experimental data.

An attempt was made to model the inhibiting effect of the R-125 as with nitrogen (i.e., assuming extinction is the result of dilution and heat absorption). The similarity in shape of the x vs. K_g curves for N_2 and R-125 argues for this approach. However, the first-order relation between the fuel (i.e., R-32) and reaction rate did not yield the close-to-straight-line fit observed in the experiments for meaningful values of activation temperature. In an alternative approach the R-125 was treated as a fuel that contributes to the heat release and maintains the overall stoichiometry constant as x is increased. The activation temperature would be expected to be higher due to the much lower reactivity of the R-125 when compared to R-32. However, the simple model used to predict the R-32 LFL and the CFR of nitrogen/R-32 assumes that a single value of C_2 exists over the entire range of x. This is invalid for a chemically acting substance, and may be the reason that the second attempt to fit the

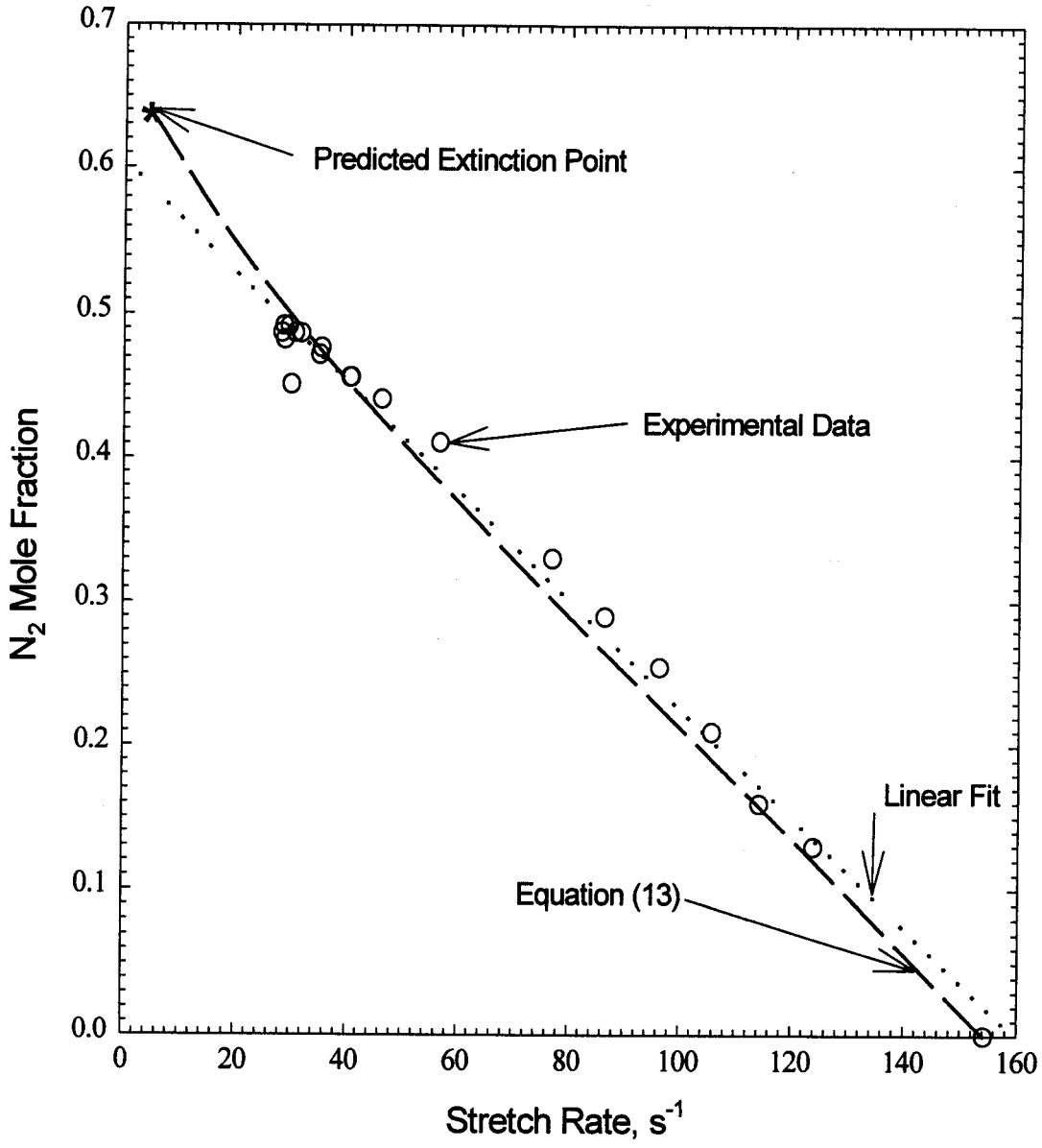

Figure 28. Comparison of non-linear and linear extrapolations to the zero stretch condition for R-32/N_2/air mixtures initially at 100 °C

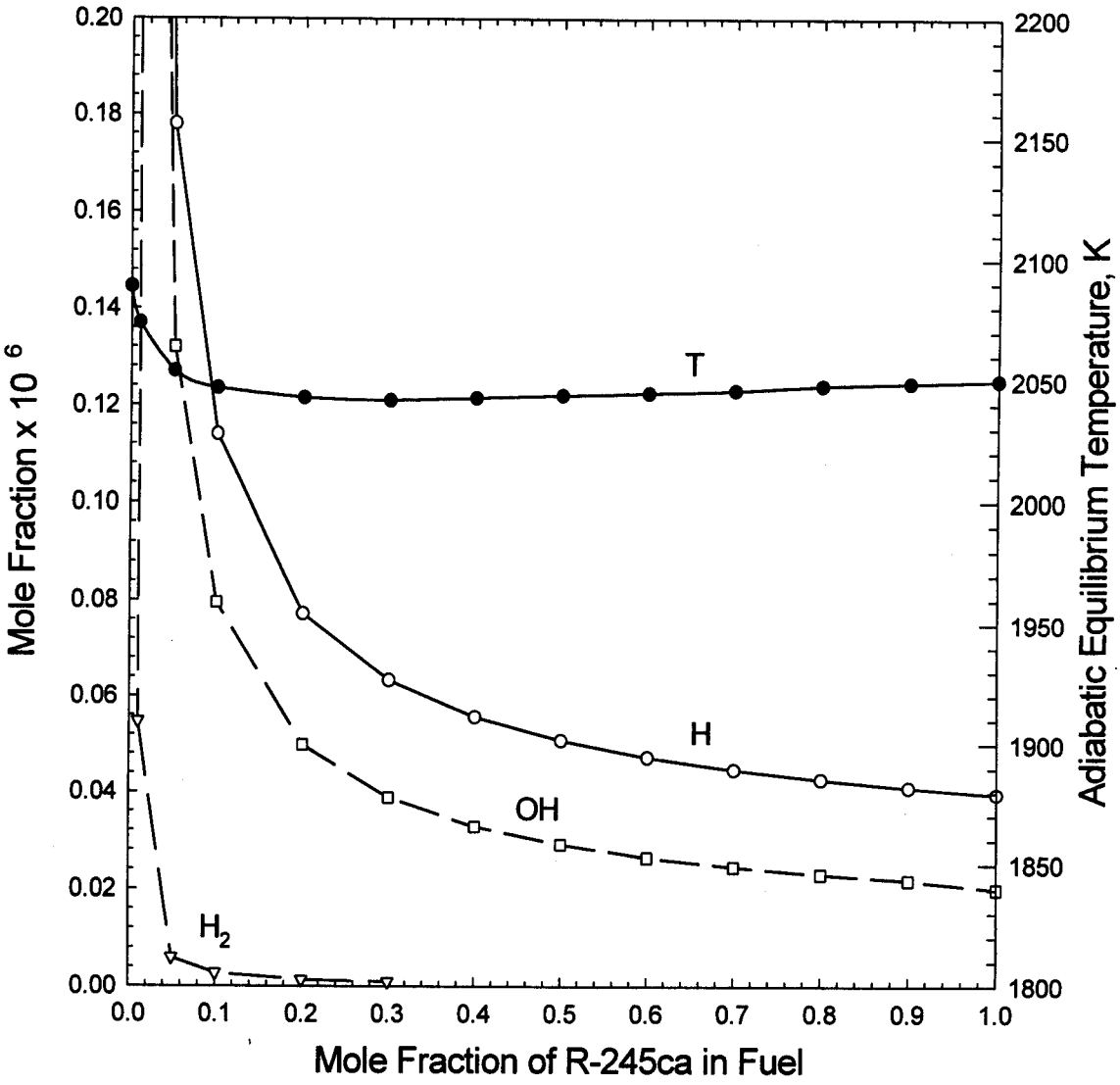

Figure 29. Adiabatic, equilibrium temperature and mole fractions of H, H_2, and OH for R-245ca/R-32 mixtures with dry air initially at 298 K.

experimental data for R-125/32 mixtures to the form of Equation (2) was unsuccessful.

In the case of R-245ca, previous unpublished measurements by others, using the ASTM constant volume apparatus, identified a region of flammability in humid air ignited at 100 °C, but none when the initial temperature was close to the ambient. Temperature sensitive and somewhat ambiguous results were also found in the current research program. No flame could be sustained for pure R-245ca/air mixtures in the counter-flow burner even when the reactants were humidified and preheated to 100 °C. A CFR just under unity was identified for R-245ca/32 mixtures by extrapolating the extinction mole fraction to zero-stretch conditions when the reactants were about 50 °C, while a small but positive extinction stretch rate was identified as being attainable for pure R-245ca/humid air mixtures preheated to 100 °C.

As with the R-125/32 mixtures, an attempt to model the influence of $x_{R\text{-}245}$ on the extinction stretch rate was unsuccessful for R-245ca/32 mixtures because of the complex flame chemistry. In this case, the heavier refrigerant inhibits the flame in low concentrations but also contributes to the flammability when it is the dominant fuel.

The adiabatic equilibrium temperatures and the concentrations of H-atom, H_2 and OH in R-245ca/32 mixtures with an overall equivalence ratio of 1.25 were estimated using reference [6], and are plotted in Figure 29. A small decrease in temperature is noted when small amounts of R-245ca are first added to the mixture, but the equilibrium temperature is almost constant for $x_{R\text{-}245}$ between 0.1 and 1.0. Hence, the inhibiting qualities of the R-245ca are less likely due to heat absorption, and more likely associated with the rapid drop in key intermediate species also observed in Figure 29. Although the concentrations in the flame are not at their equilibrium values, the high diffusivity of atomic and molecular hydrogen tends to smooth out the gradients, so that significant changes in equilibrium values of H and H_2 are reflected in similar changes within the flame. The relevance of these equilibrium calculations is that they bolster our confidence that a linear extrapolation of the extinction stretch rate to mole fractions of R-245ca below those that can be obtained in the counter-flow burner is meaningful.

CONCLUSIONS AND RECOMMENDATIONS

This research has demonstrated that a counter-flow burner is well suited for revealing the structure of refrigerant/air flames. The flame is stable enough to investigate the relationship between equivalence ratio and the stretch rates necessary for extinguishment. A plot of the mole fraction of refrigerant versus the global stretch rate shows the behavior to be close to linear down to velocities where buoyancy begins to distort the flame and heat losses become significant.

Summary of LFL and CFR Measurements

The following values of LFL and CFR, with their uncertainties, are recommended for the refrigerants examined using the premixed, counter-flow research burner (12 mm ± 0.2 mm diameter contoured nozzles, spaced 12 mm ± 0.2 mm apart):

R-32/air LFL (humidity ratio $< 10^{-2}$ $mg_{water}/g_{dry\ air}$, T= 30 °C ± 5 °C, P = 98 kPa ± 2 kPa):

$X_{R32} = 0.14 \pm 0.004$

R-32/air $ETFL_{100}$ (humidity ratio = 8.5 $mg_{water}/g_{dry\ air}$ ± 0.5 $mg_{water}/g_{dry\ air}$, T=100 °C ± 10 °C, P= 98 kPa ± 2 kPa):

$X_{R32} = 0.13 \pm 0.004$

R-125/32 CFR (humidity ratio < 10^{-2} $mg_{water}/g_{dry\ air}$, T= 30 °C ± 5 °C, P = 98 kPa ± 2 kPa):

$\chi_{R125} = 0.18 \pm 0.004$

R-125/32 CFR@100 (humidity ratio < 8.5 $mg_{water}/g_{dry\ air}$ ± 0.5 $mg_{water}/g_{dry\ air}$, T= 100 °C ± 5 °C, P = 98 kPa ± 2 kPa):

$\chi_{R125} = 0.22 \pm 0.004$

R-245ca/air $ETFL_{100}$ (humidity ratio = 8.5 $mg_{water}/g_{dry\ air}$ ± 0.5 $mg_{water}/g_{dry\ air}$, T=100 °C ± 5 °C, P= 98 kPa ± 2 kPa):

$X_{R245} = 1.35 \pm 0.15$

R-245ca/air LFL (humidity ratio = 8.5 $mg_{water}/g_{dry\ air}$ ± 0.5 $mg_{water}/g_{dry\ air}$, T= 50 °C ± 5 °C, P = 98 kPa ± 2 kPa):

Non-flammable

R-245ca/32 CFR (humidity ratio = 8.5 $mg_{water}/g_{dry\ air}$ ± 0.5 $mg_{water}/g_{dry\ air}$, T= 50 °C ± 5 °C, P = 98 kPa ± 2 kPa):

$\chi_{R245} = 0.98 \pm 0.02$

R-245ca/air LFL (humidity ratio < 10^{-2} $mg_{water}/g_{dry\ air}$, T= 100 °C ± 5 °C, P = 98 kPa ± 2 kPa):

Non-flammable

R-245ca/32 CFR (humidity ratio< 10^{-2} $mg_{water}/g_{dry\ air}$, T= 100 °C ± 5 °C, P = 98 kPa ± 2 kPa):

$\chi_{R245} < 0.98$

N_2/R-32 CFR@100 (humidity ratio = 8.5 $mg_{water}/g_{dry\ air}$ ± 0.5 $mg_{water}/g_{dry\ air}$, T= 100 °C ± 5 °C, P = 98 kPa ± 2 kPa):

$\chi_{N2} = 0.61 \pm 0.004$

These results demonstrate that the major objective of the research has been met: to design and operate a counter-flow burner that produces accurate and repeatable flame limits and critical flammability ratios at temperatures up to 100 °C, with flammable and marginally flammable liquid and gaseous refrigerants.

Industrial Burner Design

The measured LFL is sensitive to some geometric variations, the most significant being that smaller diameter burners tend to widen the flammability limits, and larger diameter burners decrease them. The 12 mm diameter burner, however, gives results consistent with LFL measurements of R-32/air, methane/air and propane/air mixtures in fixed volume experiments and flame tubes. It is recommended that the inner diameter of the counter-flow burner be held between 10 mm and 12 mm, and that the spacing be maintained about equal to the diameter, ± 1 mm. The exact character of the nozzle, the nitrogen annulus, and precise alignment of the burner were found to be of lesser importance in determining the zero-stretch mixtures as long as no changes in geometry or operational procedure occur within a single test sequence.

A new burner has been designed based upon the above findings. The objective has been to

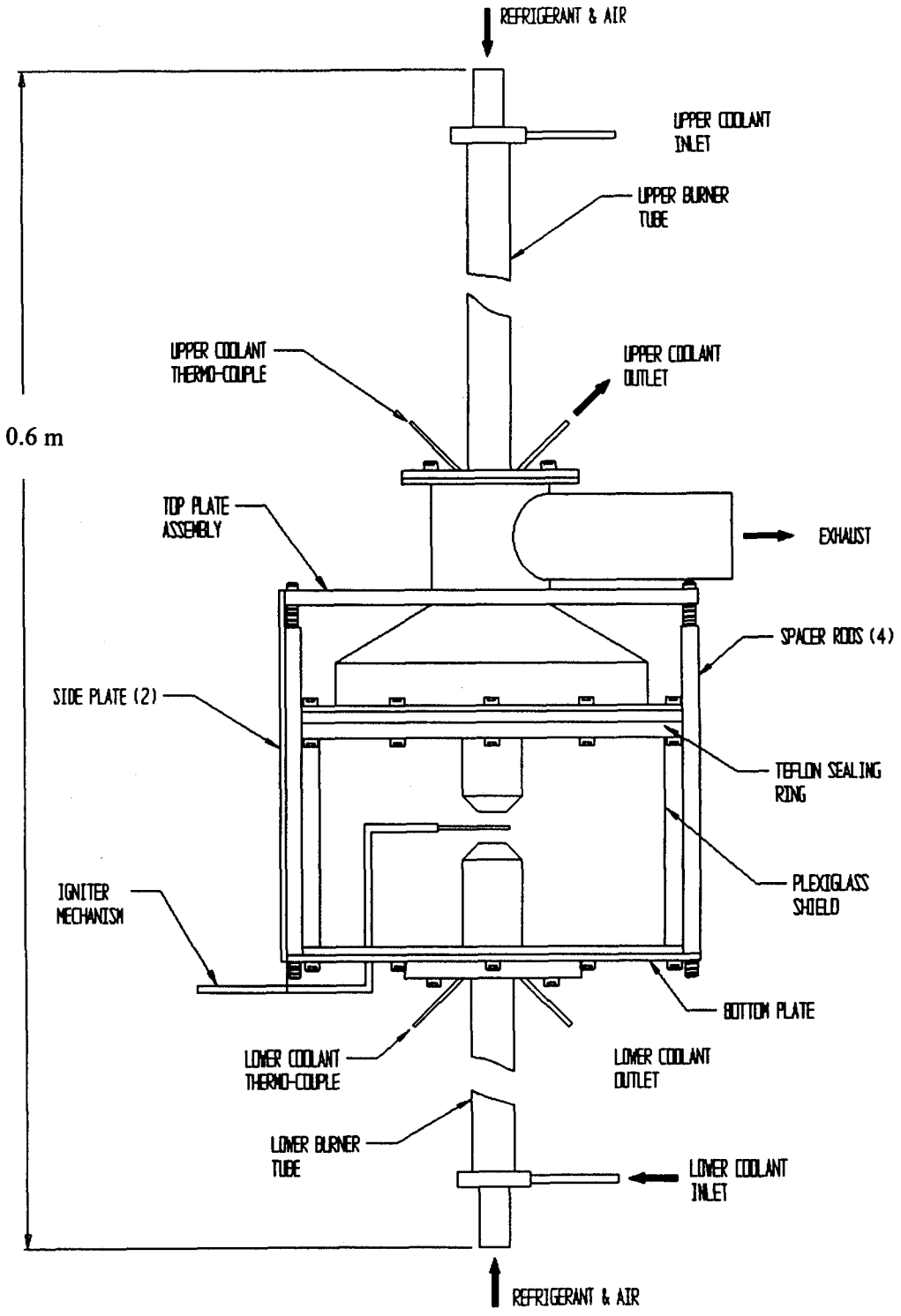

Figure 30. Overall view of industrial-grade counter-flow burner

minimize the investment in facility development and operation to the refrigeration industry, while maintaining a satisfactory level of confidence and reproducibility of the data. Figure 30 shows an overall view of the new burner. The upper and lower burner tubes are similar, and made of three concentric stainless steel tubes of standard diameters (1/2", 3/4" and 1"). The refrigerant and air pass through the inner tube; the 19 mm (3/4") tube directs water to the tip of the burner to maintain close control of the gas temperature and to protect the outer tube from overheating in the hot exhaust stream. Four adjustable spacer rods permit the burner tubes to be aligned conveniently. A 152 mm diameter Plexiglas tube shields the flame and directs the toxic combustion products to the exhaust. To simplify the design, no provision is made for a concentric flow of nitrogen gas at the burner outlets. A heated electrical wire or miniature torch can be rotated onto the centerline to ignite the refrigerant/air mixture. Thermocouples are located in the water at the burner tip to monitor the initial gas temperature.

Appendix E contains detailed drawings of the burner components and a suggested arrangement for metering all the flows. Estimates for fabricating a burner ranged between $2500 and $10,000 for the first unit. It is recommended that several be built and delivered to different laboratories. A round-robin testing program is required to determine if the industrial burner is suitable as designed to produce consistent results. If so, and if the operation is straight-forward, consideration should be given to supplementing or replacing the constant volume ASTM E 681-1994 method with a procedure based upon the counter-flow burner.

Unresolved Issues and Recommendations for Further Research

The counter-flow burner test method circumvents the most troubling issue that is intrinsic to ASTM E 681-1994: Does that which is observed in the ASTM test constitute a self-propagating flame? The answer to the question is tied inextricably to the details of the design of the ASTM test set-up, the operational procedure, the opinion of the observer, and the purpose of the test. The ASTM method combines a fundamental property measurement (which should be unassailable) with an assessment of risk (which inherently involves personal judgment). Because the ignition process and flame propagation are transient and three-dimensional in the ASTM apparatus, meaningful analysis and extrapolation to other environments becomes impossible.

The counter-flow burner method is based upon flame extinction (an unequivocal event) to define the flammability limit. It is designed to measure a fundamental property, divorced from the question of risk. The quasi-steady, one-dimensional nature of the containerless flame makes it amenable to detailed, theoretical analysis, which is essential before risks can be predicted for different possible fire scenarios.

To be most useful to the refrigeration industry, a methodology needs to be developed to assess the risk of a fire from a given working fluid in a particular realistic application. If one knows the laminar flame speed of a refrigerant/air mixture, and how it varies with environmental conditions, then meaningful predictions of the fire risk associated with a given geometry, ignition source, and leak scenario can be made. A number of carefully planned full scale tests with refrigeration machine mock-ups could be performed using a range of class 2 and class 3 refrigerants to bracket the uncertainty of the predictive method.

A comprehensive model of the counter-flow burner is currently lacking. Further research is necessary to produce such a model, which would then permit the laminar flame speed to be determined. The following tasks are recommended:

- extend the chemical kinetics data set to include additional refrigerants of interest, such as ammonia and the three carbon propane analogues;

- perform a parametric study to identify the primary reaction pathways that govern the flame extinction process;
- develop a two-dimensional fluid mechanical model of the counter-flow burner that accounts for heat loss and buoyancy;
- couple the fluid mechanical model to the chemical kinetics mechanism and conduct a laboratory study on the counter-flow burner to demonstrate the model's ability to predict flame extinction over a range of burner diameter, nozzle spacing, and inlet conditions;
- using the predictive model to identify worst case conditions, design a full-scale test to determine the fire hazard posed by a range of class 2 and class 1/2 refrigerant leaks.

Taken together with the round-robin testing on the industrial burner recommended above, the results of this research would allow the air-conditioning and refrigeration industry to move away from an ad hoc and confusing prescriptive test method towards a scientifically sound, performance-based safety

REFERENCES

[1] ANSI/ASHRAE Standard 34-1997, "Designation and Safety Classification of Refrigerants," American Society of Heating, Refrigerating and Air-conditioning Engineers, Inc., Atlanta, GA, 1997.

[2] ASTM E 681-1994, "Standard Test Method for Concentration Limits of Flammability of Chemicals," American Society for Testing and Materials, Philadelphia, PA.

[3] Law, C.K., Zhu, D.L., and Yu, G., *Twenty-first Symposium (International) on Combustion*, The Combustion Institute, 1986, p. 1419.

[4] Womeldorf, C., King, M., and Grosshandler, W., "Lean Flammability Limit as a Fundamental Refrigerant Property," Phase I Interim Technical Report, DOE/CE/23810-58, The Air-conditioning and Refrigeration Technology Institute, ARTI MCLR Project Number DE-FG02-91CE23810, March 31, 1995.

[5] Womeldorf, C., and Grosshandler, W., "Lean Flammability Limit as a Fundamental Refrigerant Property, Phase II," Interim Technical Report, DOE/CE/23810-68, ARTI MCLR Project No. DE-FG02-91CE 23810, April 30, 1996.

[6] Gordon, S., and McBride, B., *Computer Program for Calculation of Complex Chemical Equilibrium Compositions and Application*, NASA Reference Publication 1311, NASA Scientific and Technical Information Program, October 1994.

[7] Burgess, D.R., Jr., Zachariah, M.R., Tsang, W., and Westmoreland, P.R., *Progress in Energy and Combustion Science 21*: 453 (1996).

[8] Morel, T., *Journal of Fluids Engineering*, June 1975, p. 225.

[9] Pitts, W. M., Mulholland, G. W., Breuel, B. D., Johnsson, E. L., Chung, S., Harris, R. H., in *Fire Suppression System Performance of Alternative Agents in Aircraft Engine and Dry Bay Laboratory Simulations* (R.G. Gann, Ed.), NIST SP 890: Vol. II, Gaithersburg, MD, Nov. 1995,p.348.

[10] Greenspan, L., *Journal of Research of the National Bureau of Standards-A. Physics and Chemistry 81A*, No. 1, pp.89-96 (1977).

[11] Luna, R. E., "A Study of Impinging Jets and Their Application to Size Classification of Small Particles," Ph.D. thesis, Department of Aerospace and Mechanical Sciences, Princeton University, Report No. 744, 1965.

[12] Dekleva, T.W., Lindley A.A., Powell, P., *ASHRAE Journal* 35(6):40 (1993).

[13] Richard, R.G., and Shankland, I.R., *ASHRAE Journal* 34(4):20 (1992).

[14] Tanoff, M.A., Smooke, M.D., Osborne, R.J., Brown, T.M., and Pitz, R.W., *Twenty-Sixth Symposium (International) on Combustion*, The Combustion Institute, 1996, pp. 1121-1128.

[15] Egolfopoulos, FN., Zhu, D.L., and Law, C.K., *Twenty-Third Symposium (International) on Combustion,* The Combustion Institute, 1990, pp. 471-478.

[16] Kee, R.J., Grcar, J.F., Smooke, M.D., and Miller, J.A., *PREMIX: A Fortran Program for Modeling Steady One Dimensional Premixed Flames,* Sandia Report SAND85-8240, 1985.

[17] Kee, R.J., Rupley, F.M., and Miller, J.A., *CHEMKIN-II: A Fortran Chemical Kinetic Package for the Analysis of Gas Phase Chemical Kinetics,* Report number SAND89-8009, Sandia National Laboratories, Livermore, CA, 1989.

[18] Frenklach, M., Wang, H., Goldenberg, M., Smith, G.P., Golden, D.M., Bowman, C.T., Hanson, R.K., Gardiner, W.C., and Lissianski, V., "GRI-Mech -- An Optimized Detailed Chemical Reaction Mechanism for Methane Combustion," Gas Research Institute Topical Report No. GRI-95/0058, November 1, 1995.

[19] Linteris, G.T., and Truett, L., *Combustion and Flame 105*:15 (1996).

[20] Westbrook, C.K., *Nineteenth Symposium (International) on Combustion,* The Combustion Institute, 1982, p. 127.

[21] Bui-Pham, M.N., Lutz, A.E., Miller, J.A., Desjardin, M., O'Shaugnessey, D.M., and Zondlak, R.J., *Combust. Science and Technology 109*: 71-91 (1995).

[22] Law, C.K. and Egolfopoulos, FN., *Twenty-Third Symposium (International) on Combustion,* The Combustion Institute, 1990, p. 413.

[23] Chung, S.H., Chung, D.H., Fu, C., and Cho, P., *Combustion and Flame 106*:515 (1996).

[24] Maruta, K., Yoshida, M., Ju, Y., and Niioka, T., *Twenty-Sixth Symposium (International) on Combustion,* The Combustion Institute, 1996, pp. 1283-1289.

[25] Kobayashi, H., and Kitano, M., *Combust. Science and Technology 75*:227 (1991).

[26] Zabetakis, M.G. *Flammability Characteristics of Combustible Gases and Vapors*; Bulletin 627, Bureau of Mines, National Technical Information Service, Springfield, VA, 1965.

[27] Ishizuka, S. and Law, C.K., "An Experimental Study on Extinction and Stability of Stretched Premixed Flames," *Nineteenth Symposium (International) on Combustion: The Combustion Institute*, p. 327, 1982.

[28] Yamaoka, I. and Tsuji, H. "An Experimental Study of Flammability Limits Using Counterflow Flames," *Seventeenth Symposium (International) on Combustion: The Combustion Institute,* p. 843, 1979.

[29] Sorenson, S.C., Savage, L.D., Strelow, R. A., *Combustion and Flame 24*: 347 (1975).

[30] Grob, D. "Flammability Characteristics of R-32 and R-32 Mixtures," *Proceedings of the*

Symposium to Evaluate R-32 and R-32 Mixtures in Refrigeration Applications, Environmental Protection Agency, Washington, D.C., March 19-20, 1991.

[31] Ohnishi, H. "Relationship Between Flammability and Composition Ratio of HFC-32/HFC-134a Blend," *Proceedings of the ASHRAE/NIST Refrigerants Conference: R-22/R-502 Alternatives*, Gaithersburg, MD, August 19-20, 1993.

[32] Law, C.K., and Egolfopoulos, FN., *Twenty-Fourth Symposium (International) on Combustion*, The Combustion Institute, 1992, p. 137.

[33] Hertzberg, Martin, "The Theory of Flammability Limits: Radiative Losses and Selective Diffusional Demixing," Bureau of Mines Report of Investigation, RI-8607, 1982.

[34] Wang, C-H., Ueng, G-J., and Tsay, M-S., *Combustion and Flame 113*, 242-248 (1998).

[35] Ju, Y., Guo, H., Maruta, K., and Niioka, T., *Combustion and Flame 113,* 603-614 (1998).

[36] Huber, M., Gallagher, J., McLinden, M., and Morrison, G., "NIST Thermodynamic Properties of Refrigerant Mixtures, Version 5.02," 141ST Standard Reference Database 23, 1996.

[37] Smith, N.D., Ratanaphruks, M.W., and Ng, A.S., *ASHRAE Journal,* 19-23, February 1993.

APPENDIX A: Step-by-step Operation

Special Safety Precautions:

Make sure acid resistant gloves are worn when lighting the burner, handling the scrubber collection vats, and at all times when reaching inside the chemical hood.

If gas flows have been left running for more than a few minutes when the flames were not lit, or if there is any reason to believe an excess of fuel may have built up inside the burner tube, DO NOT attempt to ignite the burner. Instead, shut off gas flows and turn on the blower for a few minutes before proceeding.

Operation Procedure for R-32, R-125/32, and R-245ca/32 Mixtures:

(Skip steps 1-3 if not testing R-245ca)

1. Set up the liquid delivery system. Place the syringes into position on the pump, inside the cooling coils, and attach a thermocouple to the end of each syringe. Connect the heated delivery lines to the burner inlets on the top and bottom of the burner. Turn on the recirculating cooling bath and set the temperature to approximately 0 °C. Turn on the variacs controlling the heating tape for the boilers and the heated delivery lines. Set the temperature of the boiler at least 30 °C above the boiling point of the liquid. Set the delivery lines to at least 20 °C above the boiling point of the liquid.

2. Monitor the temperature of the syringes. When the temperature is sufficiently low enough to maintain the liquid status of the fuel, the syringes may be filled. For R-245ca, the syringes were kept below 8.5 °C to maintain a constant density. To fill the syringes, first switch the valves to the fill position. Next, push the plungers all the way forward to expel any air in the syringes. Then invert the bottle of liquid fuel and attach its outlet to one of the syringe filling tubes. Open the valve on the bottle, allowing the liquid to flow into the syringe. The plunger will slowly be pushed back by the liquid. When the syringe has been filled to the desired amount, close the valve on the bottle. Then turn the syringe valves to the off position. Disconnect the bottle and repeat procedure for the other syringe.

3. Turn on computer and open flow controller program, LIQUID.VI.

(Skip step 4 if testing R-245ca)

4. Turn on computer and open flow controller program, TWINFLAM.

5. Turn on main water valve and set water flow rate to about 150 ml/min through the heat exchanger. Next, turn on the variacs that control the burner heating tape and the heat exchanger. Set the heat exchanger variac to an initial power setting of 85, and the heat tape variac to an initial power setting of 65. This will sufficiently pre-heat the burner for a 100 °C testing condition.

6. Check the gas lines running to and from the bubblers, to make sure bubblers are connected. Check that the bubbler bath is cooled to 13 °C for 50% relative humidity.

7. Open the manual valves located after the mass flow controllers (MFCs) and open all gas bottles. At the digital control box, set all mass flow controllers to "ON".

8. For each flow controller, set the digital readout at the control box to the initial setting at which it was calibrated (different for each flow controller). With the gases flowing, adjust the gage pressure on each bottle to 140 kPa. This ensures the calibration corrections will be accurate.

9. Turn off the gas flow of the fuel at the digital control box. While the air is still flowing, measure the relative humidity and dew point with the hand-held hygrometer. Record these values for later use.

10. Determine a flame ignition condition (equivalence ratio and stretch rate) for the pure gas fuel and air mixture (without R-245ca). This can be acquired using knowledge of the lighting conditions from previous tests with the gas fuel. This allows for easy lighting, then the vaporized liquid is added later.

11. In the flow controller program (TWINFLAM or LIQUID.VI) select a file name under which the data will be recorded, and set the test number. In the fuel selection box, choose the liquid fuel and gas fuel to be used. Type in the measured humidity, and nitrogen co-flow desired. Also type in the initial strain rate and equivalence ratio settings for the lighting conditions. Set the gas fuel amount to 100% for the initial lighting phase, and set the flow controller buttons to "ON". Once all selections have been made, start the gas flows by clicking on the "Go" arrow in the upper left corner of the screen.

12. Using the continuous flame igniter, light the twin flames. Be sure to wear safety gloves during this step, and whenever reaching inside the hood since HF acid may be present. When the flames are lit, turn on the blower and the water flow for the scrubber. Set the water pressure to 69 kPa. Make sure the scrubber collection container is in place.

13. The flow program calculates the correct setting for the nitrogen co-flow rotameters. Turn on the nitrogen bottle and set rotameters as indicated by the program. This must be done after flames are lit. Flames will not ignite with nitrogen present.

(Skip steps 14-16 if not testing R-245ca)

14. Once flames have stabilized, the vaporized liquid fuel may be added. Set the pump to the desired flow rate, and enter that liquid flow rate into the controller program. Turn the syringe valves to the burner delivery position and start the pump. Click on the "Read Data" button on the screen, then click on the "Go" arrow. The program will calculate the vapor flow rate, volume percent of the fuel mixture, effective equivalence ratio and the resulting strain rate.

15. Occasionally, the addition of the liquid fuel will cause either the stretch rate or effective equivalence ratio to become too high, resulting in a mixture that is beyond its upper flammability range. If this happens, repeat steps 10 through 14 using different settings for the lighting condition and/or the liquid flow rate until a flame can be sustained.

16. The flame is now a mixture of both the gas fuel and the vaporized liquid fuel. The percent of gas fuel is then slowly reduced in an attempt to burn the vaporized liquid fuel by itself. The composition of fuel mixture, and either the strain rate or equivalence ratio may be controlled. The other parameter will vary accordingly. Start with the condition resulting from the addition of the liquid vapor. Click the "Read Data" button to record the initial flows. Select whether to control the stretch rate or the

equivalence ratio by flipping the switch to point towards one or the other. Then reduce the amount of gas fuel by setting the percent gas fuel to slightly below the current amount. For best results, make very small changes to the flame settings, since large changes to the gas composition may cause the flame to become unstable and extinguish prematurely. Typically, the gas fuel is reduced in steps of 1% of the total fuel flow, or less. Once the new settings have been selected, activate the gas flows by clicking on the "Go" arrow in the upper left corner. Either the stretch rate or equivalence ratio (whichever has been chosen to be controlled) is held constant, while the other adjusts to the new fuel composition.

(Skip step 17 if testing R-245ca)
17. After the flame stabilizes at the chosen condition, new settings can then be selected. The gas fuel may continue to be decreased until it is eliminated. Additionally, the stretch rate or equivalence ratio may be changed from its initial condition. First click "Read Data" to record the current conditions. Then, decrease the percent of gas fuel, or make a small change to either the strain rate or the equivalence ratio. Once again, small changes of around 1 s^{-1} for the strain rate, and 0.005 for the equivalence ratio are necessary to prevent instabilities. When the new conditions have been selected, click on the "Go" arrow to adjust to these settings.

18. During testing, it is important to keep watch of the current burner temperature read-outs on the screen and to make adjustment in order to maintain the desired burner temperature. Keep the upper and lower burner temperatures at 100°C ± 5°C by adjusting the flow rate of the cooling/heating water into the burner and, if necessary, the variac power settings.

19. Repeat steps 17 (or 16) and 18, changing the gas composition to approach the extinction limit. If the liquid is flammable by itself, the percent of gas fuel will reduce to 0 % and the LFL tests may then be conducted by reducing the equivalence ratio until extinction occurs. For R-245ca, the gas fuel cannot be completely eliminated, and the maximum R-245ca vapor amount is found for a particular stretch rate and equivalence ratio.

20. When flame has been extinguished, press the "Read Flows" button one more time to record the data at the extinction condition. Then set the flow control button to "Off", and click on the "Go" arrow to stop the gas flows. If testing with R-245ca, shut off the pump and close the valves after the syringes.

21. Let the scrubber continue to operate for at least five minutes after the flows have stopped, in order to clean any combustion gases that may still be present in the piping system. Check the scrubber drainage container. If it is full, or close to being full, replace with an empty container and neutralize the collected liquid.

22. If more R-245ca tests are to be run, check the syringes to see that they contain enough liquid. Then repeat steps 11 through 21. Once all tests are completed, the system may be shut down.

Shut Down Procedures:

1. Turn off valves at gas bottles.

2. Empty any remaining liquid fuel from the syringes.

3. Depressurize the gas lines by setting all MFCs to typical flows and allowing any gas left in the lines to flow out.

4. When lines are empty, shut off valves after the MFCs.

5. Set the MFCs to "off" at the digital control box.

6. Turn off the variacs for the boiler, heat exchanger, heated lines and the burner heating tape. DO NOT turn off heat exchanger water flow until all tubing lines have cooled completely.

APPENDIX B. Estimates of Test Time and Material

To complete a set of twelve lean flammability tests at 100 °C and with humid air takes approximately six hours. This includes two hours of flow calibration time, and an additional four hours of testing time. For a substance similar to R-32, about 450 grams of refrigerant are needed to complete the testing. These estimates assume that an approximate ignition condition is known.

Finding the critical flammability ratio takes about seven hours when using a base fuel with known characteristics. This allows for two hours to calibrate the refrigerant flow, and five hours to perform the set of twelve tests. For an inhibitor like R-125, at least 200 grams are necessary to complete the tests. Also, about 400 grams of the base fuel are needed. If the base fuel has not been previously calibrated, another 50 grams of fuel and two hours are needed to perform the fuel flow calibration. These estimates are for one set of tests at a predetermined equivalence ratio.

The liquid tests are more involved and require additional preparation and testing time. Individual tests may take longer than 30 minutes each, and a set of experiments takes about three days to complete, depending on the number of tests needed to map out the curve. At least 600 grams of liquid fuel, and 1000 grams of vapor base fuel are needed for one set of experiments, assuming the calibrations have already been completed. This estimate is based on testing a slightly flammable liquid, such as R-245ca, which needs to be mixed with a more flammable vapor fuel in order to ignite in the opposed-flow burner.

APPENDIX C: Data Acquisition Program

a. Overview of Program

The refrigerant experiments were conducted using TWINFLAM.VI, a virtual instrument created in National Instruments LabVIEW 3.1.1. This program was written specifically for these tests and uses an IEEE Standard 488 GPIB interface to communicate with the mass flow controllers. A sample print-out of the front panel screen is included later in the appendix. Although these tests were conducted using LabVIEW, any programming tool capable of reading inputs and controlling the mass flow controllers (MFCs) could be used. A complete copy of the custom program is available from the authors. The structure of the program is outlined in the following steps:

1. The computer reads the inputs for the types of gases used, and for the desired stretch rate, equivalence ratio, and percent inhibitor, and calculates the respective output flow rates for each gas using the basic equations.

2. The computer reads the inputs for the relative humidity, barometric pressure and the current temperatures in the lab and at each burner outlet. It then computes the settings necessary to obtain the correct gas flow rates for the conditions chosen. It also calculates the settings for the nitrogen rotameters based on their calibration, and displays these so that they may be set manually if a nitrogen co-flow is desired.

3. A digital signal is sent to the MFCs to begin the flows.

4. The computer then monitors the actual flow rates of the gases. The computer queries the settings at the MFCs. It then obtains the current temperatures, humidity, and barometric pressure, and computes the volumetric flow rate of each gas as described in the section "Determination of Flow". This information is reported on the screen.

5. Using the actual flow rates of the gases, current values for the strain rate, equivalence ratio, percent inhibitor, and the velocity at the burner outlet are calculated. This process of reading flow rates and calculating current conditions is repeated every few seconds and the screen is continually updated accordingly.

6. When the "Read Flows" command is activated, the computer stops updating conditions, and records all the current data to the chosen file. The computer then goes into stand-by mode as it waits for the next command. This means that the gases continue to flow at their present settings, but the screen is no longer updated. The computer waits for the user to either indicate new inputs and run the program again, or to shut off gas flows and end the program.

b. Determination of Flow

The mass flow controllers set and measure flow as an absolute amount of mass that passes through the controller in a given amount of time. This mass flow rate measured at the controllers is changed to the volumetric flow rate through the burner by the following series of conversions:

1. The mass flow controller measures the flowing gas in units of mass per unit of time. Internally, the MFC converts this measurement into a volume flow rate for nitrogen (the default gas) at standard temperature and pressure. This number is then transmitted to the computer via a GPIB connection.

2. Next, the computer program changes the nitrogen flow rate into the corresponding flow rate for the actual gas being used. Prior to conducting the experiments, each flow meter is calibrated with its designated gas at standard temperature and pressure, using a bubble flow meter. This calibration determines the linear relationship between the default nitrogen flow rate, and the measured flow of the actual gas, as well as any zero offset in the meter itself. The computer program uses these values to calculate the flow rate of the actual gas at standard temperature and pressure using the equation:

$$Q_{STP} = m \times Q_{N_2} + b$$

   where *m* is about equal to the ratio of the nitrogen specific heat times density to the actual gas specific heat times density, and *b* is the zero offset.

3. The flow rate for the gas must then be corrected from standard temperature and pressure, to the measured pressure in the laboratory and the temperature at the burner outlet. This is done using the ideal gas law.

$$Q = Q_{STP}\left(\frac{T_{actual}}{T_{STP}}\right)\left(\frac{P_{STP}}{P_{actual}}\right)$$

4. Finally, the flow is corrected for humidity effects using the saturation vapor pressure of the water. The saturation vapor pressure is calculated as:

$$P_V = (-16.558) + (2.8535T) - (0.079649T^2) + (0.001286T^3)$$

   where *T* is temperature measured in degrees Kelvin and *Pv* is in torr. The final corrected flow rate is computed by:

$$Q_{corr} = Q\left(\frac{P_{actual}}{P_{actual} - (P_V)(RH)}\right)$$

   where *RH* is the relative humidity and P_{actual} is the measured barometric pressure in torr.

c. Basic Equations

The following equations describe the relationships between the quantities measured in these experiments. The program uses these equations to calculate the initial flow rates to be set *(Q_{R1}, Q_{R2}, and Q_{air})* when the desired equivalence ratio, stretch rate and percent inhibitor are given as inputs. It then applies these equations to calculate the resulting equivalence ratio, stretch rate and percent inhibitor based on the measured, updated flow rates.

Equivalence Ratio: $$\Phi = \left(\frac{Q_{R1} + Q_{R2}}{Q_{air}}\right)(K)$$

RI = more flammable refrigerant
R2 = less flammable refrigerant
K = stoichiometric air/fuel ratio

Velocity: $$v = \left(\frac{Q_{air} + Q_{R1} + Q_{R2}}{outlet\ area\ one\ nozzle}\right)$$

Stretch Rate: $$SR = \left(\frac{v}{\left(\frac{nozzle\ separation}{2}\right)}\right)$$

Percent Inhibitor: $$\%\,Inhibitor = \left(\frac{Q_{R2}}{Q_{R1} + Q_{R2}}\right)(100)$$

d. Front Panel

The front panel of the program TWINFLAM.VI is shown on the following page. It is composed of the elements listed below. The front panel is the only program screen used when conducting the flammability tests and contains all the computer controls needed. All inputs, and the resulting calculated outputs appear on this screen, as well.

Manual Inputs:
- File Name
- Fuel Selector (choose gases used during testing)
- Run Number (differentiate between tests in same file)
- Stretch Rate (s^{-1})
- Equivalence Ratio
- Percent Inhibitor (volume percent of fuel)
- Relative Humidity (percent)
- Nitrogen Co-flow

Automatic Inputs:
- Barometric Pressure (torr)
- Upper Burner Temperature (°C)
- Lower Burner Temperature (°C)
- Room Temperature (°C)

Controls:
- Go (runs program)
- Read Flows (records data to file)
- All MFCs On/Off
- Individual MFCs On/Off

Calculated Outputs:
- Actual Equivalence Ratio
- Actual Stretch Rate
- Percent Inhibitor
- Total Fuel Flow (LPM)
- Total Air Flow (LPM)
- Total Inhibitor Flow (LPM)
- Velocity of Flow (cm/s)
- Temperature Difference (between upper and lower burner outlets)
- Nitrogen Rotameter settings
- Nitrogen Flow (LPM)

TWINFLAM.VI
03/27/98 05:47 PM

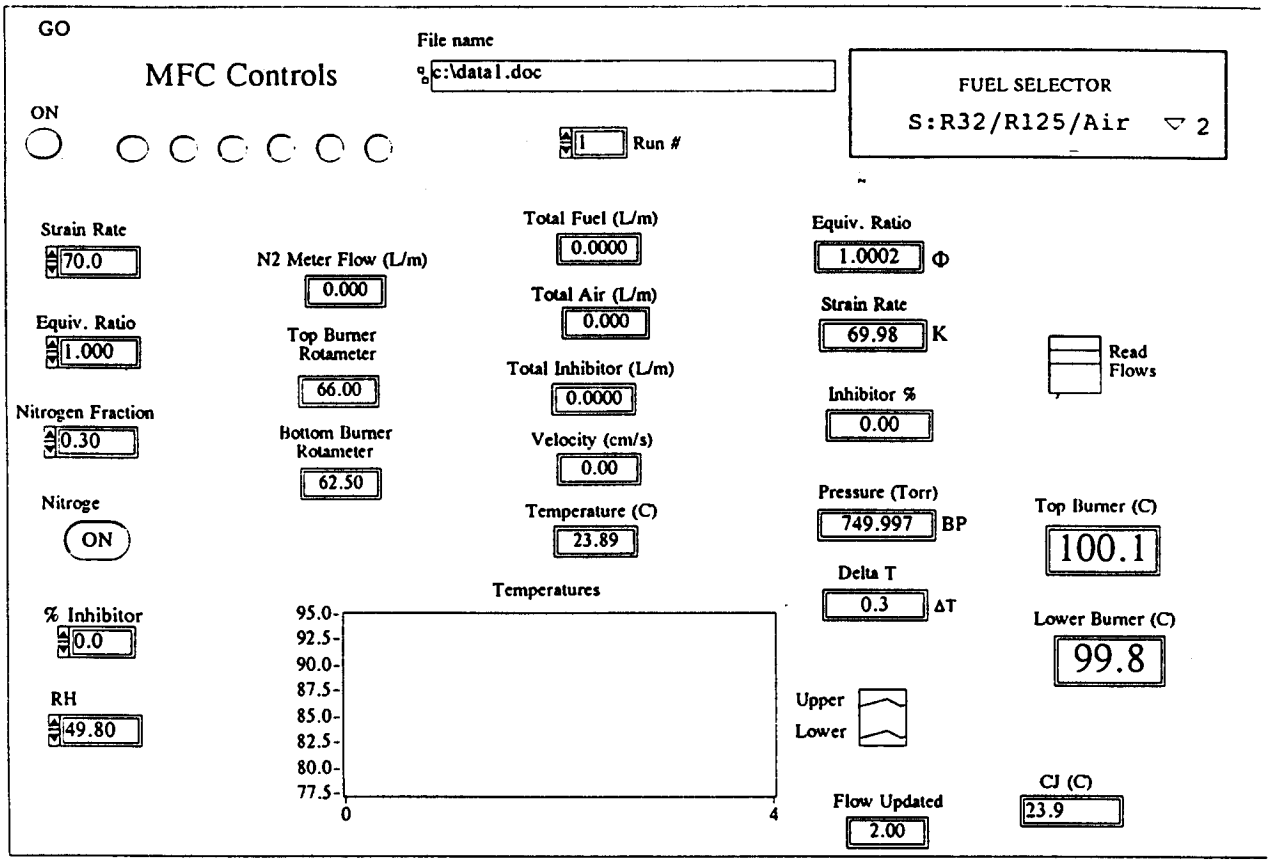

Data Acquisition System Front Panel Display

APPENDIX D. C-H-O-F Chemical Kinetics Mechanism [7, 16, 17, 18]

CHEMKIN INTERPRETER OUTPUT: CHEMKIN-II Version 3.9 Aug. 1994

species	phase	MW	temperature low	temperature high	element count H	O	C	N	F	Ar
1. O2	G	31.99880	200	3500	0	2	0	0	0	0
2. CO2	G	44.00995	200	3500	0	2	1	0	0	0
3. H2O	G	18.01534	200	3500	2	1	0	0	0	0
4. CO	G	28.01055	200	3500	0	1	1	0	0	0
5. CH4	G	16.04303	200	3500	4	0	1	0	0	0
6. CH2F2	G	52.02389	300	3000	2	0	1	0	2	0
7. H2	G	2.01594	200	3500	2	0	0	0	0	0
8. OH	G	17.00737	200	3500	1	1	0	0	0	0
9. H	G	1.00797	200	3500	1	0	0	0	0	0
10. O	G	15.99940	200	3500	0	1	0	0	0	0
11. HF	G	20.00637	300	5000	1	0	0	0	1	0
12. CF2:O	G	66.00735	300	3000	0	1	1	0	2	0
13. CF4	G	88.00475	300	3000	0	0	1	0	4	0
14. CH3	G	15.03506	200	3500	3	0	1	0	0	0
15. CH2	G	14.02709	200	3500	2	0	1	0	0	0
16. CH	G	13.01912	200	3500	1	0	1	0	0	0
17. HO2	G	33.00677	200	3500	1	2	0	0	0	0
18. H2O2	G	34.01474	200	3500	2	2	0	0	0	0
19. CH2(S)	G	14.02709	200	3500	2	0	1	0	0	0
20. C	G	12.01115	200	3500	0	0	1	0	0	0
21. C2H6	G	30.07012	200	3500	6	0	2	0	0	0
22. C2H5	G	29.06215	200	3500	5	0	2	0	0	0
23. C2H4	G	28.05418	200	3500	4	0	2	0	0	0
24. C2H3	G	27.04621	200	3500	3	0	2	0	0	0
25. C2H2	G	26.03824	200	3500	2	0	2	0	0	0
26. C2H	G	25.03027	200	3500	1	0	2	0	0	0
27. CH3OH	G	32.04243	200	3500	4	1	1	0	0	0
28. CH3O	G	31.03446	300	3000	3	1	1	0	0	0
29. CH2OH	G	31.03446	200	3500	3	1	1	0	0	0
30. CH2O	G	30.02649	200	3500	2	1	1	0	0	0
31. HCO	G	29.01852	200	3500	1	1	1	0	0	0
32. CH2CO	G	42.03764	200	3500	2	1	2	0	0	0
33. HCCO	G	41.02967	300	4000	1	1	2	0	0	0
34. HCCOH	G	42.03764	300	5000	2	1	2	0	0	0
35. F	G	18.99840	300	5000	0	0	0	0	1	0
36. CH3F	G	34.03346	300	3000	3	0	1	0	1	0
37. CHF3	G	70.01432	300	3000	1	0	1	0	3	0
38. CH2F	G	33.02549	300	3000	2	0	1	0	1	0
39. CHF2	G	51.01592	300	3000	1	0	1	0	2	0
40. CF3	G	69.00635	300	3000	0	0	1	0	3	0
41. CHF	G	32.01752	300	3000	1	0	1	0	1	0
42. CF2	G	50.00795	300	3000	0	0	1	0	2	0
43. CF	G	31.00955	300	3000	0	0	1	0	1	0
44. CF3O	G	85.00575	300	3000	0	1	1	0	3	0
45. CHF:O	G	48.01692	300	3000	1	1	1	0	1	0
46. CF:O	G	47.00895	300	3000	0	1	1	0	1	0
47. CHFCO	G	60.02807	300	3000	1	1	2	0	1	0
48. CF2CO	G	78.01850	300	3000	0	1	2	0	2	0
49. FCCO-E	G	59.02010	300	3000	0	1	2	0	1	0
50. CH3-CH2F	G	48.06055	300	1500	5	0	2	0	1	0
51. CH3-CHF2	G	66.05098	300	1500	4	0	2	0	2	0
52. CH3-CF3	G	84.04141	300	1500	3	0	2	0	3	0
53. CH2F-CH2F	G	66.05098	300	1500	4	0	2	0	2	0
54. CH2F-CHF2	G	84.04141	300	3000	3	0	2	0	3	0
55. CH2F-CF3	G	102.03184	300	1500	2	0	2	0	4	0
56. CHF2-CHF2	G	102.03184	300	3000	2	0	2	0	4	0
57. CHF2-CF3	G	120.02227	300	1500	1	0	2	0	5	0
58. CF3-CF3	G	138.01270	300	3000	0	0	2	0	6	0
59. CH3-CHF	G	47.05258	300	1500	4	0	2	0	1	0
60. CH3-CF2	G	65.04301	300	1500	3	0	2	0	2	0
61. CH2F-CH2	G	47.05258	300	1500	4	0	2	0	1	0
62. CH2F-CHF	G	65.04301	300	1500	3	0	2	0	2	0
63. CH2F-CF2	G	83.03344	300	1500	2	0	2	0	3	0
64. CHF2-CH2	G	65.04301	300	1500	3	0	2	0	2	0
65. CHF2-CHF	G	83.03344	300	1500	2	0	2	0	3	0
66. CHF2-CF2	G	101.02387	300	1500	1	0	2	0	4	0
67. CF3-CH2	G	83.03344	300	1500	2	0	2	0	3	0
68. CF3-CHF	G	101.02387	300	1500	1	0	2	0	4	0
69. CF3-CF2	G	119.01430	300	1500	0	0	2	0	5	0
70. CH2:CHF	G	46.04461	300	3000	3	0	2	0	1	0
71. CH2:CF2	G	64.03504	300	1500	2	0	2	0	2	0
72. CHF:CHF-Z	G	64.03504	300	3000	2	0	2	0	2	0
73. CHF:CF2	G	82.02547	300	3000	1	0	2	0	3	0
74. CF2:CF2	G	100.01590	300	3000	0	0	2	0	4	0
75. CH2:CF	G	45.03664	300	3000	2	0	2	0	1	0
76. CHF:CH-Z	G	45.03664	300	3000	2	0	2	0	1	0
77. CHF:CF-Z	G	63.02707	300	3000	1	0	2	0	2	0
78. CF2:CH	G	63.02707	300	3000	1	0	2	0	2	0
79. CF2:CF	G	81.01750	300	3000	0	0	2	0	3	0
80. C2HF	G	44.02867	300	3000	1	0	2	0	1	0
81. C2F2	G	62.01910	300	3000	0	0	2	0	2	0
82. N2	G	28.01340	300	5000	0	0	0	2	0	0
83. AR	G	39.94800	300	5000	0	0	0	0	0	1

k = A T**b exp(-E/RT) NOTE: A units mole-cm-sec-K, E units cal/mole

Reactions Considered		A	b	E
1. 2O+M<=>O2+M		1.20E+17	-1.0	0.0
H2	Enhanced by	2.400E+00		
H2O	Enhanced by	1.540E+01		
CH4	Enhanced by	2.000E+00		
CO	Enhanced by	1.750E+00		
CO2	Enhanced by	3.600E+00		
C2H6	Enhanced by	3.000E+00		
AR	Enhanced by	8.300E-01		
2. O+H+M<=>OH+M		5.00E+17	-1.0	0.0
H2	Enhanced by	2.000E+00		
H2O	Enhanced by	6.000E+00		
CH4	Enhanced by	2.000E+00		
CO	Enhanced by	1.500E+00		
CO2	Enhanced by	2.000E+00		
C2H6	Enhanced by	3.000E+00		
AR	Enhanced by	7.000E-01		
3. O+H2<=>H+OH		5.00E+04	2.7	6290.0
4. O+HO2<=>OH+O2		2.00E+13	0.0	0.0
5. O+H2O2<=>OH+HO2		9.63E+06	2.0	4000.0
6. O+CH<=>H+CO		5.70E+13	0.0	0.0
7. O+CH2<=>H+HCO		8.00E+13	0.0	0.0
8. O+CH2(S)<=>H2+CO		1.50E+13	0.0	0.0
9. O+CH2(S)<=>H+HCO		1.50E+13	0.0	0.0
10. O+CH3<=>H+CH2O		8.43E+13	0.0	0.0
11. O+CH4<=>OH+CH3		1.02E+09	1.5	8600.0
12. O+CO+M<=>CO2+M		6.02E+14	0.0	3000.0
H2	Enhanced by	2.000E+00		
O2	Enhanced by	6.000E+00		
H2O	Enhanced by	6.000E+00		
CH4	Enhanced by	2.000E+00		
CO	Enhanced by	1.500E+00		
CO2	Enhanced by	3.500E+00		
C2H6	Enhanced by	3.000E+00		
AR	Enhanced by	5.000E-01		
13. O+HCO<=>OH+CO		3.00E+13	0.0	0.0
14. O+HCO<=>H+CO2		3.00E+13	0.0	0.0
15. O+CH2O<=>OH+HCO		3.90E+13	0.0	3540.0
16. O+CH2OH<=>OH+CH2O		1.00E+13	0.0	0.0
17. O+CH3O<=>OH+CH2O		1.00E+13	0.0	0.0
18. O+CH3OH<=>OH+CH2OH		3.88E+05	2.5	3100.0
19. O+CH3OH<=>OH+CH3O		1.30E+05	2.5	5000.0
20. O+C2H<=>CH+CO		5.00E+13	0.0	0.0
21. O+C2H2<=>H+HCCO		1.02E+07	2.0	1900.0
22. O+C2H2<=>OH+C2H		4.60E+19	-1.4	28950.0
23. O+C2H2<=>CO+CH2		1.02E+07	2.0	1900.0
24. O+C2H3<=>H+CH2CO		3.00E+13	0.0	0.0
25. O+C2H4<=>CH3+HCO		1.92E+07	1.8	220.0
26. O+C2H5<=>CH3+CH2O		1.32E+14	0.0	0.0
27. O+C2H6<=>OH+C2H5		8.98E+07	1.9	5690.0
28. O+HCCO<=>H+2CO		1.00E+14	0.0	0.0
29. O+CH2CO<=>OH+HCCO		1.00E+13	0.0	8000.0
30. O+CH2CO<=>CH2+CO2		1.75E+12	0.0	1350.0
31. O2+CO<=>O+CO2		2.50E+12	0.0	47800.0
32. O2+CH2O<=>HO2+HCO		1.00E+14	0.0	40000.0
33. H+O2+M<=>HO2+M		2.80E+18	-0.9	0.0
O2	Enhanced by	0.000E+00		
H2O	Enhanced by	0.000E+00		
CO	Enhanced by	7.500E-01		
CO2	Enhanced by	1.500E+00		
C2H6	Enhanced by	1.500E+00		
N2	Enhanced by	0.000E+00		
AR	Enhanced by	0.000E+00		
34. H+2O2<=>HO2+O2		3.00E+20	-1.7	0.0
35. H+O2+H2O<=>HO2+H2O		9.38E+18	-0.8	0.0
36. H+O2+N2<=>HO2+N2		3.75E+20	-1.7	0.0
37. H+O2+AR<=>HO2+AR		7.00E+17	-0.8	0.0
38. H+O2<=>O+OH		8.30E+13	0.0	14413.0
39. 2H+M<=>H2+M		1.00E+18	-1.0	0.0
H2	Enhanced by	0.000E+00		
H2O	Enhanced by	0.000E+00		
CH4	Enhanced by	2.000E+00		
CO2	Enhanced by	0.000E+00		
C2H6	Enhanced by	3.000E+00		
AR	Enhanced by	6.300E-01		
40. 2H+H2<=>2H2		9.00E+16	-0.6	0.0
41. 2H+H2O<=>H2+H2O		6.00E+19	-1.3	0.0
42. 2H+CO2<=>H2+CO2		5.50E+20	-2.0	0.0
43. H+OH+M<=>H2O+M		2.20E+22	-2.0	0.0
H2	Enhanced by	7.300E-01		
H2O	Enhanced by	3.650E+00		
CH4	Enhanced by	2.000E+00		
C2H6	Enhanced by	3.000E+00		
AR	Enhanced by	3.800E-01		
44. H+HO2<=>O+H2O		3.97E+12	0.0	671.0
45. H+HO2<=>O2+H2		2.80E+13	0.0	1068.0
46. H+HO2<=>2OH		1.34E+14	0.0	635.0
47. H+H2O2<=>HO2+H2		1.21E+07	2.0	5200.0
48. H+H2O2<=>OH+H2O		1.00E+13	0.0	3600.0
49. H+CH<=>C+H2		1.10E+14	0.0	0.0
50. H+CH2(+M)<=>CH3(+M)		2.50E+16	-0.8	0.0
Low pressure limit:		0.32000E+28	-0.31400E+01	0.12300E+04
TROE centering:		0.68000E+00	0.78000E+02	0.19950E+04 0.55900E+04
H2	Enhanced by	2.000E+00		
H2O	Enhanced by	6.000E+00		

```
    CH4             Enhanced by   2.000E+00
    CO              Enhanced by   1.500E+00
    CO2             Enhanced by   2.000E+00
    C2H6            Enhanced by   3.000E+00
    AR              Enhanced by   7.000E-01
51. H+CH2(S)<=>CH+H2                 3.00E+13   0.0      0.0
52. H+CH3(+M)<=>CH4(+M)              1.27E+16  -0.6    383.0
  Low pressure limit:  0.24770E+34 -0.47600E+01  0.24400E+04
  TROE centering:      0.78300E+00  0.74000E+02  0.29410E+04  0.69640E+04
    H2              Enhanced by   2.000E+00
    H2O             Enhanced by   6.000E+00
    CH4             Enhanced by   2.000E+00
    CO              Enhanced by   1.500E+00
    CO2             Enhanced by   2.000E+00
    C2H6            Enhanced by   3.000E+00
    AR              Enhanced by   7.000E-01
53. H+CH4<=>CH3+H2                   6.60E+08   1.6    10840.0
54. H+HCO(+M)<=>CH2O(+M)             1.09E+12   0.5     -260.0
  Low pressure limit:  0.13500E+25 -0.25700E+01  0.14250E+04
  TROE centering:      0.78240E+00  0.27100E+03  0.27550E+04  0.65700E+04
    H2              Enhanced by   2.000E+00
    H2O             Enhanced by   6.000E+00
    CH4             Enhanced by   2.000E+00
    CO              Enhanced by   1.500E+00
    CO2             Enhanced by   2.000E+00
    C2H6            Enhanced by   3.000E+00
    AR              Enhanced by   7.000E-01
55. H+HCO<=>H2+CO                    7.34E+13   0.0      0.0
56. H+CH2O(+M)<=>CH2OH(+M)           5.40E+11   0.5   3600.0
  Low pressure limit:  0.12700E+33 -0.48200E+01  0.65300E+04
  TROE centering:      0.71870E+00  0.10300E+03  0.12910E+04  0.41600E+04
    H2              Enhanced by   2.000E+00
    H2O             Enhanced by   6.000E+00
    CH4             Enhanced by   2.000E+00
    CO              Enhanced by   1.500E+00
    CO2             Enhanced by   2.000E+00
    C2H6            Enhanced by   3.000E+00
57. H+CH2O(+M)<=>CH3O(+M)            5.40E+11   0.5   2600.0
  Low pressure limit:  0.22000E+31 -0.48000E+01  0.55600E+04
  TROE centering:      0.75800E+00  0.94000E+02  0.15550E+04  0.42000E+04
    H2              Enhanced by   2.000E+00
    H2O             Enhanced by   6.000E+00
    CH4             Enhanced by   2.000E+00
    CO              Enhanced by   1.500E+00
    CO2             Enhanced by   2.000E+00
    C2H6            Enhanced by   3.000E+00
58. H+CH2O<=>HCO+H2                  2.30E+10   1.1   3275.0
59. H+CH2OH(+M)<=>CH3OH(+M)          1.80E+13   0.0      0.0
  Low pressure limit:  0.30000E+32 -0.48000E+01  0.33000E+04
  TROE centering:      0.76790E+00  0.33800E+03  0.18120E+04  0.50810E+04
    H2              Enhanced by   2.000E+00
    H2O             Enhanced by   6.000E+00
    CH4             Enhanced by   2.000E+00
    CO              Enhanced by   1.500E+00
    CO2             Enhanced by   2.000E+00
    C2H6            Enhanced by   3.000E+00
60. H+CH2OH<=>H2+CH2O                2.00E+13   0.0      0.0
61. H+CH2OH<=>OH+CH3                 1.20E+13   0.0      0.0
62. H+CH2OH<=>CH2(S)+H2O             6.00E+12   0.0      0.0
63. H+CH3O(+M)<=>CH3OH(+M)           5.00E+13   0.0      0.0
  Low pressure limit:  0.86000E+29 -0.40000E+01  0.30250E+04
  TROE centering:      0.89020E+00  0.14400E+03  0.28380E+04  0.45569E+05
    H2              Enhanced by   2.000E+00
    H2O             Enhanced by   6.000E+00
    CH4             Enhanced by   2.000E+00
    CO              Enhanced by   1.500E+00
    CO2             Enhanced by   2.000E+00
    C2H6            Enhanced by   3.000E+00
64. H+CH3O<=>H+CH2OH                 3.40E+06   1.6      0.0
65. H+CH3O<=>H2+CH2O                 2.00E+13   0.0      0.0
66. H+CH3O<=>OH+CH3                  3.20E+13   0.0      0.0
67. H+CH3O<=>CH2(S)+H2O              1.60E+13   0.0      0.0
68. H+CH3OH<=>CH2OH+H2               1.70E+07   2.1   4870.0
69. H+CH3OH<=>CH3O+H2                4.20E+06   2.1   4870.0
70. H+C2H(+M)<=>C2H2(+M)             1.00E+17  -1.0      0.0
  Low pressure limit:  0.37500E+34 -0.48000E+01  0.19000E+04
  TROE centering:      0.64640E+00  0.13200E+03  0.13150E+04  0.55660E+04
    H2              Enhanced by   2.000E+00
    H2O             Enhanced by   6.000E+00
    CH4             Enhanced by   2.000E+00
    CO              Enhanced by   1.500E+00
    CO2             Enhanced by   2.000E+00
    C2H6            Enhanced by   3.000E+00
    AR              Enhanced by   7.000E-01
71. H+C2H2(+M)<=>C2H3(+M)            5.60E+12   0.0   2400.0
  Low pressure limit:  0.38000E+41 -0.72700E+01  0.72200E+04
  TROE centering:      0.75070E+00  0.98500E+02  0.13020E+04  0.41670E+04
    H2              Enhanced by   2.000E+00
    H2O             Enhanced by   6.000E+00
    CH4             Enhanced by   2.000E+00
    CO              Enhanced by   1.500E+00
    CO2             Enhanced by   2.000E+00
    C2H6            Enhanced by   3.000E+00
    AR              Enhanced by   7.000E-01
72. H+C2H3(+M)<=>C2H4(+M)            6.08E+12   0.3    280.0
  Low pressure limit:  0.14000E+31 -0.38600E+01  0.33200E+04
  TROE centering:      0.78200E+00  0.20750E+03  0.26630E+04  0.60950E+04
    H2              Enhanced by   2.000E+00
```

```
    H2O          Enhanced by   6.000E+00
    CH4          Enhanced by   2.000E+00
    CO           Enhanced by   1.500E+00
    CO2          Enhanced by   2.000E+00
    C2H6         Enhanced by   3.000E+00
    AR           Enhanced by   7.000E-01
73. H+C2H3<=>H2+C2H2                 3.00E+13   0.0      0.0
74. H+C2H4(+M)<=>C2H5(+M)            1.08E+12   0.5    1820.0
  Low pressure limit:  0.12000E+43 -0.76200E+01  0.69700E+04
  TROE centering:      0.97530E+00  0.21000E+03  0.98400E+03  0.43740E+04
    H2           Enhanced by   2.000E+00
    H2O          Enhanced by   6.000E+00
    CH4          Enhanced by   2.000E+00
    CO           Enhanced by   1.500E+00
    CO2          Enhanced by   2.000E+00
    C2H6         Enhanced by   3.000E+00
    AR           Enhanced by   7.000E-01
75. H+C2H4<=>C2H3+H2                 1.33E+06   2.5    12240.0
76. H+C2H5(+M)<=>C2H6(+M)            5.21E+17  -1.0     1580.0
  Low pressure limit:  0.19900E+42 -0.70800E+01  0.66850E+04
  TROE centering:      0.84220E+00  0.12500E+03  0.22190E+04  0.68820E+04
    H2           Enhanced by   2.000E+00
    H2O          Enhanced by   6.000E+00
    CH4          Enhanced by   2.000E+00
    CO           Enhanced by   1.500E+00
    CO2          Enhanced by   2.000E+00
    C2H6         Enhanced by   3.000E+00
    AR           Enhanced by   7.000E-01
77. H+C2H5<=>H2+C2H4                 2.00E+12   0.0      0.0
78. H+C2H6<=>C2H5+H2                 1.15E+08   1.9    7530.0
79. H+HCCO<=>CH2(S)+CO               1.00E+14   0.0      0.0
80. H+CH2CO<=>HCCO+H2                5.00E+13   0.0    8000.0
81. H+CH2CO<=>CH3+CO                 1.13E+13   0.0    3428.0
82. H+HCCOH<=>H+CH2CO                1.00E+13   0.0      0.0
83. H2+CO(+M)<=>CH2O(+M)             4.30E+07   1.5   79600.0
  Low pressure limit:  0.50700E+28 -0.34200E+01  0.84350E+05
  TROE centering:      0.93200E+00  0.19700E+03  0.15400E+04  0.10300E+05
    H2           Enhanced by   2.000E+00
    H2O          Enhanced by   6.000E+00
    CH4          Enhanced by   2.000E+00
    CO           Enhanced by   1.500E+00
    CO2          Enhanced by   2.000E+00
    C2H6         Enhanced by   3.000E+00
    AR           Enhanced by   7.000E-01
84. OH+H2<=>H+H2O                    2.16E+08   1.5    3430.0
85. 2OH(+M)<=>H2O2(+M)               7.40E+13  -0.4      0.0
  Low pressure limit:  0.23000E+19 -0.90000E+00 -0.17000E+04
  TROE centering:      0.73460E+00  0.94000E+02  0.17560E+04  0.51820E+04
    H2           Enhanced by   2.000E+00
    H2O          Enhanced by   6.000E+00
    CH4          Enhanced by   2.000E+00
    CO           Enhanced by   1.500E+00
    CO2          Enhanced by   2.000E+00
    C2H6         Enhanced by   3.000E+00
    AR           Enhanced by   7.000E-01
86. 2OH<=>O+H2O                      3.57E+04   2.4   -2110.0
87. OH+HO2<=>O2+H2O                  2.90E+13   0.0    -500.0
88. OH+H2O2<=>HO2+H2O                1.75E+12   0.0     320.0
  Declared duplicate reaction...
89. OH+H2O2<=>HO2+H2O                5.80E+14   0.0    9560.0
  Declared duplicate reaction...
90. OH+C<=>H+CO                      5.00E+13   0.0      0.0
91. OH+CH<=>H+HCO                    3.00E+13   0.0      0.0
92. OH+CH2<=>H+CH2O                  2.00E+13   0.0      0.0
93. OH+CH2<=>CH+H2O                  1.13E+07   2.0    3000.0
94. OH+CH2(S)<=>H+CH2O               3.00E+13   0.0      0.0
95. OH+CH3(+M)<=>CH3OH(+M)           6.30E+13   0.0      0.0
  Low pressure limit:  0.27000E+39 -0.63000E+01  0.31000E+04
  TROE centering:      0.21050E+00  0.83500E+02  0.53980E+04  0.83700E+04
    H2           Enhanced by   2.000E+00
    H2O          Enhanced by   6.000E+00
    CH4          Enhanced by   2.000E+00
    CO           Enhanced by   1.500E+00
    CO2          Enhanced by   2.000E+00
    C2H6         Enhanced by   3.000E+00
96. OH+CH3<=>CH2+H2O                 5.60E+07   1.6    5420.0
97. OH+CH3<=>CH2(S)+H2O              2.50E+13   0.0      0.0
98. OH+CH4<=>CH3+H2O                 1.00E+08   1.6    3120.0
99. OH+CO<=>H+CO2                    4.76E+07   1.2      70.0
100. OH+HCO<=>H2O+CO                 5.00E+13   0.0      0.0
101. OH+CH2O<=>HCO+H2O               3.43E+09   1.2    -447.0
102. OH+CH2OH<=>H2O+CH2O             5.00E+12   0.0      0.0
103. OH+CH3O<=>H2O+CH2O              5.00E+12   0.0      0.0
104. OH+CH3OH<=>CH2OH+H2O            1.44E+06   2.0    -840.0
105. OH+CH3OH<=>CH3O+H2O             6.30E+06   2.0    1500.0
106. OH+C2H<=>H+HCCO                 2.00E+13   0.0      0.0
107. OH+C2H2<=>H+CH2CO               2.18E-04   4.5   -1000.0
108. OH+C2H2<=>H+HCCOH               5.04E+05   2.3   13500.0
109. OH+C2H2<=>C2H+H2O               3.37E+07   2.0   14000.0
110. OH+C2H2<=>CH3+CO                4.83E-04   4.0   -2000.0
111. OH+C2H3<=>H2O+C2H2              5.00E+12   0.0      0.0
112. OH+C2H4<=>C2H3+H2O              3.60E+06   2.0    2500.0
113. OH+C2H6<=>C2H5+H2O              3.54E+06   2.1     870.0
114. OH+CH2CO<=>HCCO+H2O             7.50E+12   0.0    2000.0
115. 2HO2<=>O2+H2O2                  1.30E+11   0.0   -1630.0
  Declared duplicate reaction...
116. 2HO2<=>O2+H2O2                  4.20E+14   0.0   12000.0
  Declared duplicate reaction...
```

117. HO2+CH2<=>OH+CH2O 2.00E+13 0.0 0.0
118. HO2+CH3<=>O2+CH4 1.00E+12 0.0 0.0
119. HO2+CH3<=>OH+CH3O 2.00E+13 0.0 0.0
120. HO2+CO<=>OH+CO2 1.50E+14 0.0 23600.0
121. HO2+CH2O<=>HCO+H2O2 1.00E+12 0.0 8000.0
122. C+O2<=>O+CO 5.80E+13 0.0 576.0
123. C+CH2<=>H+C2H 5.00E+13 0.0 0.0
124. C+CH3<=>H+C2H2 5.00E+13 0.0 0.0
125. CH+O2<=>O+HCO 3.30E+13 0.0 0.0
126. CH+H2<=>H+CH2 1.11E+08 1.8 1670.0
127. CH+H2O<=>H+CH2O 1.71E+13 0.0 -755.0
128. CH+CH2<=>H+C2H2 4.00E+13 0.0 0.0
129. CH+CH3<=>H+C2H3 3.00E+13 0.0 0.0
130. CH+CH4<=>H+C2H4 6.00E+13 0.0 0.0
131. CH+CO(+M)<=>HCCO(+M) 5.00E+13 0.0 0.0
Low pressure limit: 0.26900E+29 -0.37400E+01 0.19360E+04
TROE centering: 0.57570E+00 0.23700E+03 0.16520E+04 0.50690E+04
H2 Enhanced by 2.000E+00
H2O Enhanced by 6.000E+00
CH4 Enhanced by 2.000E+00
CO Enhanced by 1.500E+00
CO2 Enhanced by 2.000E+00
C2H6 Enhanced by 3.000E+00
AR Enhanced by 7.000E-01
132. CH+CO2<=>HCO+CO 3.40E+12 0.0 690.0
133. CH+CH2O<=>H+CH2CO 9.46E+13 0.0 -515.0
134. CH+HCCO<=>CO+C2H2 5.00E+13 0.0 0.0
135. CH2+O2<=>OH+HCO 1.32E+13 0.0 1500.0
136. CH2+H2<=>H+CH3 5.00E+05 2.0 7230.0
137. 2CH2<=>H2+C2H2 3.20E+13 0.0 0.0
138. CH2+CH3<=>H+C2H4 4.00E+13 0.0 0.0
139. CH2+CH4<=>2CH3 2.46E+06 2.0 8270.0
140. CH2+CO(+M)<=>CH2CO(+M) 8.10E+11 0.5 4510.0
Low pressure limit: 0.26900E+34 -0.51100E+01 0.70950E+04
TROE centering: 0.59070E+00 0.27500E+03 0.12260E+04 0.51850E+04
H2 Enhanced by 2.000E+00
H2O Enhanced by 6.000E+00
CH4 Enhanced by 2.000E+00
CO Enhanced by 1.500E+00
CO2 Enhanced by 2.000E+00
C2H6 Enhanced by 3.000E+00
AR Enhanced by 7.000E-01
141. CH2+HCCO<=>C2H3+CO 3.00E+13 0.0 0.0
142. CH2(S)+N2<=>CH2+N2 1.50E+13 0.0 600.0
143. CH2(S)+AR<=>CH2+AR 9.00E+12 0.0 600.0
144. CH2(S)+O2<=>H+OH+CO 2.80E+13 0.0 0.0
145. CH2(S)+O2<=>CO+H2O 1.20E+13 0.0 0.0
146. CH2(S)+H2<=>CH3+H 7.00E+13 0.0 0.0
147. CH2(S)+H2O(+M)<=>CH3OH(+M) 2.00E+13 0.0 0.0
Low pressure limit: 0.27000E+39 -0.63000E+01 0.31000E+04
TROE centering: 0.15070E+00 0.13400E+03 0.23830E+04 0.72650E+04
H2 Enhanced by 2.000E+00
H2O Enhanced by 6.000E+00
CH4 Enhanced by 2.000E+00
CO Enhanced by 1.500E+00
CO2 Enhanced by 2.000E+00
C2H6 Enhanced by 3.000E+00
148. CH2(S)+H2O<=>CH2+H2O 3.00E+13 0.0 0.0
149. CH2(S)+CH3<=>H+C2H4 1.20E+13 0.0 -570.0
150. CH2(S)+CH4<=>2CH3 1.60E+13 0.0 -570.0
151. CH2(S)+CO<=>CH2+CO 9.00E+12 0.0 0.0
152. CH2(S)+CO2<=>CH2+CO2 7.00E+12 0.0 0.0
153. CH2(S)+CO2<=>CO+CH2O 1.40E+13 0.0 0.0
154. CH2(S)+C2H6<=>CH3+C2H5 4.00E+13 0.0 -550.0
155. CH3+O2<=>O+CH3O 2.68E+13 0.0 28800.0
156. CH3+O2<=>OH+CH2O 3.60E+10 0.0 8940.0
157. CH3+H2O2<=>HO2+CH4 2.45E+04 2.5 5180.0
158. 2CH3(+M)<=>C2H6(+M) 2.12E+16 -1.0 620.0
Low pressure limit: 0.17700E+51 -0.96700E+01 0.62200E+04
TROE centering: 0.53250E+00 0.15100E+03 0.10380E+04 0.49700E+04
H2 Enhanced by 2.000E+00
H2O Enhanced by 6.000E+00
CH4 Enhanced by 2.000E+00
CO Enhanced by 1.500E+00
CO2 Enhanced by 2.000E+00
C2H6 Enhanced by 3.000E+00
AR Enhanced by 7.000E-01
159. 2CH3<=>H+C2H5 4.99E+12 0.1 10600.0
160. CH3+HCO<=>CH4+CO 2.65E+13 0.0 0.0
161. CH3+CH2O<=>HCO+CH4 3.32E+03 2.8 5860.0
162. CH3+CH3OH<=>CH2OH+CH4 3.00E+07 1.5 9940.0
163. CH3+CH3OH<=>CH3O+CH4 1.00E+07 1.5 9940.0
164. CH3+C2H4<=>C2H3+CH4 2.27E+05 2.0 9200.0
165. CH3+C2H6<=>C2H5+CH4 6.14E+06 1.7 10450.0
166. HCO+H2O<=>H+CO+H2O 2.24E+18 -1.0 17000.0
167. HCO+M<=>H+CO+M 1.87E+17 -1.0 17000.0
H2 Enhanced by 2.000E+00
H2O Enhanced by 0.000E+00
CH4 Enhanced by 2.000E+00
CO Enhanced by 1.500E+00
CO2 Enhanced by 2.000E+00
C2H6 Enhanced by 3.000E+00
168. HCO+O2<=>HO2+CO 7.60E+12 0.0 400.0
169. CH2OH+O2<=>HO2+CH2O 1.80E+13 0.0 900.0
170. CH3O+O2<=>HO2+CH2O 4.28E-13 7.6 -3530.0
171. C2H+O2<=>HCO+CO 5.00E+13 0.0 1500.0
172. C2H+H2<=>H+C2H2 4.07E+05 2.4 200.0
173. C2H3+O2<=>HCO+CH2O 3.98E+12 0.0 -240.0

174. C2H4(+M)<=>H2+C2H2(+M) 8.00E+12 0.4 88770.0
Low pressure limit: 0.70000E+51 -0.93100E+01 0.99860E+05
TROE centering: 0.73450E+00 0.18000E+03 0.10350E+04 0.54170E+04
H2 Enhanced by 2.000E+00
H2O Enhanced by 6.000E+00
CH4 Enhanced by 2.000E+00
CO Enhanced by 1.500E+00
CO2 Enhanced by 2.000E+00
C2H6 Enhanced by 3.000E+00
AR Enhanced by 7.000E-01
175. C2H5+O2<=>HO2+C2H4 8.40E+11 0.0 3875.0
176. HCCO+O2<=>OH+2CO 1.60E+12 0.0 854.0
177. 2HCCO<=>2CO+C2H2 1.00E+13 0.0 0.0
178. HF+M=H+F 3.12E+13 0.0 99320.0
179. H2+F=H+HF 2.56E+12 0.5 650.0
180. OH+F=O+HF 2.00E+13 0.0 0.0
181. HO2+F=O2+HF 2.89E+12 0.5 0.0
182. H2O+F=OH+HF 1.30E+09 1.5 0.0
183. H2O2+F=HO2+HF 1.73E+12 0.5 0.0
184. CH2(S)+HF=CH3F 1.91E+23 -3.6 1780.0
185. CHF+H2=CH3F 2.25E+17 -2.9 13000.0
186. CH2F+H=CH3F 3.03E+21 -3.4 3460.0
187. CH2(S)+HF=CHF+H2 2.08E+07 1.3 8330.0
188. CH2F+H=CH2(S)+HF 8.19E+15 -0.6 505.0
189. CH2F+H=CHF+H2 5.21E+08 1.2 1000.0
190. CHF+HF=CH2F2 3.64E+24 -4.3 4060.0
191. CF2+H2=CH2F2 1.70E+06 -0.7 40900.0
192. CHF2+H=CH2F2 2.75E+06 -0.3 7690.0
193. CHF+HF=CF2+H2 5.77E+06 1.4 17900.0
194. CHF2+H=CHF+HF 1.49E+14 -0.1 101.0
195. CHF2+H=CF2+H2 5.50E+03 2.4 -420.0
196. CHF3+M=CF2+HF 3.40E+30 -4.0 69050.0
H2 Enhanced by 2.000E+00
H2O Enhanced by 6.000E+00
CH4 Enhanced by 2.000E+00
CO Enhanced by 1.500E+00
CO2 Enhanced by 2.000E+00
C2H6 Enhanced by 3.000E+00
AR Enhanced by 7.000E-01
197. CF3+H=CF2+HF 5.50E+13 0.0 0.0
198. CF3+F=CF4 1.60E+38 -7.9 8950.0
199. CH3+F=CH2(S)+HF 1.62E+16 -0.9 -981.0
200. CH2F+F=CHF+HF 5.00E+13 0.0 0.0
201. CHF2+F=CF2+HF 3.00E+13 0.0 0.0
202. CH3+F=CH2F+H 1.36E+12 -0.4 -265.0
203. CH3F+H=CH2F+H2 2.70E+03 3.0 5300.0
204. CH2F2+H=CHF2+H2 1.65E+03 3.0 5600.0
205. CF3+H2=CHF3+H 6.30E+01 3.0 5300.0
206. CH3F+H=CH3+HF 2.75E+14 0.0 31400.0
207. CH2F2+H=CH2F+HF 5.50E+13 0.0 34100.0
208. CHF3+H=CHF2+HF 8.00E+13 0.0 40300.0
209. CF4+H=CF3+HF 1.10E+15 0.0 44600.0
210. CH3F+O=CH2F+OH 6.50E+07 1.5 7000.0
211. CH2F2+O=CHF2+OH 2.25E+07 1.5 6100.0
212. CHF3+O=CF3+OH 1.00E+08 1.5 9250.0
213. CH3F+OH=CH2F+H2O 2.60E+08 1.5 2940.0
214. CH2F2+OH=CHF2+H2O 2.80E+07 1.7 2540.0
215. CHF3+OH=CF3+H2O 5.77E+06 1.8 4292.0
216. CH2F+H2O2=CH3F+HO2 1.20E+10 0.0 -600.0
217. CHF2+H2O2=CH2F2+HO2 1.20E+10 0.0 -600.0
218. CF3+H2O2=CHF3+HO2 1.20E+10 0.0 -600.0
219. CH3F+CH3=CH2F+CH4 1.50E+11 0.0 11400.0
220. CH3F+C2H5=CH2F+C2H6 1.50E+11 0.0 16300.0
221. CH3F+C2H3=CH2F+C2H4 1.50E+11 0.0 10300.0
222. CH2F2+CH3=CHF2+CH4 8.70E+10 0.0 10200.0
223. CH2F2+C2H5=CHF2+C2H6 9.00E+10 0.0 14600.0
224. CH2F2+C2H3=CHF2+C2H4 9.00E+10 0.0 9200.0
225. CF3+CH4=CHF3+CH3 8.34E+11 0.0 10920.0
226. CF3+C2H6=CHF3+C2H5 7.59E+11 0.0 7980.0
227. CF3+C2H4=CHF3+C2H3 8.00E+11 0.0 12000.0
228. CH3F+CF3=CH2F+CHF3 1.35E+12 0.0 11200.0
229. CH2F2+CH2F=CHF2+CH3F 9.00E+10 0.0 14000.0
230. CH2F2+CF3=CHF2+CHF3 7.20E+11 0.0 11200.0
231. CH2O+CH2F=HCO+CH3F 5.54E+03 2.8 8300.0
232. CH2O+CHF2=HCO+CH2F2 5.54E+03 2.8 7800.0
233. CH2O+CF3=HCO+CHF3 5.54E+03 2.8 4600.0
234. CH3OH+CH2F=CH3O+CH3F 1.44E+01 3.1 9800.0
235. CH3OH+CHF2=CH3O+CH2F2 1.44E+01 3.1 9000.0
236. CH3OH+CF3=CH3O+CHF3 1.44E+01 3.1 5500.0
237. CH3OH+CH2F=CH2OH+CH3F 3.20E+01 3.2 10000.0
238. CH3OH+CHF2=CH2OH+CH2F2 3.20E+01 3.2 9300.0
239. CH3OH+CF3=CH2OH+CHF3 3.20E+01 3.2 5700.0
240. HCO+CH2F=CO+CH3F 9.00E+13 0.0 0.0
241. HCO+CHF2=CO+CH2F2 9.00E+13 0.0 0.0
242. HCO+CF3=CO+CHF3 9.00E+13 0.0 0.0
243. HCO+CH2F=CH2CO+HF 2.70E+13 0.0 0.0
244. HCO+CHF2=CHFCO+HF 2.70E+13 0.0 0.0
245. HCO+CF3=CF2CO+HF 2.70E+13 0.0 0.0
246. CH2F+O2=>CHF:O+O+H 2.26E+09 1.1 28500.0
247. CHF2+O2=>CF2:O+O+H 2.26E+09 1.1 24500.0
248. CF3+O2=CF3O+O 2.26E+09 1.1 21500.0
249. CH2F+O=CHF:O+H 5.70E+13 0.0 0.0
250. CHF2+O=CF2:O+H 3.70E+13 0.0 0.0
251. CF3+O=CF2:O+F 1.90E+13 0.0 0.0
252. CH2F+OH=CH2O+HF 2.50E+13 0.0 0.0
253. CHF2+OH=CHF:O+HF 2.50E+13 0.0 0.0
254. CF3+OH=CF2:O+HF 2.00E+13 0.0 0.0
255. CH2F+HO2=>CHF:O+OH+H 1.50E+13 0.0 0.0

256. CHF2+HO2=>CF2:O+OH+H		1.50E+13	0.0	0.0
257. CF3+HO2=CF3O+OH		1.00E+13	0.0	0.0
258. CH2F+HO2=CH3F+O2		3.00E+12	0.0	0.0
259. CHF2+HO2=CH2F2+O2		3.00E+12	0.0	0.0
260. CF3+HO2=CHF3+O2		2.00E+12	0.0	0.0
261. CF3O+M=CF2:O+F		9.03E+26	-3.4	21700.0
H2	Enhanced by 2.000E+00			
H2O	Enhanced by 6.000E+00			
CH4	Enhanced by 2.000E+00			
CO	Enhanced by 1.500E+00			
CO2	Enhanced by 2.000E+00			
C2H6	Enhanced by 3.000E+00			
AR	Enhanced by 7.000E-01			
262. CF3O+H=CF2:O+HF		1.00E+14	0.0	0.0
263. CF3O+H2=>CF2:O+HF+H		1.00E+13	0.0	5000.0
264. CF3O+H2O=>CF2:O+HF+OH		1.00E+13	0.0	5000.0
265. CF3O+CH4=>CF2:O+HF+CH3		8.00E+12	0.0	2300.0
266. CF3O+C2H6=>CF2:O+HF+C2H5		1.20E+13	0.0	2300.0
267. CF3O+C2H4=>CF2:O+HF+C2H3		1.00E+13	0.0	5000.0
268. CF3O+C2H2=>CF2:O+CH2:CF		1.00E+13	0.0	5000.0
269. CF3O+CH2O=>CF2:O+HF+HCO		5.00E+12	0.0	5000.0
270. CF3O+HCO=>CF2:O+HF+CO		5.00E+12	0.0	2000.0
271. CHF+O2=CHF:O+O		2.00E+13	0.0	16500.0
272. CF2+O2=CF2:O+O		2.00E+13	0.0	26500.0
273. CHF+O=CO+HF		9.00E+13	0.0	0.0
274. CF2+O=CF:O+F		7.00E+13	0.0	1000.0
275. CF+F=CF2		6.00E+13	0.0	0.0
276. CHF+OH=HCO+HF		4.00E+12	0.0	0.0
277. CF2+OH=CF:O+HF		4.00E+12	0.0	3500.0
278. CHF+OH=CHF:O+H		2.00E+13	0.0	0.0
279. CF2+OH=CF2:O+H		2.00E+13	0.0	3500.0
280. CHF+HO2=CHF:O+OH		1.00E+13	0.0	0.0
281. CF2+HO2=CF2:O+OH		1.00E+13	0.0	3500.0
282. CHF+HO2=CH2F+O2		2.00E+12	0.0	0.0
283. CF2+HO2=CHF2+O2		2.00E+12	0.0	3500.0
284. CHF+H2O=CH2O+HF		5.00E+12	0.0	6500.0
285. CF2+H2O=CHF:O+HF		5.00E+12	0.0	25000.0
286. CHF+H=CH+HF		2.95E+14	0.0	0.0
287. CF2+H=CF+HF		2.00E+14	0.0	1250.0
288. CH2O+CHF=HCO+CH2F		1.00E+13	0.0	15000.0
289. CH2O+CHF=CH2CO+HF		1.00E+13	0.0	15000.0
290. CH2O+CF2=HCO+CHF2		1.00E+13	0.0	41000.0
291. CH2O+CF2=CHFCO+HF		1.00E+13	0.0	41000.0
292. HCO+CHF=CO+CH2F		2.00E+13	0.0	15000.0
293. HCO+CF2=CO+CHF2		2.00E+13	0.0	41000.0
294. CH+HF=CF+H2		3.00E+13	0.0	0.0
295. CF+O2=CF:O+O		2.00E+13	0.0	1800.0
296. CF+H2O=CHF:O+H		2.00E+13	0.0	17000.0
297. CF+H=>CH+F		4.00E+13	0.0	750.0
298. CF+O=CO+F		4.00E+13	0.0	1000.0
299. CF+OH=CO+HF		3.00E+13	0.0	1000.0
300. CF+HO2=>CF:O+OH		3.00E+13	0.0	0.0
301. CF+CH3=>CH2:CF+H		3.00E+13	0.0	0.0
302. CF+C2H5=>CH2:CF+CH3		3.00E+13	0.0	0.0
303. CF+C2H3=>C2HF+CH2		3.00E+13	0.0	0.0
304. CF+CH2=>C2HF+H		3.00E+13	0.0	0.0
305. CF+CH2(S)=>C2HF+H		3.00E+13	0.0	0.0
306. CF+CH4=>CH2:CHF+H		5.00E+12	0.0	10000.0
307. CF+C2H4=>C2H2+CH2F		1.00E+13	0.0	0.0
308. CF+CH2O=>CHF+HCO		1.00E+13	0.0	8000.0
309. CF+HCO=>CHF+CO		1.00E+13	0.0	0.0
310. CHF:O+M=CO+HF		2.48E+25	-3.0	43000.0
H2	Enhanced by 2.000E+00			
H2O	Enhanced by 6.000E+00			
CH4	Enhanced by 2.000E+00			
CO	Enhanced by 1.500E+00			
CO2	Enhanced by 2.000E+00			
C2H6	Enhanced by 3.000E+00			
AR	Enhanced by 7.000E-01			
311. CF:O+F=CF2:O		1.00E+12	0.0	0.0
312. CF2:O+H2O=>CO2+HF+HF		7.40E-03	3.8	25100.0
313. CHF:O+H=CF:O+H2		1.10E+08	1.8	3000.0
314. CF2:O+H=CF:O+HF		2.40E+07	1.9	35900.0
Declared duplicate reaction...				
315. CF2:O+H=CF:O+HF		1.20E+10	0.8	22300.0
Declared duplicate reaction...				
316. CF2:O+H=CF:O+HF		5.50E+08	1.4	18900.0
Declared duplicate reaction...				
317. CHF:O+O=CF:O+OH		9.00E+12	0.0	3080.0
318. CHF:O+OH=CF:O+H2O		1.72E+09	1.2	-447.0
319. CF2:O+OH=>CO2+F+HF		2.70E+03	2.4	21000.0
320. CF:O+H2O2=CHF:O+HO2		1.00E+11	0.0	3900.0
321. CHF:O+CH3=CF:O+CH4		2.00E+12	0.0	9000.0
322. CHF:O+CH2F=CF:O+CH3F		2.00E+12	0.0	9000.0
323. CHF:O+CHF2=CF:O+CH2F2		2.00E+12	0.0	9000.0
324. CHF:O+CF3=CF:O+CHF3		2.00E+12	0.0	9000.0
325. CHF:O+C2H3=CF:O+C2H4		2.00E+12	0.0	5000.0
326. CHF:O+C2H5=CF:O+C2H6		2.00E+12	0.0	13000.0
327. CO+F+M=CF:O+M		1.03E+19	-1.4	-487.0
H2	Enhanced by 2.000E+00			
H2O	Enhanced by 6.000E+00			
CH4	Enhanced by 2.000E+00			
CO	Enhanced by 1.500E+00			
CO2	Enhanced by 2.000E+00			
C2H6	Enhanced by 3.000E+00			
AR	Enhanced by 7.000E-01			
328. CF:O+O2=>CO2+F+O		2.00E+13	0.0	24000.0
329. CF:O+H=CO+HF		1.20E+14	0.0	0.0

330. CF:O+O=CO2+F	3.00E+13	0.0	0.0
331. CF:O+OH=CO2+HF	3.00E+13	0.0	0.0
332. CF:O+HO2=>CO2+F+OH	3.00E+13	0.0	0.0
333. CF:O+CH3=CH2CO+HF	2.70E+13	0.0	0.0
334. CF:O+CH2F=CHFCO+HF	2.70E+13	0.0	0.0
335. CF:O+CHF2=CF2CO+HF	2.70E+13	0.0	0.0
336. CF:O+CF:O=CO+CF2:O	2.23E+13	0.0	318.0
337. CH3-CH2F=C2H4+HF	2.63E+13	0.0	59900.0
338. CH3-CHF2=CH2:CHF+HF	7.94E+13	0.0	61900.0
339. CH3-CF3=CH2:CF2+HF	1.00E+14	0.0	68700.0
340. CH2F-CH2F=CH2:CHF+HF	2.50E+13	0.0	62900.0
341. CH2F-CHF2=CHF:CHF-Z+HF	1.26E+14	0.0	69100.0
342. CH2F-CHF2=CH2:CF2+HF	1.00E+13	0.0	65400.0
343. CH2F-CF3=CHF:CF2+HF	2.63E+13	0.0	70700.0
344. CHF2-CHF2=CHF:CF2+HF	2.00E+13	0.0	69400.0
345. CHF2-CF3=CF2:CF2+HF	4.00E+13	0.0	71600.0
346. CH2F-CH2+H=C2H4+HF	1.44E+20	-2.1	1730.0
347. CH3-CHF+H=C2H4+HF	2.27E+20	-2.2	1950.0
348. CH2F-CHF+H=CH2:CHF+HF	2.06E+23	-3.2	2280.0
349. CHF2-CH2+H=CH2:CHF+HF	5.24E+16	-0.9	880.0
350. CH3-CF2+H=CH2:CHF+HF	2.09E+16	-0.9	848.0
351. CHF2-CHF+H=CHF:CHF-Z+HF	1.86E+20	-2.3	1750.0
352. CHF2-CHF+H=CH2:CF2+HF	9.95E+19	-2.3	1780.0
353. CH2F-CF2+H=CHF:CHF-Z+HF	6.32E+19	-2.2	1630.0
354. CH2F-CF2+H=CH2:CF2+HF	3.36E+19	-2.3	1660.0
355. CF3-CH2+H=CH2:CF2+HF	1.12E+21	-2.3	2240.0
356. CHF2-CF2+H=CHF:CF2+HF	1.81E+22	-2.9	3070.0
357. CF3-CF2+H=CF2:CF2+HF	1.41E+21	-2.4	3630.0
358. CH2F-CH2+H=CH3+CH2F	3.80E+11	0.6	633.0
359. CH3-CHF+H=CH3+CH2F	3.47E+10	0.9	1370.0
360. CH2F-CHF+H=CH2F+CH2F	1.79E+14	-0.1	1320.0
361. CHF2-CH2+H=CH3+CHF2	2.02E+06	2.2	451.0
362. CH3-CF2+H=CH3+CHF2	1.62E+05	2.5	1370.0
363. CHF2-CHF+H=CH2F+CHF2	6.36E+12	0.3	1460.0
364. CH2F-CF2+H=CH2F+CHF2	3.64E+12	0.3	1180.0
365. CF3-CH2+H=CH3+CF3	2.48E+11	0.8	2870.0
366. CHF2-CF2+H=CHF2+CHF2	3.25E+15	-0.5	3000.0
367. CF3-CF2+H=CHF2+CF3	4.37E+16	-0.7	4360.0
368. CH2F-CH2+H=CH3-CH2F	1.19E+35	-8.5	8140.0
369. CH3-CHF+H=CH3-CH2F	9.57E+38	-9.2	7360.0
370. CH2F-CHF+H=CH2F-CH2F	1.56E+45	-10.8	8070.0
371. CHF2-CH2+H=CH3-CHF2	2.96E+37	-9.1	7160.0
372. CH3-CF2+H=CH3-CHF2	3.11E+40	-9.6	7190.0
373. CHF2-CHF+H=CH2F-CHF2	1.20E+44	-10.6	7520.0
374. CH2F-CF2+H=CH2F-CHF2	2.74E+43	-10.5	7670.0
375. CF3-CH2+H=CH3-CF3	7.27E+42	-9.9	7360.0
376. CHF2-CF2+H=CHF2-CHF2	3.77E+46	-10.8	8980.0
377. CF3-CF2+H=CHF2-CF3	1.12E+47	-10.8	4100.0
378. CH3+CH2F=C2H4+HF	2.35E+19	-1.9	1870.0
379. CH2F+CH2F=CH2:CHF+HF	7.56E+21	-2.8	2590.0
380. CH3+CHF2=CH2:CHF+HF	1.90E+15	-0.6	634.0
381. CH2F+CHF2=CHF:CHF-Z+HF	3.88E+20	-2.4	2888.0
382. CH2F+CHF2=CH2:CF2+HF	2.23E+20	-2.4	2910.0
383. CH3+CF3=CH2:CF2+HF	5.53E+19	-1.9	2440.0
384. CHF2+CHF2=CHF:CF2+HF	2.20E+19	-2.0	4100.0
385. CHF2+CF3=CF2:CF2+HF	7.00E+16	-1.2	4330.0
386. CH3+CH2F=CH3-CH2F	1.57E+31	-6.3	4440.0
387. CH2F+CH2F=CH2F-CH2F	2.37E+24	-3.8	2290.0
388. CH3+CHF2=CH3-CHF2	1.93E+35	-7.7	5760.0
389. CH2F+CHF2=CH2F-CHF2	9.61E+38	-8.4	6940.0
390. CH3+CF3=CH3-CF3	1.78E+33	-6.6	5020.0
391. CHF2+CHF2=CHF2-CHF2	2.26E+24	-3.5	3360.0
392. CHF2+CF3=CHF2-CF3	2.61E+26	-4.2	4100.0
393. CF3+CF3=CF3-CF3	1.63E+36	-7.3	7050.0
394. CH2F-CH2+H=CH3-CHF+H	1.87E+01	3.1	137.0
395. CHF2-CH2+H=CH3-CF2+H	1.59E-03	4.3	157.0
396. CH2F-CF2+H=CHF2-CHF+H	6.40E-01	3.5	1830.0
397. CF3-CF3+H=CF3-CF2+HF	1.00E+15	0.0	30000.0
398. CH3F+CH2(S)=C2H4+HF	3.00E+13	0.0	0.0
399. CH2F2+CH2(S)=CH2:CHF+HF	2.00E+13	0.0	0.0
400. CHF3+CH2(S)=CH2:CF2+HF	1.00E+13	0.0	0.0
401. CF4+CH2(S)=CHF:CF2+HF	4.00E+13	0.0	31000.0
402. CH4+CHF=C2H4+HF	4.00E+13	0.0	15000.0
403. CH3F+CHF=CH2:CHF+HF	3.00E+13	0.0	15000.0
404. CH2F2+CHF=CH2:CF2+HF	1.00E+13	0.0	15000.0
405. CH2F2+CHF=CHF:CHF-Z+HF	1.00E+13	0.0	15000.0
406. CHF3+CHF=CHF:CF2+HF	1.00E+13	0.0	15000.0
407. CF4+CHF=CF2:CF2+HF	4.00E+13	0.0	31000.0
408. CH4+CF2=CH2:CHF+HF	4.00E+13	0.0	41000.0
409. CH3F+CF2=CH2:CF2+HF	1.50E+13	0.0	41000.0
410. CH3F+CF2=CHF:CHF-Z+HF	1.50E+13	0.0	41000.0
411. CH2F2+CF2=CHF:CF2+HF	2.00E+13	0.0	41000.0
412. CHF3+CF2=CF2:CF2+HF	1.00E+13	0.0	41000.0
413. CF4+CF2=>CF3-CF3	4.00E+13	0.0	51000.0
414. CH3+CH2F=CH4+CHF	3.00E+13	0.0	3400.0
415. CH2F+CH2F=CH3F+CHF	3.00E+13	0.0	4800.0
416. CHF2+CH2F=CH2F2+CHF	3.00E+13	0.0	4400.0
417. CF3+CH2F=CHF3+CHF	3.00E+13	0.0	4600.0
418. CH3+CHF2=CH4+CF2	3.00E+13	0.0	800.0
419. CH2F+CHF2=CH3F+CF2	3.00E+13	0.0	2200.0
420. CHF2+CHF2=CH2F2+CF2	3.00E+13	0.0	1600.0
421. CF3+CHF2=CHF3+CF2	3.00E+13	0.0	2000.0
422. CH3-CH2F+H=CH2F-CH2+H2	5.50E+08	1.6	9100.0
423. CH3-CH2F+O=CH2F-CH2+OH	2.90E+08	1.6	6100.0
424. CH3-CH2F+OH=CH2F-CH2+H2O	5.50E+07	1.6	1093.0
425. CH3-CH2F+H=CH3-CHF+H2	3.30E+08	1.6	9100.0
426. CH3-CH2F+O=CH3-CHF+OH	1.60E+08	1.6	6100.0
427. CH3-CH2F+OH=CH3-CHF+H2O	3.30E+07	1.6	1093.0

428. CH3-CHF2+H=CHF2-CH2+H2	1.50E+08	1.6	9600.0
429. CH3-CHF2+O=CHF2-CH2+OH	7.50E+08	1.6	6600.0
430. CH3-CHF2+OH=CHF2-CH2+H2O	1.54E+07	1.6	1132.0
431. CH3-CHF2+H=CH3-CF2+H2	4.40E+07	1.6	9300.0
432. CH3-CHF2+O=CH3-CF2+OH	2.20E+07	1.6	6300.0
433. CH3-CHF2+OH=CH3-CF2+H2O	4.40E+06	1.6	1332.0
434. CH3-CF3+H=CF3-CH2+H2	4.00E+10	1.1	12700.0
435. CH3-CF3+O=CF3-CH2+OH	2.00E+10	1.1	9700.0
436. CH3-CF3+OH=CF3-CH2+H2O	4.08E+09	1.1	4670.0
437. CH2F-CH2F+H=CH2F-CHF+H2	6.00E+08	1.7	9600.0
438. CH2F-CH2F+O=CH2F-CHF+OH	3.00E+08	1.7	6600.0
439. CH2F-CH2F+OH=CH2F-CHF+H2O	6.16E+07	1.7	1610.0
440. CH2F-CHF2+H=CHF2-CHF+H2	2.00E+08	1.7	9800.0
441. CH2F-CHF2+O=CHF2-CHF+OH	1.00E+08	1.7	6800.0
442. CH2F-CHF2+OH=CHF2-CHF+H2O	2.05E+07	1.7	1800.0
443. CH2F-CHF2+H=CH2F-CF2+H2	1.00E+08	1.7	11000.0
444. CH2F-CHF2+O=CH2F-CF2+OH	5.00E+07	1.7	8000.0
445. CH2F-CHF2+OH=CH2F-CF2+H2O	1.06E+07	1.7	3000.0
446. CH2F-CF3+H=CF3-CHF+H2	2.00E+08	1.7	10500.0
447. CH2F-CF3+O=CF3-CHF+OH	1.00E+08	1.7	7500.0
448. CH2F-CF3+OH=CF3-CHF+H2O	2.10E+07	1.7	2524.0
449. CHF2-CHF2+H=CHF2-CF2+H2	1.60E+07	1.7	10600.0
450. CHF2-CHF2+O=CHF2-CF2+OH	8.00E+07	1.7	7600.0
451. CHF2-CHF2+OH=CHF2-CF2+H2O	1.60E+07	1.7	2643.0
452. CHF2-CF3+H=CF3-CF2+H2	1.40E+07	1.6	10200.0
453. CHF2-CF3+O=CF3-CF2+OH	7.00E+07	1.6	7200.0
454. CHF2-CF3+OH=CF3-CF2+H2O	1.40E+07	1.6	2246.0
455. CH3-CHF+H2O2=CH3-CH2F+HO2	9.00E+09	0.0	1000.0
456. CH3-CF2+H2O2=CH3-CHF2+HO2	9.00E+09	0.0	1000.0
457. CH2F-CH2+H2O2=CH3-CH2F+HO2	9.00E+09	0.0	1000.0
458. CH2F-CHF+H2O2=CH2F-CH2F+HO2	9.00E+09	0.0	1000.0
459. CH2F-CF2+H2O2=CH2F-CHF2+HO2	9.00E+09	0.0	1000.0
460. CHF2-CH2+H2O2=CH3-CHF2+HO2	9.00E+09	0.0	1000.0
461. CHF2-CHF+H2O2=CH2F-CHF2+HO2	9.00E+09	0.0	1000.0
462. CHF2-CF2+H2O2=CHF2-CHF2+HO2	9.00E+09	0.0	1000.0
463. CF3-CH2+H2O2=CH3-CF3+HO2	9.00E+09	0.0	1000.0
464. CF3-CHF+H2O2=CH2F-CF3+HO2	9.00E+09	0.0	1000.0
465. CF3-CF2+H2O2=CHF2-CF3+HO2	9.00E+09	0.0	1000.0
466. CH3-CH2F+CH3=CH2F-CH2+CH4	2.00E+11	0.0	13400.0
467. CH3-CH2F+C2H5=CH2F-CH2+C2H6	2.00E+11	0.0	16000.0
468. CH3-CH2F+C2H3=CH2F-CH2+C2H4	2.00E+11	0.0	10000.0
469. CH3-CH2F+CH3=CH3-CHF+CH4	1.50E+11	0.0	10000.0
470. CH3-CH2F+C2H5=CH3-CHF+C2H6	1.50E+11	0.0	13000.0
471. CH3-CH2F+C2H3=CH3-CHF+C2H4	1.50E+11	0.0	7000.0
472. CH3-CHF2+CH3=CHF2-CH2+CH4	2.00E+11	0.0	12000.0
473. CH3-CHF2+C2H5=CHF2-CH2+C2H6	2.00E+11	0.0	15000.0
474. CH3-CHF2+C2H3=CHF2-CH2+C2H4	2.00E+11	0.0	9000.0
475. CH3-CHF2+CH3=CH3-CF2+CH4	8.00E+10	0.0	10000.0
476. CH3-CHF2+C2H3=CH3-CF2+C2H4	8.00E+10	0.0	7000.0
477. CH3-CHF2+C2H5=CH3-CF2+C2H6	8.00E+10	0.0	13000.0
478. CH3-CF3+CH3=CF3-CH2+CH4	2.00E+11	0.0	12000.0
479. CH3-CF3+C2H3=CF3-CH2+C2H4	2.00E+11	0.0	9000.0
480. CH3-CF3+C2H5=CF3-CH2+C2H6	2.00E+11	0.0	15000.0
481. CH2F-CH2F+CH3=CH2F-CHF+CH4	3.00E+11	0.0	10400.0
482. CH2F-CH2F+C2H3=CH2F-CHF+C2H4	3.00E+11	0.0	7000.0
483. CH2F-CH2F+C2H5=CH2F-CHF+C2H6	3.00E+11	0.0	13000.0
484. CH2F-CHF2+CH3=CHF2-CHF+CH4	2.00E+11	0.0	10000.0
485. CH2F-CHF2+C2H3=CHF2-CHF+C2H4	2.00E+11	0.0	7000.0
486. CH2F-CHF2+C2H5=CHF2-CHF+C2H6	2.00E+11	0.0	13000.0
487. CH2F-CHF2+CH3=CH2F-CF2+CH4	1.00E+11	0.0	9600.0
488. CH2F-CHF2+C2H3=CH2F-CF2+C2H4	1.00E+11	0.0	7000.0
489. CH2F-CHF2+C2H5=CH2F-CF2+C2H6	1.00E+11	0.0	13000.0
490. CH2F-CF3+CH3=CF3-CHF+CH4	2.00E+11	0.0	10000.0
491. CH2F-CF3+C2H3=CF3-CHF+C2H4	2.00E+11	0.0	7000.0
492. CH2F-CF3+C2H5=CF3-CHF+C2H6	2.00E+11	0.0	13000.0
493. CHF2-CHF2+CH3=CHF2-CF2+CH4	3.00E+11	0.0	10000.0
494. CHF2-CHF2+C2H3=CHF2-CF2+C2H4	3.00E+11	0.0	7000.0
495. CHF2-CHF2+C2H5=CHF2-CF2+C2H6	3.00E+11	0.0	13000.0
496. CHF2-CF3+CH3=CF3-CF2+CH4	5.70E+10	0.0	9500.0
497. CHF2-CF3+C2H3=CF3-CF2+C2H4	6.00E+10	0.0	7000.0
498. CHF2-CF3+C2H5=CF3-CF2+C2H6	6.00E+10	0.0	13000.0
499. CH3-CH2F+CH2F=CH2F-CH2+CH3F	2.00E+11	0.0	13000.0
500. CH3-CH2F+CH2F=CH3-CHF+CH3F	1.50E+11	0.0	10000.0
501. CH3-CHF2+CH2F=CHF2-CH2+CH3F	2.00E+11	0.0	12000.0
502. CH3-CHF2+CH2F=CH3-CF2+CH3F	8.00E+10	0.0	10000.0
503. CH3-CF3+CH2F=CF3-CH2+CH3F	2.00E+11	0.0	12000.0
504. CH2F-CH2F+CH2F=CH2F-CHF+CH3F	3.00E+11	0.0	10000.0
505. CH2F-CHF2+CH2F=CHF2-CHF+CH3F	2.00E+11	0.0	10000.0
506. CH2F-CHF2+CH2F=CH2F-CF2+CH3F	1.00E+11	0.0	10000.0
507. CH2F-CF3+CH2F=CF3-CHF+CH3F	2.00E+11	0.0	10000.0
508. CHF2-CHF2+CH2F=CHF2-CF2+CH3F	3.00E+11	0.0	11000.0
509. CHF2-CF3+CH2F=CF3-CF2+CH3F	2.00E+11	0.0	10000.0
510. CH3-CH2F+CHF2=CH2F-CH2+CH2F2	2.00E+11	0.0	13000.0
511. CH3-CH2F+CHF2=CH3-CHF+CH2F2	1.50E+11	0.0	10000.0
512. CH3-CHF2+CHF2=CHF2-CH2+CH2F2	2.00E+11	0.0	12000.0
513. CH3-CHF2+CHF2=CH3-CF2+CH2F2	8.00E+10	0.0	10000.0
514. CH3-CF3+CHF2=CF3-CH2+CH2F2	2.00E+11	0.0	12000.0
515. CH2F-CH2F+CHF2=CH2F-CHF+CH2F2	3.00E+11	0.0	10000.0
516. CH2F-CHF2+CHF2=CHF2-CHF+CH2F2	2.00E+11	0.0	10000.0
517. CH2F-CHF2+CHF2=CH2F-CF2+CH2F2	1.00E+11	0.0	10000.0
518. CH2F-CF3+CHF2=CF3-CHF+CH2F2	2.00E+11	0.0	10000.0
519. CHF2-CHF2+CHF2=CHF2-CF2+CH2F2	3.00E+11	0.0	10000.0
520. CHF2-CF3+CHF2=CF3-CF2+CH2F2	2.00E+11	0.0	10000.0
521. CH3-CH2F+CF3=CH2F-CH2+CHF3	9.50E+11	0.0	8200.0
522. CH3-CH2F+CF3=CH3-CHF+CHF3	9.50E+11	0.0	8200.0
523. CH3-CHF2+CF3=CHF2-CH2+CHF3	3.10E+10	0.0	7100.0
524. CH3-CHF2+CF3=CH3-CF2+CHF3	3.10E+10	0.0	7100.0
525. CH3-CF3+CF3=CF3-CH2+CHF3	1.45E+12	0.0	13500.0

526. CH2F-CH2F+CF3=CH2F-CHF+CHF3	5.00E+11	0.0	7600.0
527. CH2F-CHF2+CF3=CHF2-CHF+CHF3	3.00E+11	0.0	7200.0
528. CH2F-CHF2+CF3=CH2F-CF2+CHF3	2.00E+11	0.0	8000.0
529. CH2F-CF3+CF3=CF3-CHF+CHF3	3.00E+11	0.0	6400.0
530. CHF2-CHF2+CF3=CHF2-CF2+CHF3	5.70E+11	0.0	11900.0
531. CHF2-CF3+CF3=CF3-CF2+CHF3	1.40E+11	0.0	10100.0
532. CH3-CHF+O2=CH2:CHF+HO2	2.56E+19	-2.8	1977.0
533. CH3-CF2+O2=CH2:CF2+HO2	2.56E+19	-2.8	1977.0
534. CH2F-CH2+O2=CH2:CHF+HO2	2.56E+19	-2.8	1977.0
535. CH2F-CHF+O2=CHF:CHF-Z+HO2	2.56E+19	-2.8	1977.0
536. CH2F-CF2+O2=CHF:CF2+HO2	2.56E+19	-2.8	1977.0
537. CHF2-CH2+O2=CH2:CF2+HO2	2.56E+19	-2.8	1977.0
538. CHF2-CHF+O2=CHF:CF2+HO2	2.56E+19	-2.8	1977.0
539. CHF2-CF2+O2=CF2:CF2+HO2	2.56E+19	-2.8	1977.0
540. CF3-CH2+O2=>CF3+CH2O+O	1.30E+13	0.0	44000.0
541. CF3-CHF+O2=>CF3+CHF:O+O	1.30E+13	0.0	23000.0
542. CF3-CF2+O2=>CF3+CF2:O+O	1.30E+13	0.0	23000.0
543. CH2F-CH2+O=CH2CO+HF+H	6.60E+13	0.0	0.0
544. CHF2-CH2+O=CHFCO+HF+H	6.60E+13	0.0	0.0
545. CF3-CH2+O=CF2CO+HF+H	6.60E+13	0.0	0.0
546. CH3-CHF+O=CH2CO+HF+H	4.40E+13	0.0	0.0
547. CH2F-CHF+O=CHFCO+HF+H	4.40E+13	0.0	0.0
548. CHF2-CHF+O=CF2CO+HF+H	4.40E+13	0.0	0.0
549. CF3-CHF+O=>CF3+CF:O+H	4.40E+13	0.0	0.0
550. CH3-CF2+O=CH2CO+HF+F	2.20E+13	0.0	0.0
551. CH2F-CF2+O=CHFCO+HF+F	2.20E+13	0.0	0.0
552. CHF2-CF2+O=CF2CO+HF+F	2.20E+13	0.0	0.0
553. CF3-CF2+O=>CF3+CF:O+F	2.20E+13	0.0	0.0
554. CH2F-CH2+O=CH2O+CH2F	3.30E+13	0.0	0.0
555. CHF2-CH2+O=CH2O+CHF2	3.30E+13	0.0	0.0
556. CF3-CH2+O=CH2O+CF3	3.30E+13	0.0	0.0
557. CH3-CHF+O=CHF:O+CH3	2.20E+13	0.0	0.0
558. CH2F-CHF+O=CHF:O+CH2F	2.20E+13	0.0	0.0
559. CHF2-CHF+O=CHF:O+CHF2	2.20E+13	0.0	0.0
560. CF3-CHF+O=CHF:O+CF3	2.20E+13	0.0	0.0
561. CH3-CF2+O=CF2:O+CH3	1.10E+13	0.0	0.0
562. CH2F-CF2+O=CF2:O+CH2F	1.10E+13	0.0	0.0
563. CHF2-CF2+O=CF2:O+CHF2	1.10E+13	0.0	0.0
564. CF3-CF2+O=CF2:O+CF3	1.10E+13	0.0	0.0
565. CH2F-CH2+OH=>CH2CO+HF+H2	6.60E+13	0.0	0.0
566. CHF2-CH2+OH=>CHFCO+HF+H2	6.60E+13	0.0	0.0
567. CF3-CH2+OH=>CF2CO+HF+H2	6.60E+13	0.0	0.0
568. CH3-CHF+OH=>CH2CO+H2+HF	4.40E+13	0.0	0.0
569. CH2F-CHF+OH=>CH2CO+HF+HF	4.40E+13	0.0	0.0
570. CHF2-CHF+OH=>CHFCO+HF+HF	4.40E+13	0.0	0.0
571. CF3-CHF+OH=>CF2CO+HF+HF	4.40E+13	0.0	0.0
572. CH3-CF2+OH=>CH2CO+HF+HF	2.20E+13	0.0	0.0
573. CH2F-CF2+OH=>CHFCO+HF+HF	2.20E+13	0.0	0.0
574. CHF2-CF2+OH=>CF2CO+HF+HF	2.20E+13	0.0	0.0
575. CF3-CF2+OH=>CF3+CF:O+HF	2.20E+13	0.0	0.0
576. CH2F-CH2+OH=CH2:CHF+H2O	6.60E+13	0.0	1510.0
577. CHF2-CH2+OH=CH2:CF2+H2O	4.40E+13	0.0	1510.0
578. CH3-CHF+OH=CH2:CHF+H2O	6.60E+13	0.0	1510.0
579. CH2F-CHF+OH=CHF:CHF-Z+H2O	4.40E+13	0.0	1510.0
580. CHF2-CHF+OH=CHF:CF2+H2O	2.20E+13	0.0	1510.0
581. CH3-CF2+OH=CH2:CF2+H2O	6.60E+13	0.0	1510.0
582. CH2F-CF2+OH=CHF:CF2+H2O	4.40E+13	0.0	1510.0
583. CHF2-CF2+OH=CF2:CF2+H2O	2.20E+13	0.0	1510.0
584. CH2F-CH2+CH3=CH2:CHF+CH4	1.30E+13	-0.5	0.0
585. CHF2-CH2+CH3=CH2:CF2+CH4	6.50E+12	-0.5	0.0
586. CH3-CHF+CH3=CH2:CHF+CH4	1.95E+13	-0.5	0.0
587. CH2F-CHF+CH3=CHF:CHF-Z+CH4	1.30E+13	-0.5	0.0
588. CHF2-CHF+CH3=CHF:CF2+CH4	6.50E+12	-0.5	0.0
589. CH3-CF2+CH3=CH2:CF2+CH4	1.95E+13	-0.5	0.0
590. CH2F-CF2+CH3=CHF:CF2+CH4	1.30E+13	-0.5	0.0
591. CHF2-CF2+CH3=CF2:CF2+CH4	6.50E+12	-0.5	0.0
592. CH3-CHF+HO2=>CH3+CHF:O+OH	3.00E+13	0.0	0.0
593. CH3-CF2+HO2=>CH3+CF2:O+OH	3.00E+13	0.0	0.0
594. CH2F-CH2+HO2=>CH2F+CH2O+OH	3.00E+13	0.0	0.0
595. CH2F-CHF+HO2=>CH2F+CHF:O+OH	3.00E+13	0.0	0.0
596. CH2F-CF2+HO2=>CH2F+CF2:O+OH	3.00E+13	0.0	0.0
597. CHF2-CH2+HO2=>CHF2+CH2O+OH	3.00E+13	0.0	0.0
598. CHF2-CHF+HO2=>CHF2+CHF:O+OH	3.00E+13	0.0	0.0
599. CHF2-CF2+HO2=>CHF2+CF2:O+OH	3.00E+13	0.0	0.0
600. CF3-CH2+HO2=>CF3+CH2O+OH	3.00E+13	0.0	0.0
601. CF3-CHF+HO2=>CF3+CHF:O+OH	3.00E+13	0.0	0.0
602. CF3-CF2+HO2=>CF3+CF2:O+OH	3.00E+13	0.0	0.0
603. CH3-CHF+HO2=CH2:CHF+H2O2	3.00E+11	0.0	0.0
604. CH3-CF2+HO2=CH2:CF2+H2O2	3.00E+11	0.0	0.0
605. CH2F-CH2+HO2=CH2:CHF+H2O2	2.00E+11	0.0	0.0
606. CH2F-CHF+HO2=CHF:CHF-Z+H2O2	4.00E+11	0.0	0.0
607. CH2F-CF2+HO2=CHF:CF2+H2O2	2.00E+11	0.0	0.0
608. CHF2-CH2+HO2=CH2:CF2+H2O2	1.00E+11	0.0	0.0
609. CHF2-CHF+HO2=CHF:CF2+H2O2	1.00E+11	0.0	0.0
610. CHF2-CF2+HO2=CF2:CF2+H2O2	1.00E+11	0.0	0.0
611. CH3-CHF+HO2=CH3-CH2F+O2	3.00E+11	0.0	0.0
612. CH3-CF2+HO2=CH3-CHF2+O2	3.00E+11	0.0	0.0
613. CH2F-CH2+HO2=CH3-CH2F+O2	3.00E+11	0.0	0.0
614. CH2F-CHF+HO2=CH2F-CH2F+O2	3.00E+11	0.0	0.0
615. CH2F-CF2+HO2=CH2F-CHF2+O2	3.00E+11	0.0	0.0
616. CHF2-CH2+HO2=CH3-CHF2+O2	3.00E+11	0.0	0.0
617. CHF2-CHF+HO2=CH2F-CHF2+O2	3.00E+11	0.0	0.0
618. CHF2-CF2+HO2=CHF2-CHF2+O2	3.00E+11	0.0	0.0
619. CF3-CH2+HO2=CH3-CF3+O2	3.00E+11	0.0	0.0
620. CF3-CHF+HO2=CH2F-CF3+O2	3.00E+11	0.0	0.0
621. CF3-CF2+HO2=CHF2-CF3+O2	3.00E+11	0.0	0.0
622. CH3-CHF+CH2O=CH3-CH2F+HCO	5.50E+03	2.8	5900.0
623. CH3-CF2+CH2O=CH3-CHF2+HCO	5.50E+03	2.8	5900.0

624. CH2F-CH2+CH2O=CH3-CH2F+HCO 5.50E+03 2.8 5900.0
625. CH2F-CHF+CH2O=CH2F-CH2F+HCO 5.50E+03 2.8 5900.0
626. CH2F-CF2+CH2O=CH2F-CHF2+HCO 5.50E+03 2.8 5900.0
627. CHF2-CH2+CH2O=CH3-CHF2+HCO 5.50E+03 2.8 5900.0
628. CHF2-CHF+CH2O=CH2F-CHF2+HCO 5.50E+03 2.8 5900.0
629. CHF2-CF2+CH2O=CHF2-CHF2+HCO 5.50E+03 2.8 5900.0
630. CF3-CH2+CH2O=CH3-CF3+HCO 5.50E+03 2.8 5900.0
631. CF3-CHF+CH2O=CH2F-CF3+HCO 5.50E+03 2.8 5900.0
632. CF3-CF2+CH2O=CHF2-CF3+HCO 5.50E+03 2.8 5900.0
633. CH2:CHF=C2H2+HF 1.00E+14 0.0 70800.0
634. CH2:CF2=C2HF+HF 2.50E+14 0.0 86000.0
635. CHF:CHF-Z=C2HF+HF 2.50E+14 0.0 78000.0
636. CHF:CF2=C2F2+HF 2.50E+14 0.0 100000.0
637. CH2(S)+CHF=C2H2+HF 1.70E+20 -2.1 2380.0
638. CH2(S)+CF2=C2HF+HF 1.70E+20 -2.1 2380.0
639. CHF+CHF=C2HF+HF 1.70E+20 -2.1 2380.0
640. CHF+CF2=C2F2+HF 8.51E+19 -2.1 2380.0
641. CH2(S)+CHF=CH2:CHF 3.10E+24 -3.8 2830.0
642. CH2(S)+CF2=CH2:CF2 3.10E+24 -3.8 2830.0
643. CHF+CHF=CHF:CHF-Z 3.10E+24 -3.8 2830.0
644. CHF+CF2=CHF:CF2 3.10E+24 -3.8 2830.0
645. CH2(S)+CHF=CH2:CF+H 1.64E+07 1.6 5740.0
646. CH2(S)+CHF=CHF:CH-Z+H 1.64E+07 1.6 5740.0
647. CH2(S)+CF2=CF2:CH+H 3.28E+07 1.6 5740.0
648. CHF+CHF=CHF:CF-Z+H 1.64E+07 1.6 5740.0
649. CHF+CF2=CF2:CF+H 1.64E+07 1.6 5740.0
650. CH2:CF+H=C2H2+HF 5.98E+20 -2.3 1940.0
651. CHF:CH-Z+H=C2H2+HF 5.98E+20 -2.3 1940.0
652. CF2:CH+H=C2HF+HF 5.98E+20 -2.3 1940.0
653. CHF:CF-Z+H=C2HF+HF 5.98E+20 -2.3 1940.0
654. CF2:CF+H=C2F2+HF 5.98E+20 -2.3 1940.0
655. CH2:CF+H=CH2:CHF 2.40E+34 -7.1 5040.0
656. CHF:CH-Z+H=CH2:CHF 2.40E+34 -7.1 5040.0
657. CF2:CH+H=CH2:CF2 2.40E+34 -7.1 5040.0
658. CHF:CF-Z+H=CHF:CHF-Z 2.40E+34 -7.1 5040.0
659. CF2:CF+H=CHF:CF2 2.40E+34 -7.1 5040.0
660. CF2:CF2+M=CF2+CF2+M 3.96E+50 -9.1 85300.0
H2 Enhanced by 2.000E+00
H2O Enhanced by 6.000E+00
CH4 Enhanced by 2.000E+00
CO Enhanced by 1.500E+00
CO2 Enhanced by 2.000E+00
C2H6 Enhanced by 3.000E+00
AR Enhanced by 7.000E-01
661. CH2:CHF+H(+M)=CH2F-CH2(+M) 4.20E+08 1.5 990.0
Low pressure limit: 0.31900E+28 -0.28000E+01 -0.54000E+02
H2 Enhanced by 2.000E+00
CO Enhanced by 2.000E+00
CO2 Enhanced by 3.000E+00
H2O Enhanced by 5.000E+00
662. CH2:CHF+H(+M)=CH3-CHF(+M) 4.20E+08 1.5 990.0
Low pressure limit: 0.31900E+28 -0.28000E+01 -0.54000E+02
H2 Enhanced by 2.000E+00
CO Enhanced by 2.000E+00
CO2 Enhanced by 3.000E+00
H2O Enhanced by 5.000E+00
663. CH2:CF2+H(+M)=CHF2-CH2(+M) 4.20E+08 1.5 990.0
Low pressure limit: 0.31900E+28 -0.28000E+01 -0.54000E+02
H2 Enhanced by 2.000E+00
CO Enhanced by 2.000E+00
CO2 Enhanced by 3.000E+00
H2O Enhanced by 5.000E+00
664. CH2:CF2+H(+M)=CH3-CF2(+M) 4.20E+08 1.5 990.0
Low pressure limit: 0.31900E+28 -0.28000E+01 -0.54000E+02
H2 Enhanced by 2.000E+00
CO Enhanced by 2.000E+00
CO2 Enhanced by 3.000E+00
H2O Enhanced by 5.000E+00
665. CHF:CHF-Z+H(+M)=CH2F-CHF(+M) 8.40E+08 1.5 990.0
Low pressure limit: 0.63700E+28 -0.28000E+01 -0.54000E+02
H2 Enhanced by 2.000E+00
CO Enhanced by 2.000E+00
CO2 Enhanced by 3.000E+00
H2O Enhanced by 5.000E+00
666. CHF:CF2+H(+M)=CHF2-CHF(+M) 4.20E+08 1.5 990.0
Low pressure limit: 0.31900E+28 -0.28000E+01 -0.54000E+02
H2 Enhanced by 2.000E+00
CO Enhanced by 2.000E+00
CO2 Enhanced by 3.000E+00
H2O Enhanced by 5.000E+00
667. CHF:CF2+H(+M)=CH2F-CF2(+M) 4.20E+08 1.5 990.0
Low pressure limit: 0.31900E+28 -0.28000E+01 -0.54000E+02
H2 Enhanced by 2.000E+00
CO Enhanced by 2.000E+00
CO2 Enhanced by 3.000E+00
H2O Enhanced by 5.000E+00
668. CF2:CF2+H(+M)=CHF2-CF2(+M) 8.40E+08 1.5 990.0
Low pressure limit: 0.63700E+28 -0.28000E+01 -0.54000E+02
H2 Enhanced by 2.000E+00
CO Enhanced by 2.000E+00
CO2 Enhanced by 3.000E+00
H2O Enhanced by 5.000E+00
669. CH2:CHF+H=CHF:CH-Z+H2 3.30E+05 2.5 12241.0
670. CH2:CHF+H=CH2:CF+H2 3.30E+05 2.5 12241.0
671. CH2:CF2+H=CF2:CH+H2 6.70E+05 2.5 12241.0
672. CHF:CHF-Z+H=CHF:CF-Z+H2 3.30E+05 2.5 12241.0
673. CHF:CF2+H=CF2:CF+H2 3.30E+05 2.5 12241.0
674. C2H4+F=CH2:CHF+H 2.00E+13 0.0 0.0

675. CH2:CHF+F=CH2:CF2+H	2.00E+12	0.0	0.0
676. CH2:CHF+F=CHF:CHF-Z+H	5.00E+12	0.0	0.0
677. CHF:CHF-Z+F=CHF:CF2+H	4.00E+12	0.0	0.0
678. CHF:CF2+F=CF2:CF2+H	2.00E+12	0.0	0.0
679. CH2:CHF+O=CH2F+HCO	5.30E+09	1.0	1310.0
680. CHF:CHF-Z+O=CH2F+CF:O	7.00E+09	1.0	1590.0
681. CH2:CF2+O=CHF2+HCO	4.30E+09	1.0	1490.0
682. CHF:CF2+O=CHF2+CF:O	6.00E+09	1.0	1150.0
683. CF2:CF2+O=CF2+CF2:O	1.90E+09	1.0	0.0
684. CH2:CHF+O=CH3+CF:O	5.30E+09	1.0	2300.0
685. CH2:CHF+OH=CHF:CH-Z+H2O	2.00E+06	2.0	2850.0
686. CH2:CHF+OH=CH2:CF+H2O	1.00E+06	2.0	2850.0
687. CHF:CHF-Z+OH=CHF:CF-Z+H2O	2.00E+06	2.0	2850.0
688. CH2:CF2+OH=CF2:CH+H2O	2.00E+06	2.0	2850.0
689. CHF:CF2+OH=CF2:CF+H2O	1.00E+06	2.0	2850.0
690. CH2:CF+O2=CH2O+CF:O	4.48E+26	-4.5	5480.0
Declared duplicate reaction...			
691. CHF:CH-Z+O2=CHF:O+HCO	4.48E+26	-4.5	5480.0
Declared duplicate reaction...			
692. CHF:CF-Z+O2=CHF:O+CF:O	4.48E+26	-4.5	5480.0
Declared duplicate reaction...			
693. CF2:CH+O2=CF2:O+HCO	4.48E+26	-4.5	5480.0
Declared duplicate reaction...			
694. CF2:CF+O2=CF2:O+CF:O	4.48E+26	-4.5	5480.0
Declared duplicate reaction...			
Declared duplicate reaction...			
695. CH2:CF+O2=CH2O+CF:O	1.05E+38	-8.2	7030.0
Declared duplicate reaction...			
696. CHF:CH-Z+O2=CHF:O+HCO	1.05E+38	-8.2	7030.0
Declared duplicate reaction...			
697. CHF:CF-Z+O2=CHF:O+CF:O	1.05E+38	-8.2	7030.0
Declared duplicate reaction...			
698. CF2:CH+O2=CF2:O+HCO	1.05E+38	-8.2	7030.0
Declared duplicate reaction...			
699. CF2:CF+O2=CF2:O+CF:O	1.05E+38	-8.2	7030.0
Declared duplicate reaction...			
700. CH2:CF+O=CH2CO+F	3.00E+13	0.0	0.0
701. CHF:CH-Z+O=CHFCO+H	3.00E+13	0.0	0.0
702. CHF:CF-Z+O=CHFCO+F	3.00E+13	0.0	0.0
703. CF2:CH+O=CF2CO+H	3.00E+13	0.0	0.0
704. CF2:CF+O=CF2CO+F	3.00E+13	0.0	0.0
705. CH2:CF+OH=CH2CO+HF	3.00E+13	0.0	0.0
706. CHF:CH-Z+OH=CH2CO+HF	3.00E+13	0.0	0.0
707. CHF:CF-Z+OH=CHFCO+HF	2.00E+13	0.0	0.0
708. CF2:CF+OH=CF2CO+HF	1.00E+13	0.0	0.0
709. CH2:CF+OH=CH3+CF:O	3.00E+13	0.0	0.0
710. CHF:CH-Z+OH=CH2F+HCO	3.00E+13	0.0	0.0
711. CHF:CF-Z+OH=CH2F+CF:O	4.00E+13	0.0	0.0
712. CF2:CF+OH=CHF2+CF:O	5.00E+13	0.0	0.0
713. C2HF+H(+M)=CH2:CF(+M)	2.80E+12	0.0	2410.0
Low pressure limit: 0.13300E+28 -0.35000E+01 0.24100E+04			
H2 Enhanced by 2.000E+00			
CO Enhanced by 2.000E+00			
CO2 Enhanced by 3.000E+00			
H2O Enhanced by 5.000E+00			
714. C2HF+H(+M)=CHF:CH-Z(+M)	1.40E+12	0.0	2410.0
Low pressure limit: 0.67000E+27 -0.35000E+01 0.24100E+04			
H2 Enhanced by 2.000E+00			
CO Enhanced by 2.000E+00			
CO2 Enhanced by 3.000E+00			
H2O Enhanced by 5.000E+00			
715. C2F2+H(+M)=CHF:CF-Z(+M)	2.80E+12	0.0	2410.0
Low pressure limit: 0.13300E+28 -0.35000E+01 0.24100E+04			
H2 Enhanced by 2.000E+00			
CO Enhanced by 2.000E+00			
CO2 Enhanced by 3.000E+00			
H2O Enhanced by 5.000E+00			
716. C2HF+O=FCCO-E+H	1.00E+07	2.0	1900.0
717. C2F2+O=FCCO-E+F	1.00E+07	2.0	1900.0
718. C2HF+OH=CHFCO+H	2.18E-04	4.5	-1000.0
719. C2HF+OH=CH2F+CO	2.50E-04	4.0	-2000.0
720. C2HF+OH=HCCO+HF	2.50E-04	4.0	-2000.0
721. C2F2+OH=CF2CO+H	2.18E-04	4.5	-1000.0
722. C2F2+OH=FCCO-E+HF	2.50E-04	4.0	-2000.0
723. CH2F+CH2=CH2:CHF+H	4.00E+13	0.0	0.0
724. CH2F+CH2=C2H4+F	4.00E+13	0.0	0.0
725. CHF2+CH2=CH2:CF2+H	4.00E+13	0.0	0.0
726. CHF2+CH2=CH2:CHF+F	4.00E+13	0.0	0.0
727. CF3+CH2=CH2:CF2+F	4.00E+13	0.0	0.0
728. CH2F+CH2(S)=CH2:CHF+H	4.00E+12	0.0	0.0
729. CH2F+CH2(S)=C2H4+F	2.00E+12	0.0	0.0
730. CHF2+CH2(S)=CH2:CF2+H	2.00E+12	0.0	0.0
731. CHF2+CH2(S)=CH2:CHF+F	4.00E+12	0.0	0.0
732. CF3+CH2(S)=CH2:CF2+F	6.00E+12	0.0	0.0
733. CH3+CHF=CH2:CHF+H	6.00E+12	0.0	0.0
734. CH2F+CHF=CHF:CHF-Z+H	4.00E+12	0.0	0.0
735. CH2F+CHF=CH2:CHF+F	2.00E+12	0.0	0.0
736. CHF2+CHF=CHF:CF2+H	2.00E+12	0.0	0.0
737. CHF2+CHF=CHF:CHF-Z+F	4.00E+12	0.0	0.0
738. CF3+CHF=CHF:CF2+F	6.00E+12	0.0	0.0
739. CH3+CF2=CH2:CF2+H	6.00E+12	0.0	3500.0
740. CH2F+CF2=CHF:CF2+H	4.00E+12	0.0	3500.0
741. CH2F+CF2=CH2:CF2+F	2.00E+12	0.0	3500.0
742. CHF2+CF2=CF2:CF2+H	2.00E+12	0.0	3500.0
743. CHF2+CF2=CHF:CF2+F	4.00E+12	0.0	3500.0
744. CHFCO+H=CH2F+CO	1.13E+13	0.0	3428.0
745. CF2CO+H=CHF2+CO	1.13E+13	0.0	3428.0
746. CHFCO+H=FCCO-E+H2	5.00E+13	0.0	8000.0

747. CHFCO+O=CHF:O+CO	1.00E+13	0.0	8000.0
748. CF2CO+O=CF2:O+CO	1.00E+13	0.0	8000.0
749. CHFCO+OH=FCCO-E+H2O	7.50E+12	0.0	2000.0
750. HCCO+F=CHF+CO	3.00E+13	0.0	0.0
751. FCCO-E+F=CF2+CO	3.00E+13	0.0	0.0
752. FCCO-E+H=CHF+CO	1.00E+14	0.0	0.0
753. FCCO-E+O=CF:O+CO	1.00E+14	0.0	0.0
754. CH4+F=CH3+HF	5.90E+12	0.5	450.0
755. CH3F+F=CH2F+HF	1.35E+14	0.0	1200.0
756. CH2F2+F=CHF2+HF	9.00E+13	0.0	1850.0
757. CHF3+F=CF3+HF	4.50E+13	0.0	3700.0
758. CH3OH+F=CH3O+HF	2.62E+09	1.4	-205.0
759. CH3OH+F=CH2OH+HF	4.62E+07	2.0	-300.0
760. CH2O+F=HCO+HF	6.00E+13	0.0	2000.0
761. CHF:O+F=CF:O+HF	2.65E+13	0.0	1800.0
762. CH3O+F=CH2O+HF	3.00E+13	0.0	0.0
763. HCO+F=CO+HF	1.00E+13	0.0	0.0
764. C2H6+F=C2H5+HF	8.00E+12	0.0	300.0
765. CH3-CH2F+F=CH2F-CH2+HF	9.00E+13	0.0	800.0
766. CH3-CHF2+F=CHF2-CH2+HF	1.00E+14	0.0	800.0
767. CH3-CF3+F=CF3-CH2+HF	1.00E+14	0.0	4000.0
768. CH3-CH2F+F=CH3-CHF+HF	6.00E+13	0.0	200.0
769. CH2F-CH2F+F=CH2F-CHF+HF	1.30E+14	0.0	800.0
770. CH2F-CHF2+F=CHF2-CHF+HF	1.30E+14	0.0	800.0
771. CH2F-CF3+F=CF3-CHF+HF	6.00E+13	0.0	1200.0
772. CH3-CHF2+F=CH3-CF2+HF	3.00E+13	0.0	800.0
773. CH2F-CHF2+F=CH2F-CF2+HF	3.00E+13	0.0	1200.0
774. CHF2-CHF2+F=CHF2-CF2+HF	6.00E+13	0.0	1200.0
775. CHF2-CF3+F=CF3-CF2+HF	4.00E+13	0.0	1400.0
776. C2H4+F=C2H3+HF	1.00E+14	0.0	2000.0
777. CF2:CF2+F=CF3+CF2	3.00E+13	0.0	0.0
778. C2H3+F=C2H2+HF	2.00E+13	0.0	0.0
779. CHF:CF-Z+F=CHF+CF2	1.00E+13	0.0	0.0
780. CF2:CF+F=CF2+CF2	2.00E+13	0.0	0.0

NOTE: A units mole-cm-sec-K, E units cal/mole

APPENDIX E. Detailed Drawings of Industrial Burner (dimensions in inches and mm)

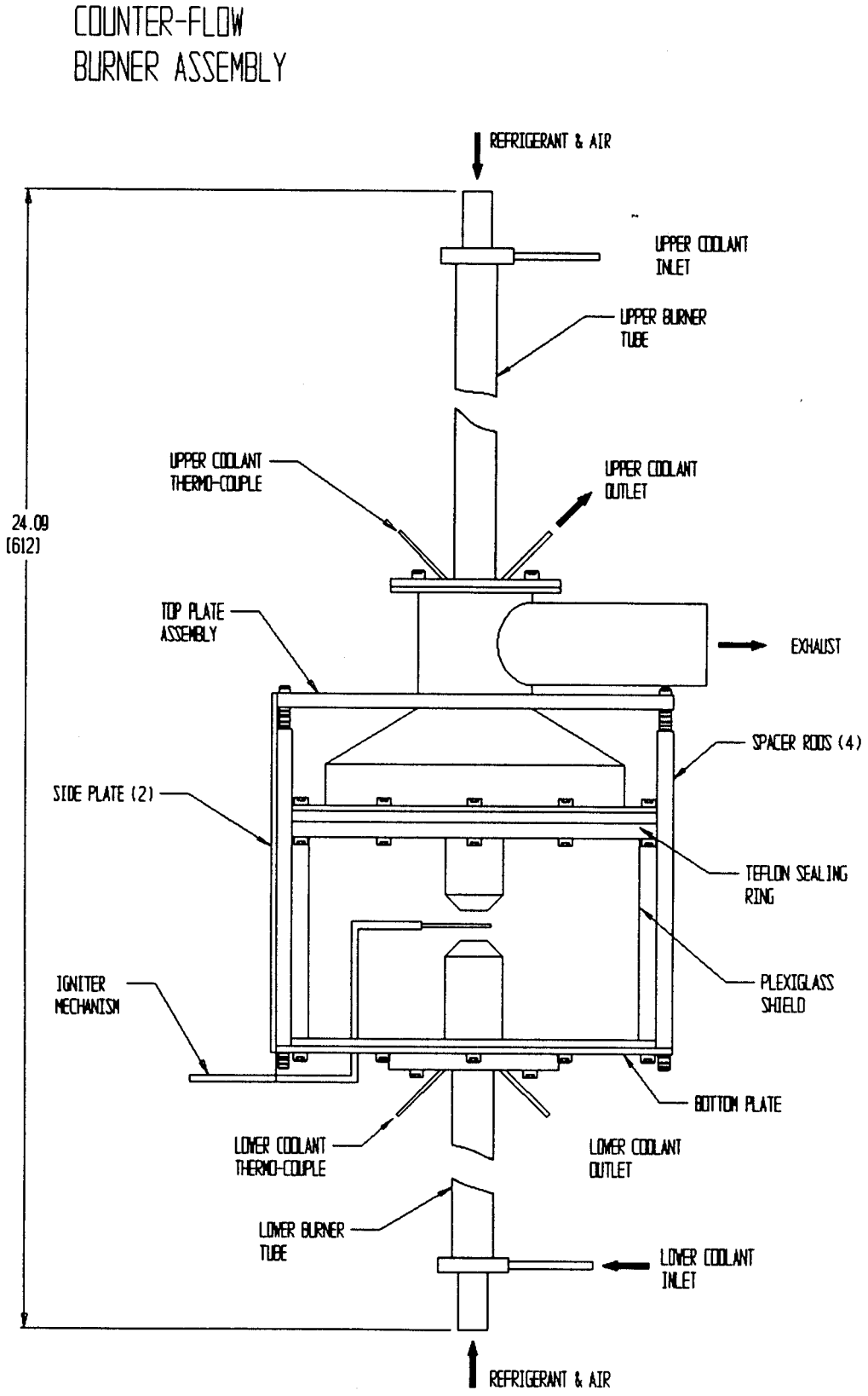

BURNER TUBE

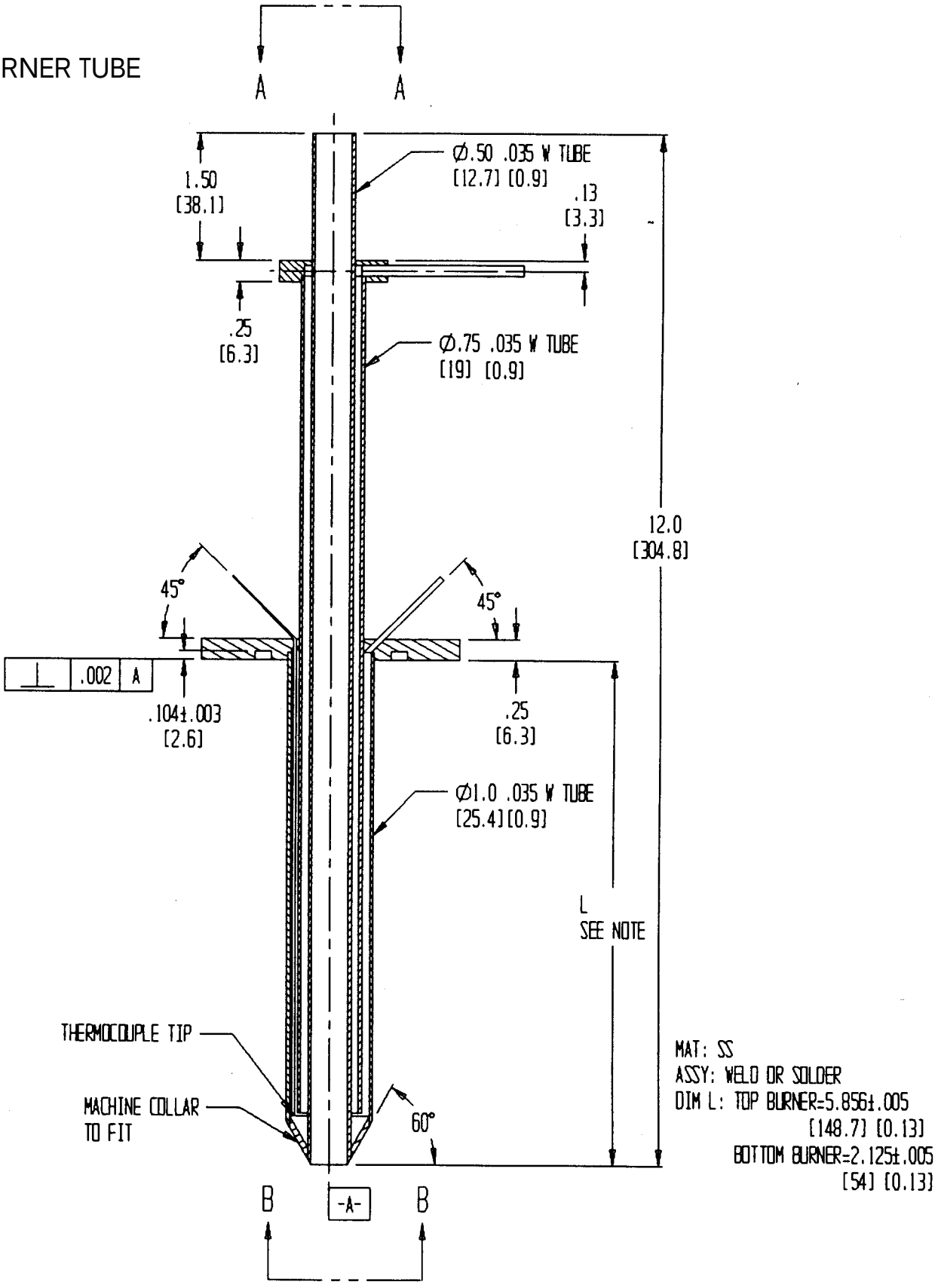
A
A
1.50
[38.1]
Ø.50 .035 W TUBE
[12.7] [0.9]
.13
[3.3]
.25
[6.3]
Ø.75 .035 W TUBE
[19] [0.9]
12.0
[304.8]
45°
45°
.002 A
.104±.003
[2.6]
.25
[6.3]
Ø1.0 .035 W TUBE
[25.4] [0.9]
L
SEE NOTE
THERMOCOUPLE TIP
MACHINE COLLAR
TO FIT
60°
MAT: SS
ASSY: WELD OR SOLDER
DIM L: TOP BURNER=5.856±.005
[148.7] [0.13]
BOTTOM BURNER=2.125±.005
[54] [0.13]
B
-A-
B

BURNER TUBE

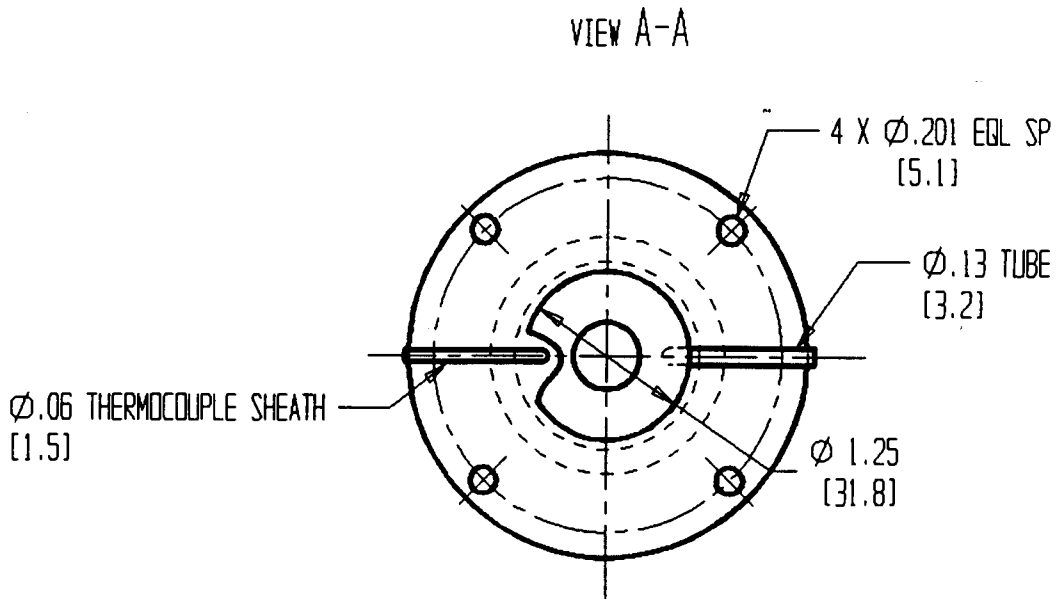

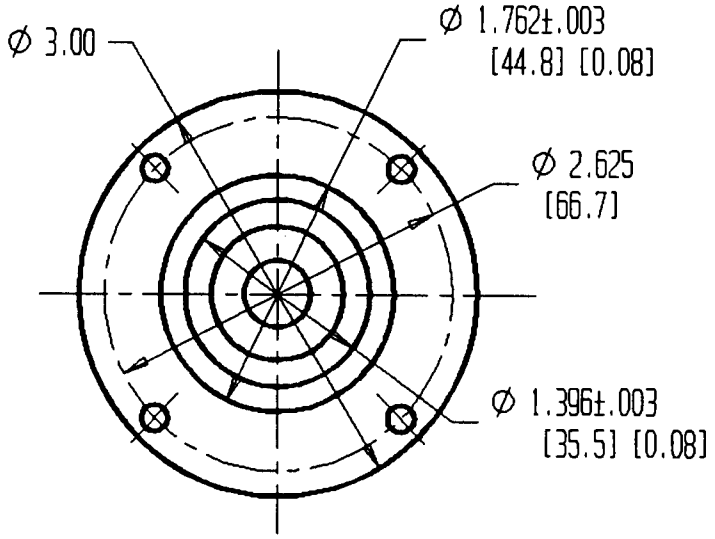

MAT: SS 304
NO REQ:ONE

VIEW B-B

BURNER EXHAUST H00D

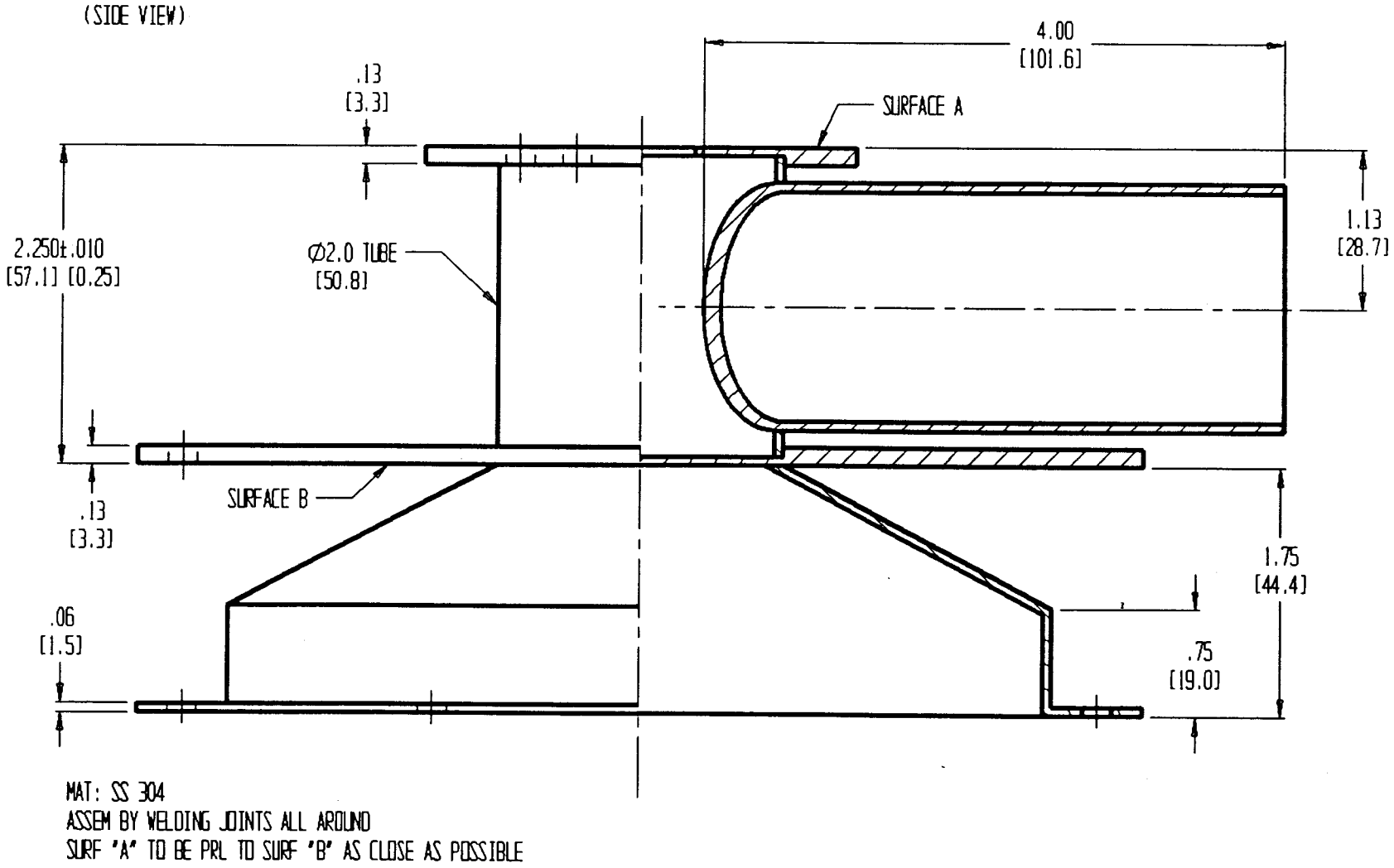

MAT: SS 304
ASSEM BY WELDING JOINTS ALL AROUND
SURF "A" TO BE PRL TO SURF "B" AS CLOSE AS POSSIBLE

BURNER EXHAUST H00D

(TOP VIEW)

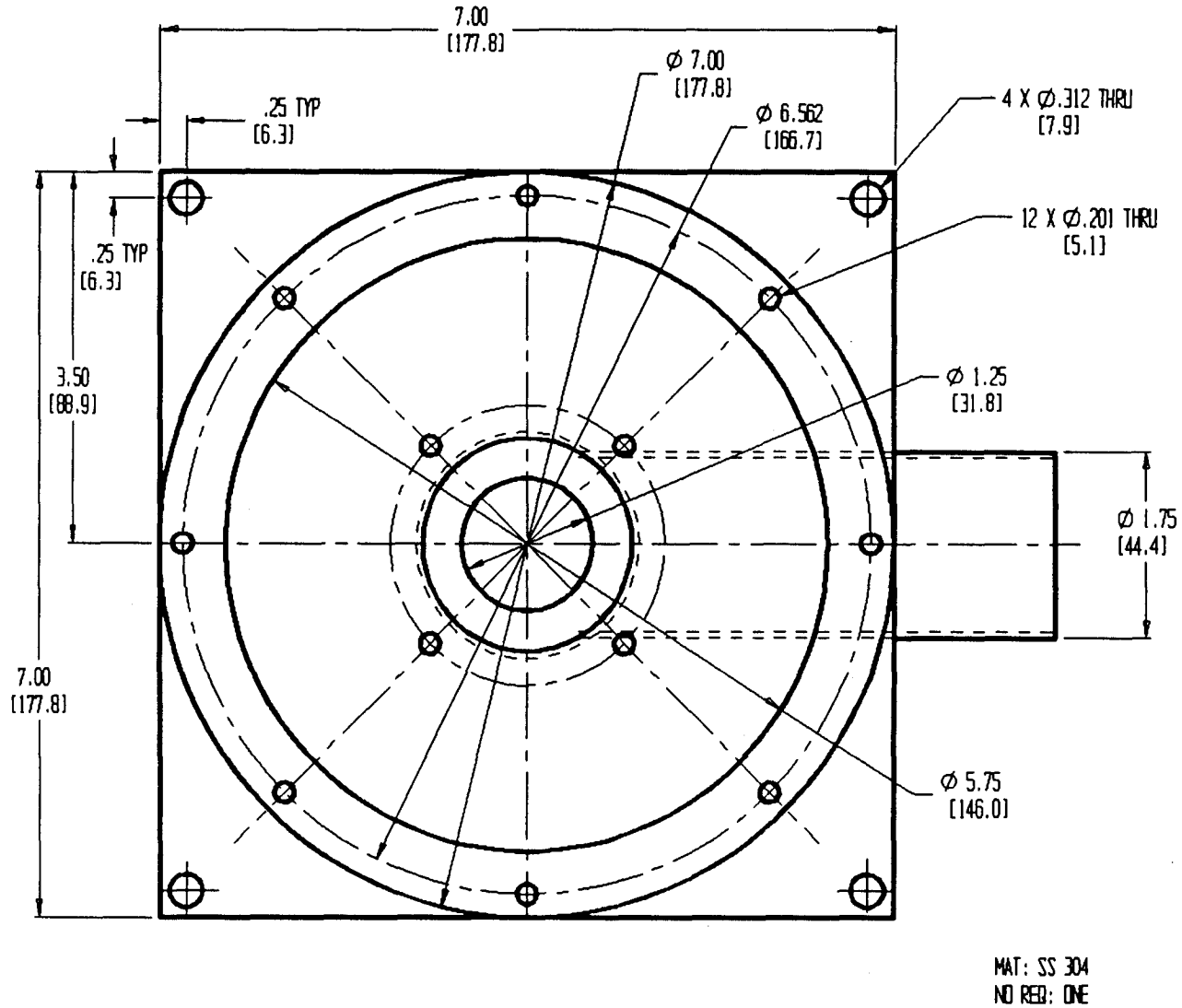

BOTTOM PLATE

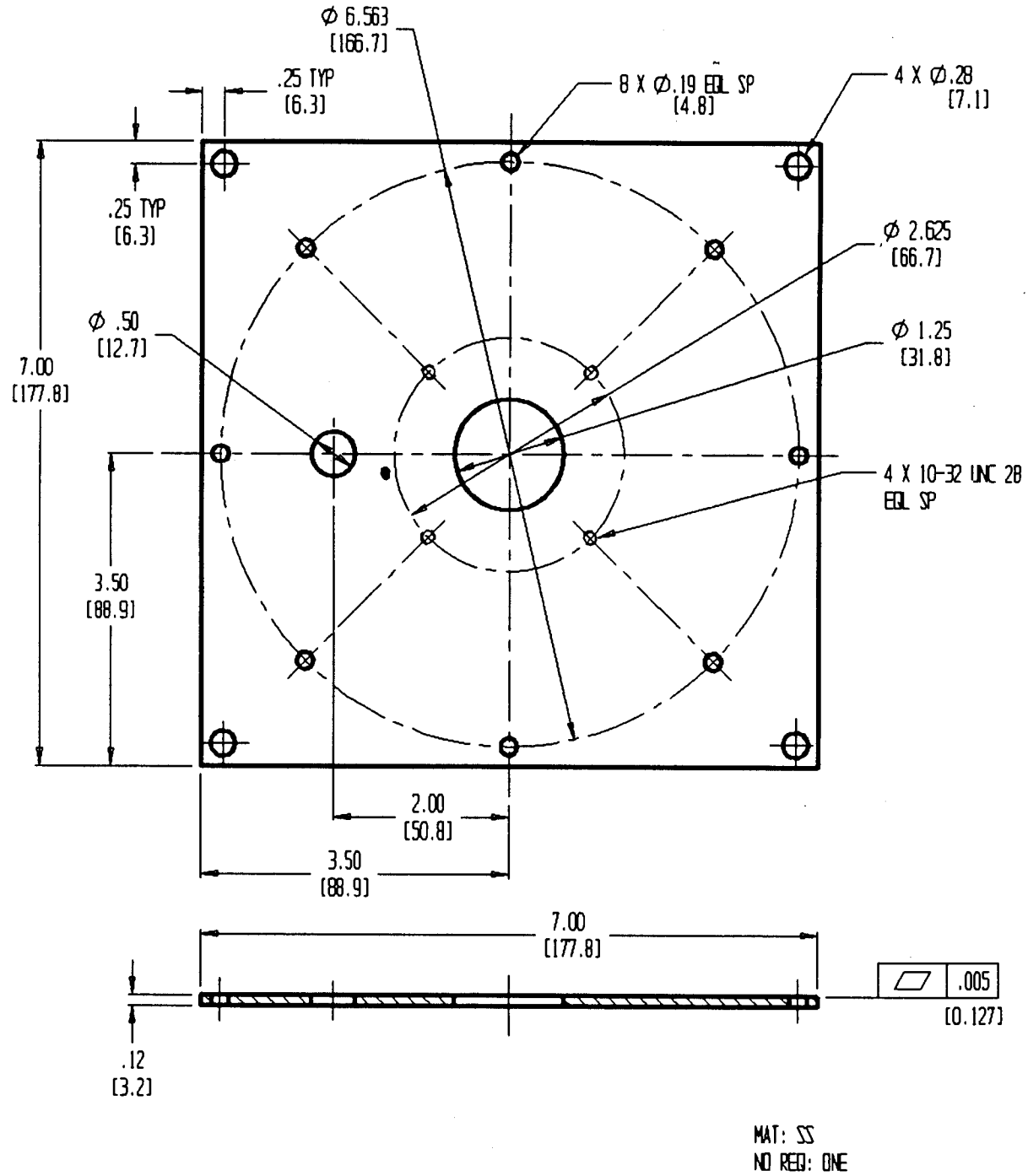

SPACER R0D

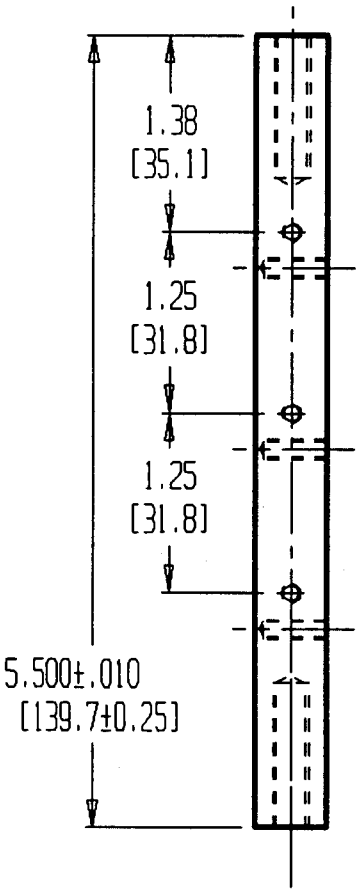

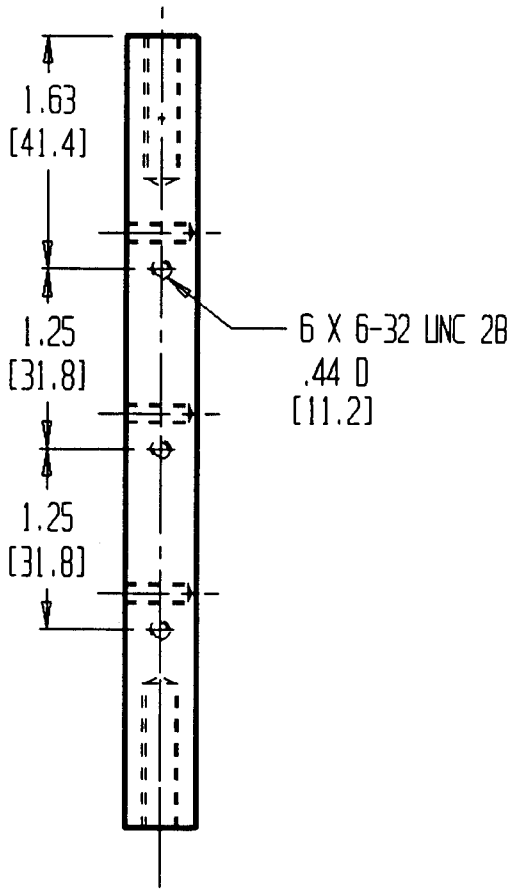

MAT: SS
NO REQ: 4

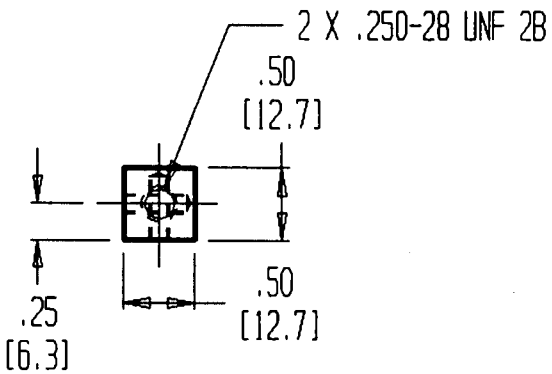

SIDE PLATE

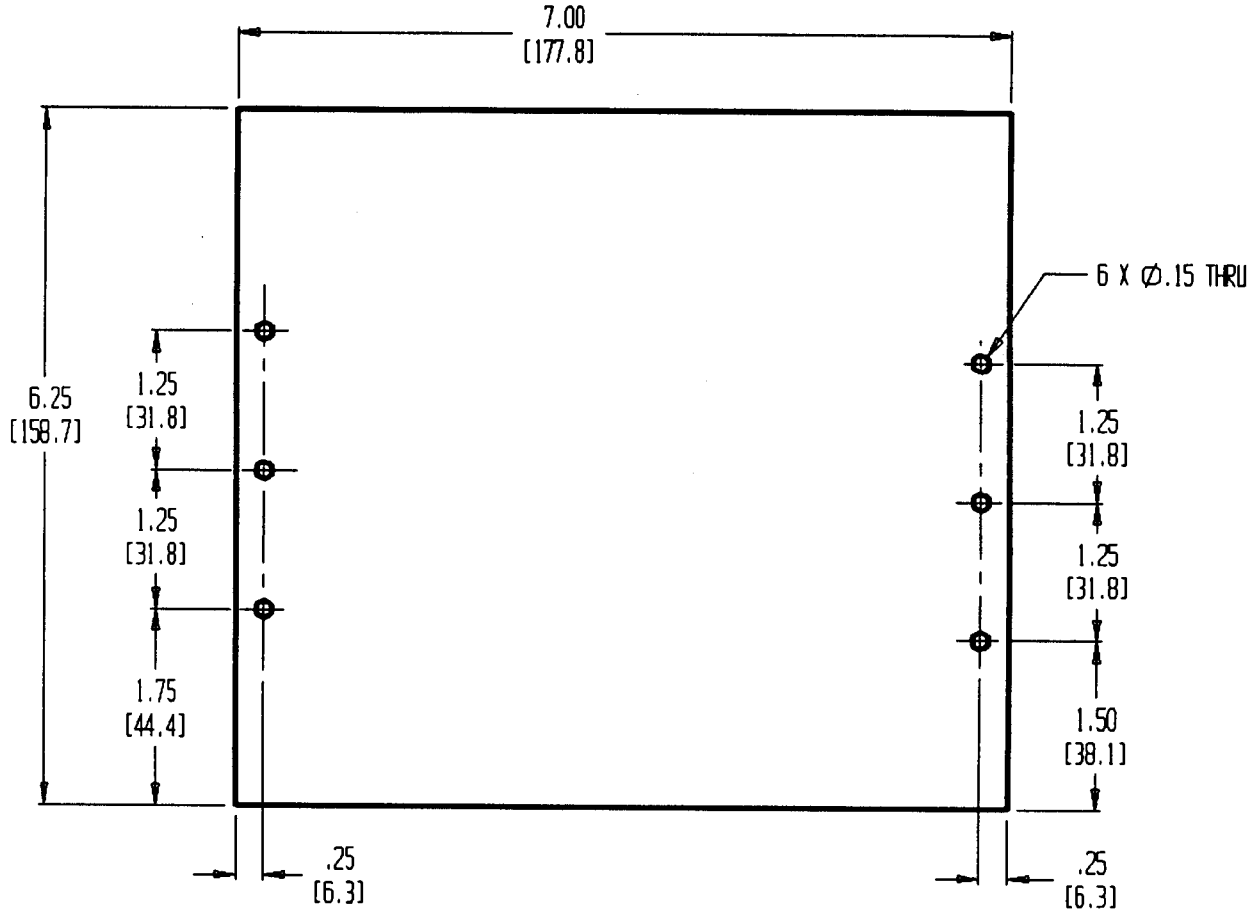

MAT: SS .062 [1.6] THK
NO REQ: TWO

IGNITER BRACKET

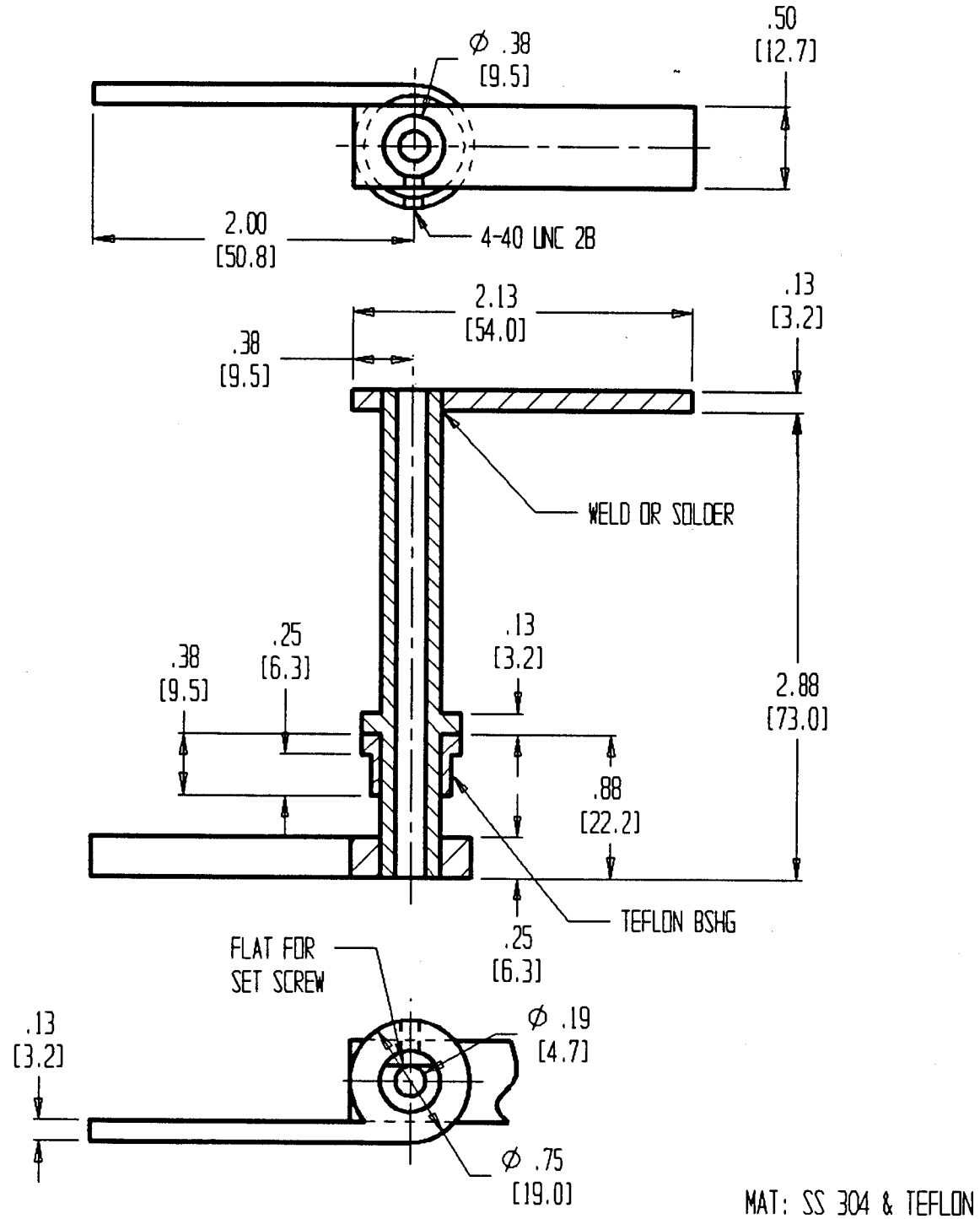

MAT: SS 304 & TEFLON

ACRYLIC BURNER SHIELD

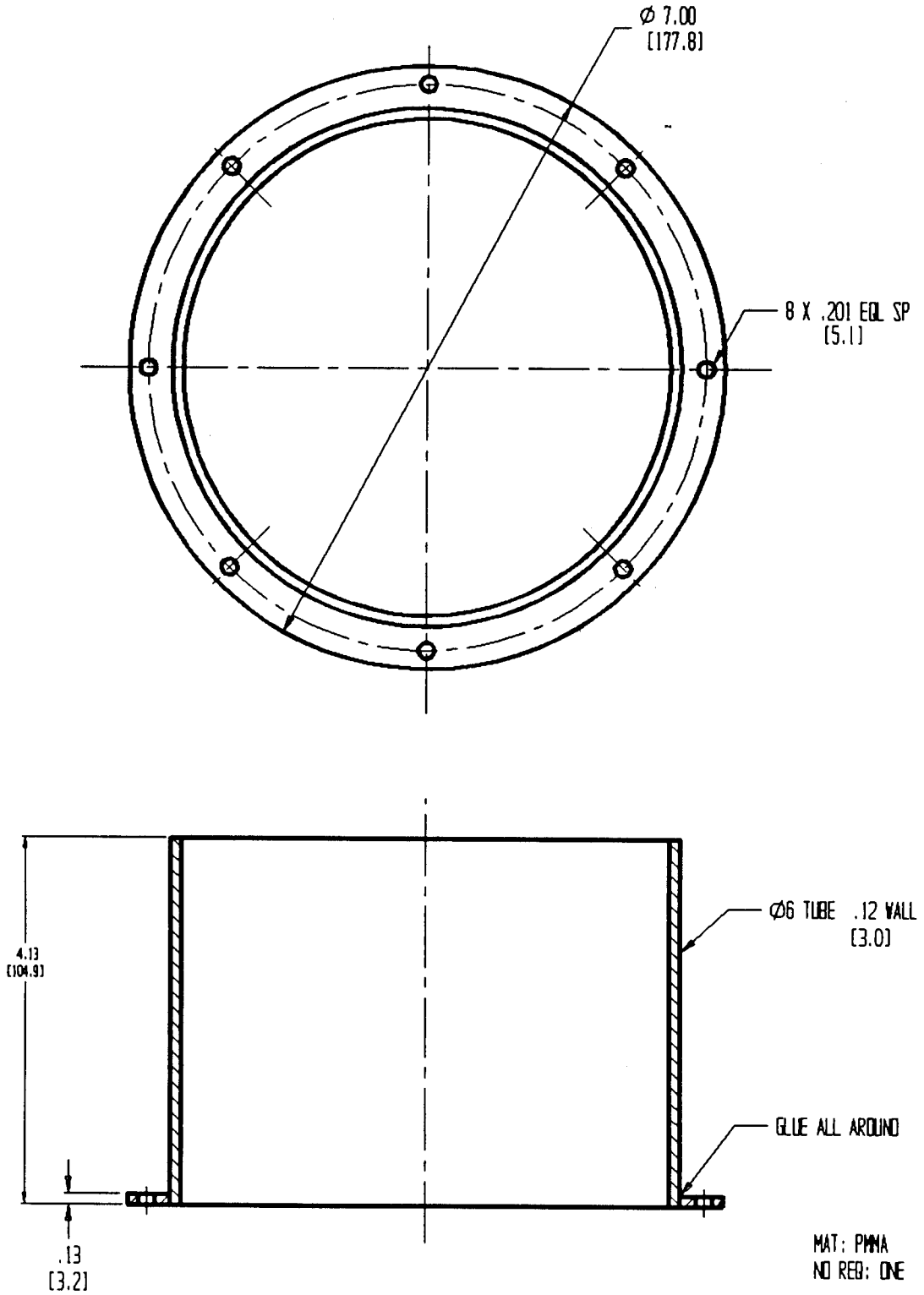

TEFLON SEALING RING

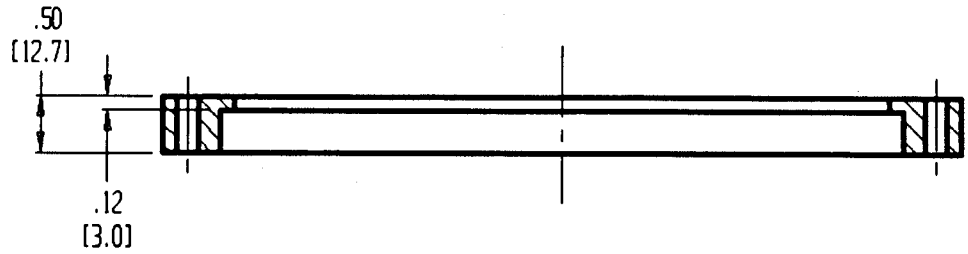

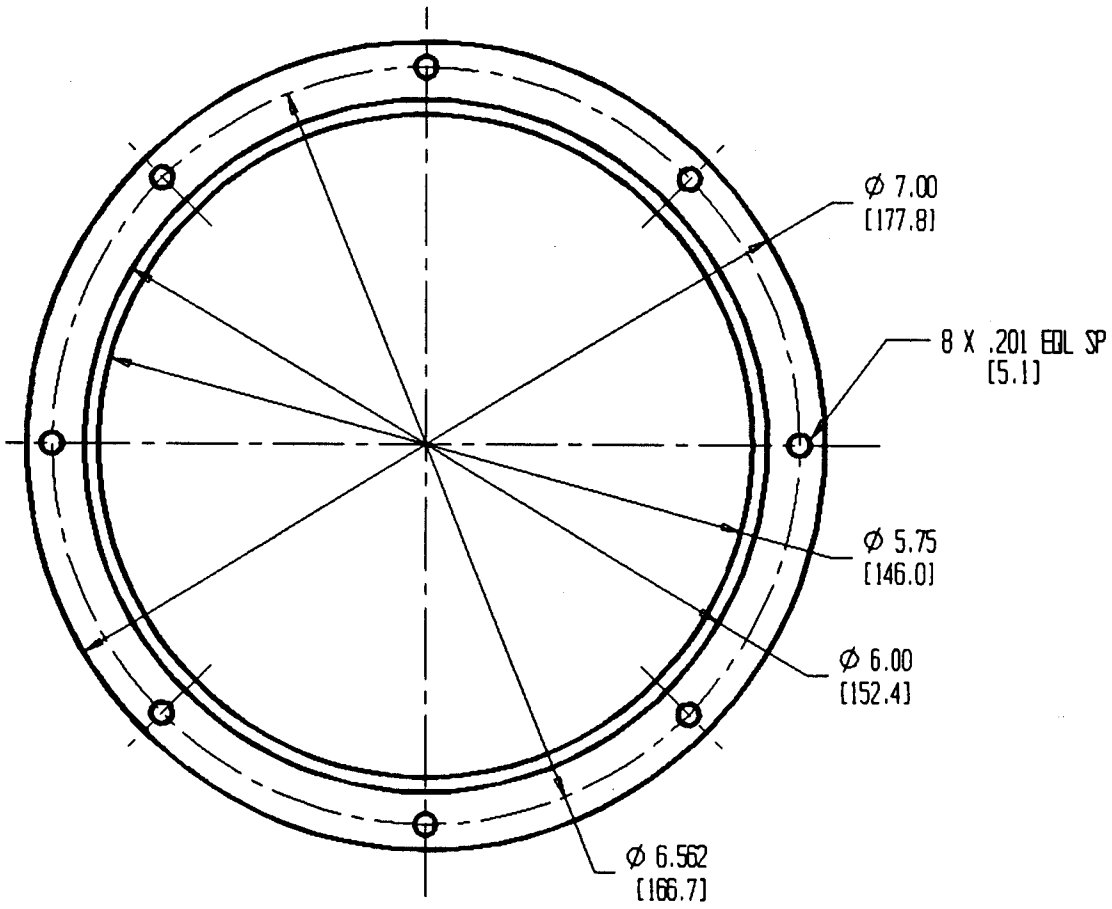

MAT: TEFLON
NO REQ: ONE

APPENDIX F: Drawings of Research Burner

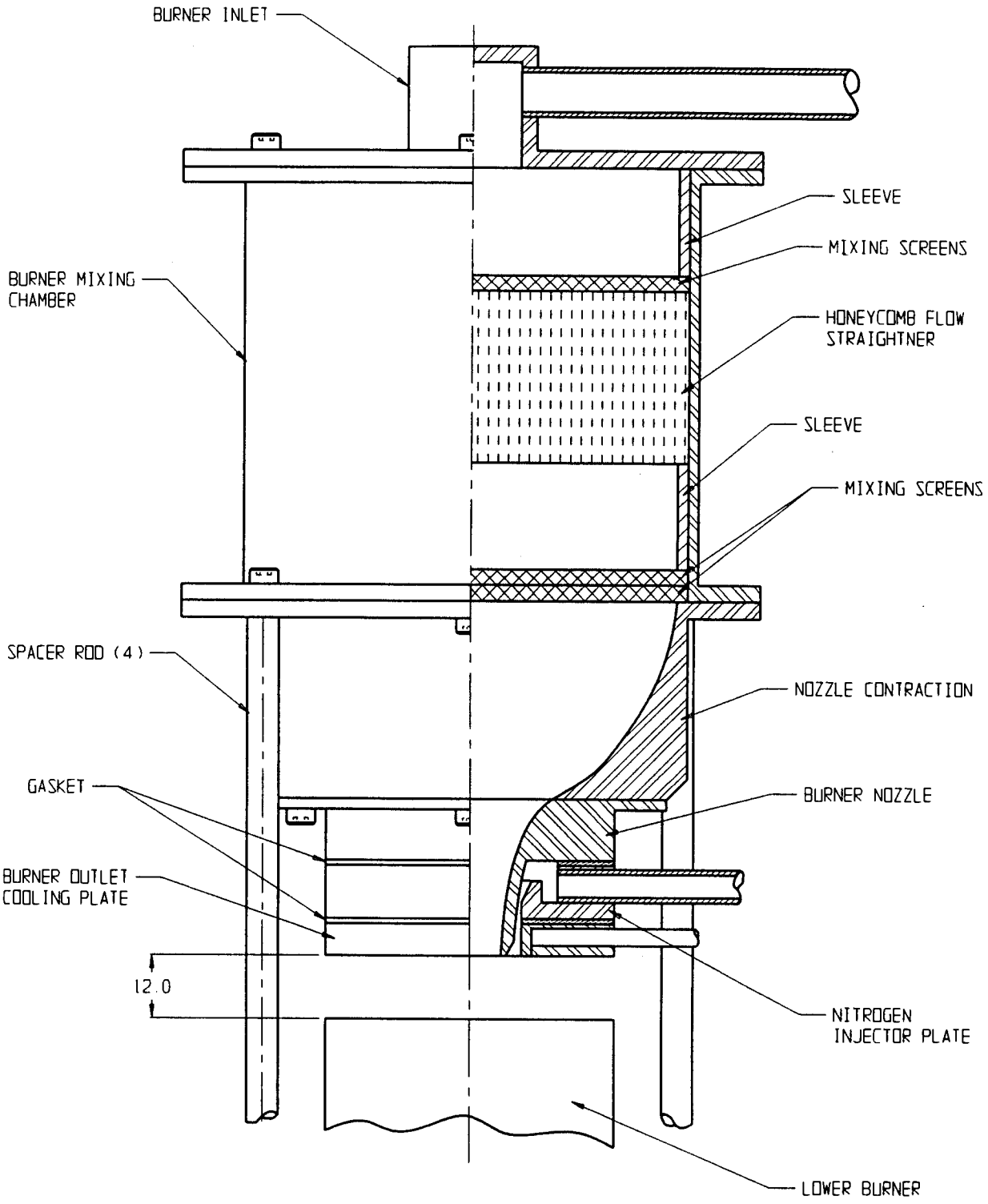

C0UNTER FL0W BURNER ASSEMBLY

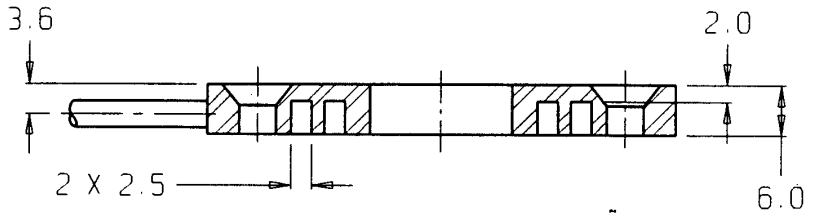

SECTION C-C

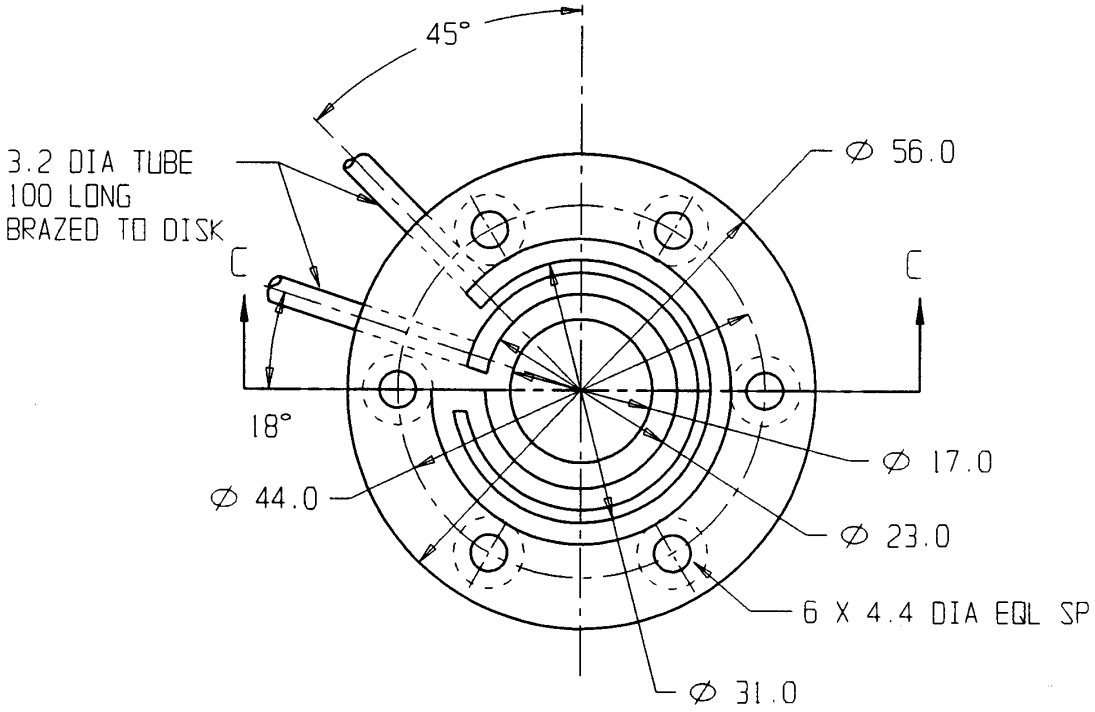

BURNER OUTLET COOLING PLATE
MAT: SS304
DIM: MILLIMETERS

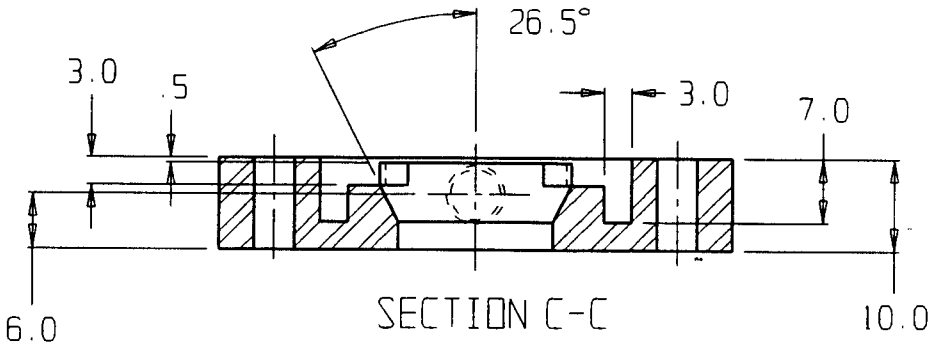

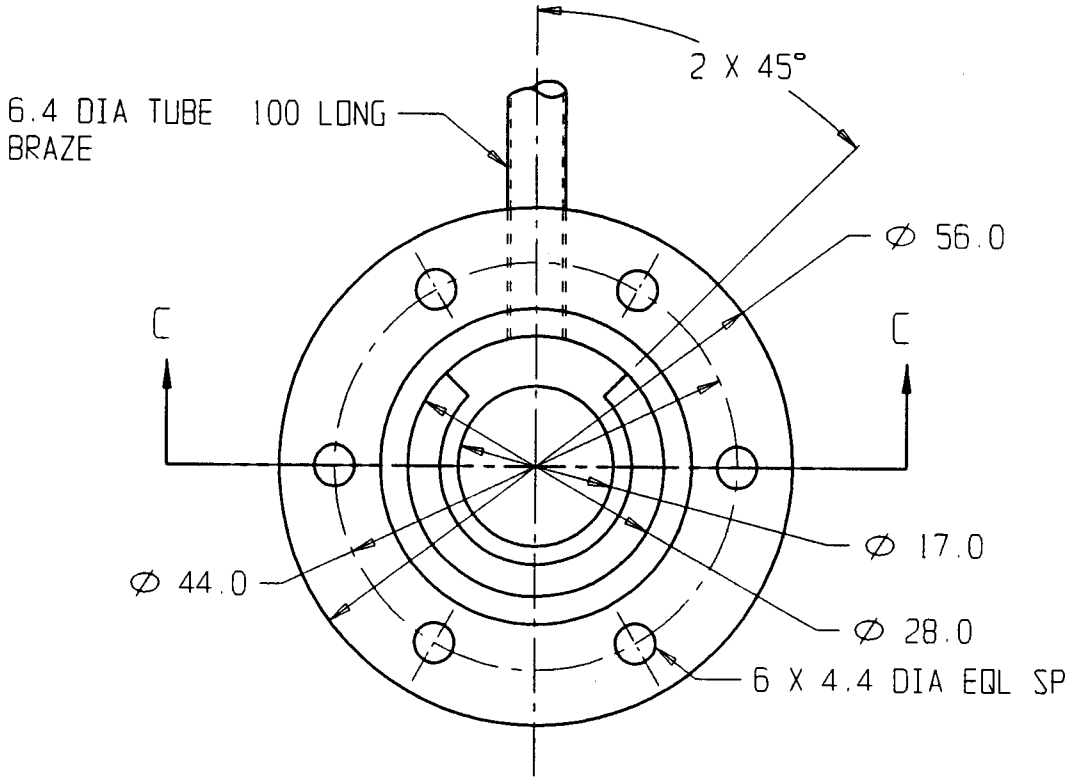

NITR0GEN INJECT0R PLATE
MAT: SS304
DIM: MILLIMETERS

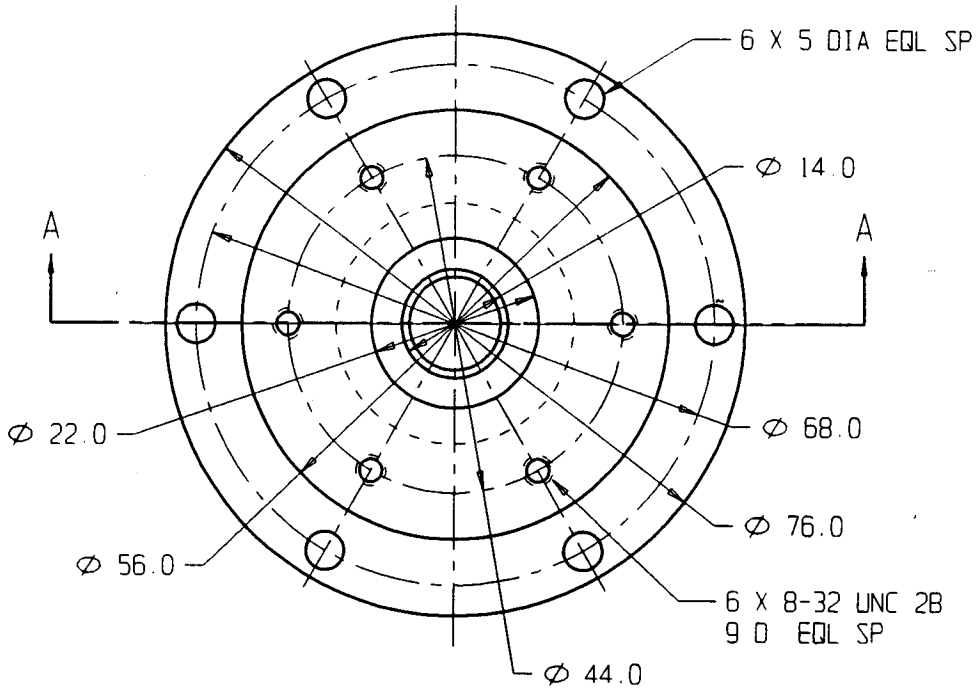

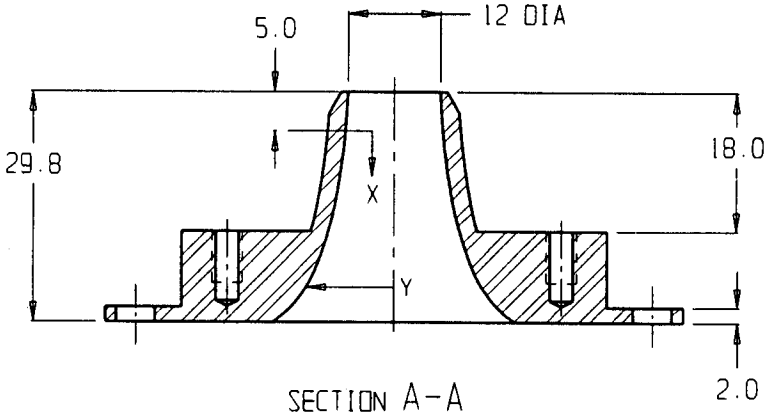

BURNER N0ZZLE
MAT: SS 304
DIM: MILLIMETERS
Y=6+ .0008824 XCUBED

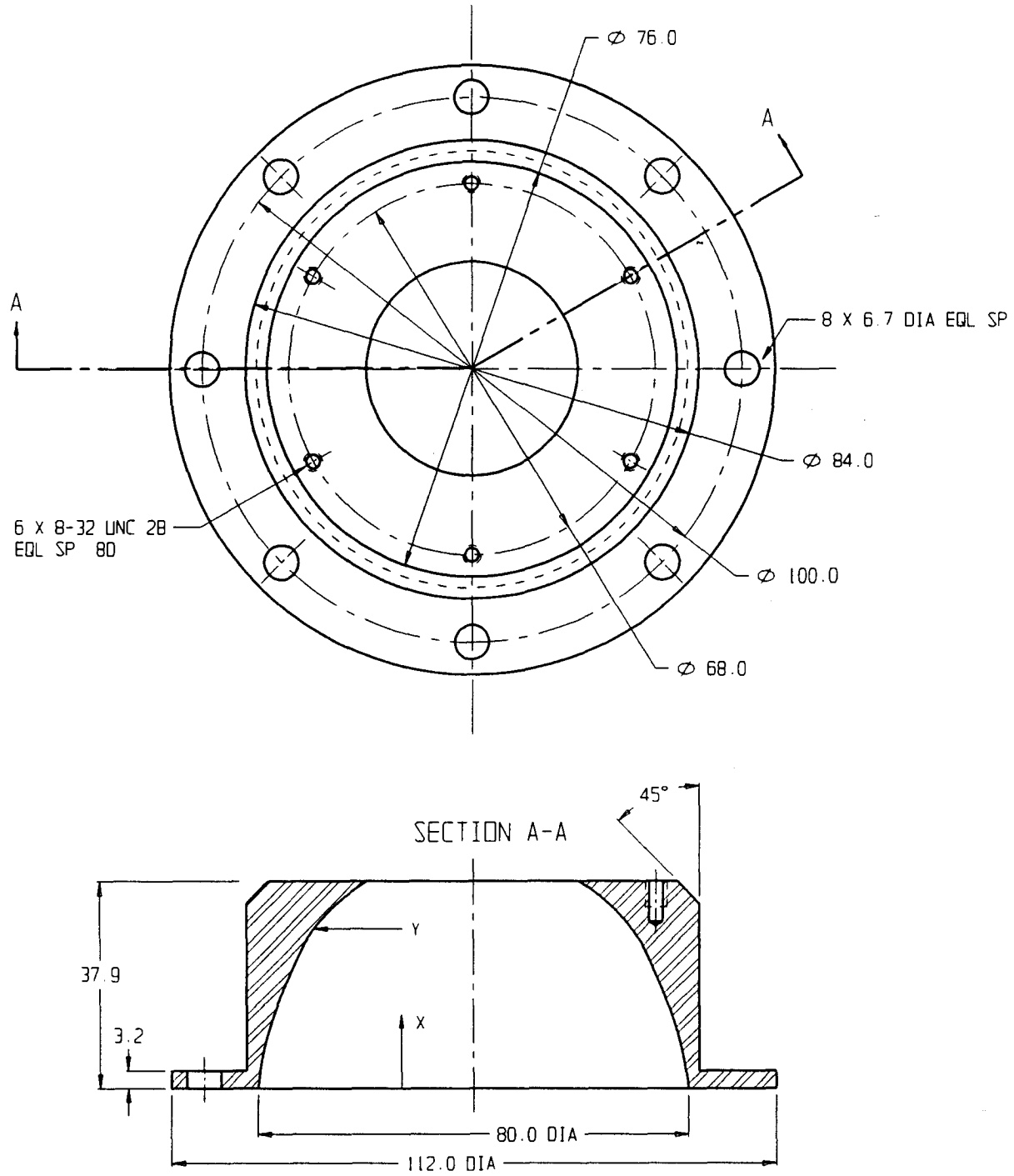

BURNER N0ZZLE C0NTRACTI0N
MAT: SS 304
DIM: MILLIMETERS
Y=40- .0003773 XCUBED

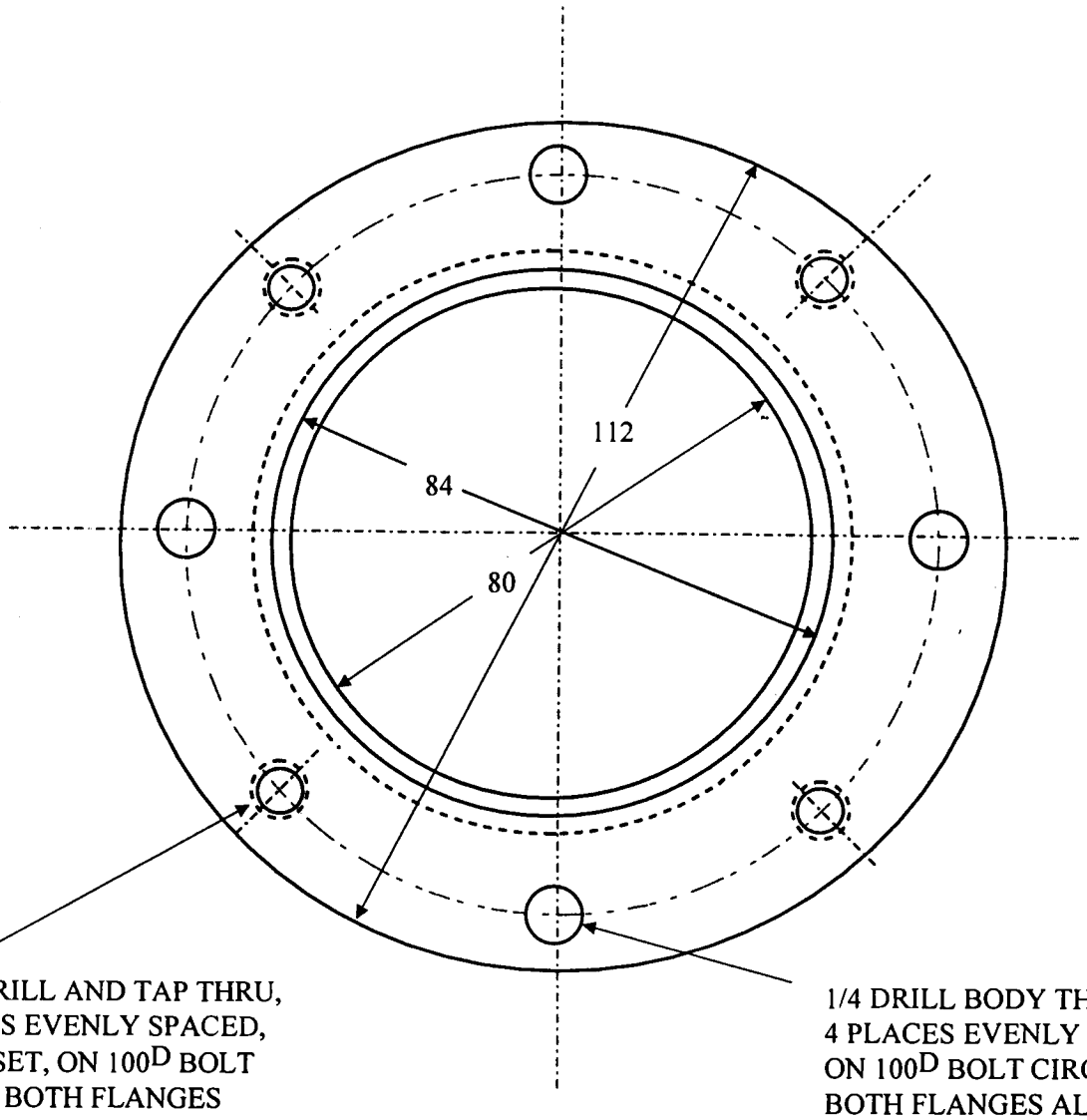

TITLE: BURNER MIXING CHAMBER,
SHEET 1 OF 2

MATERIAL: STAINLESS STEEL 304

DIMENSIONS: mm

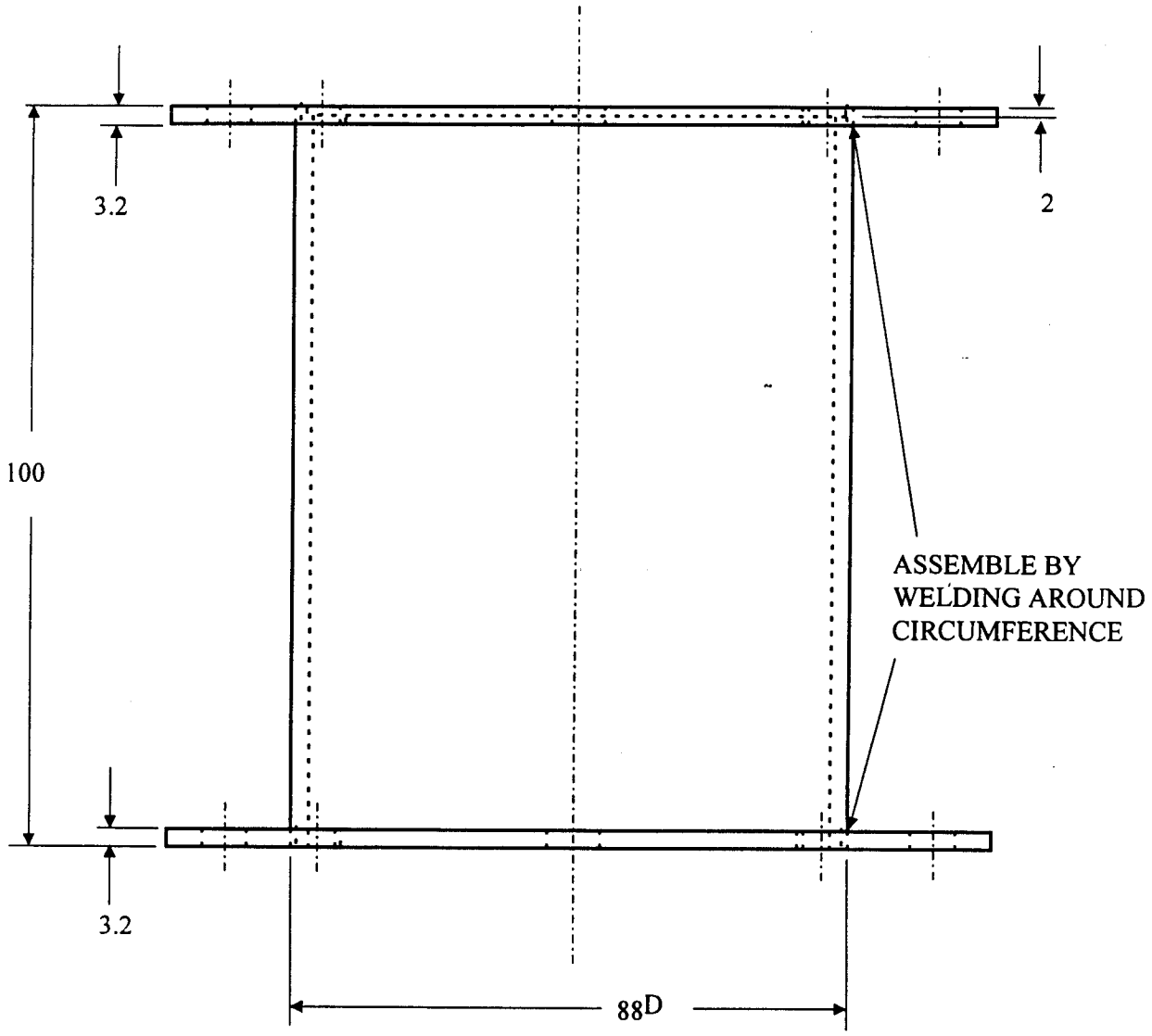

TITLE: BURNER MIXING CHAMBER, SHEET 2 OF 2

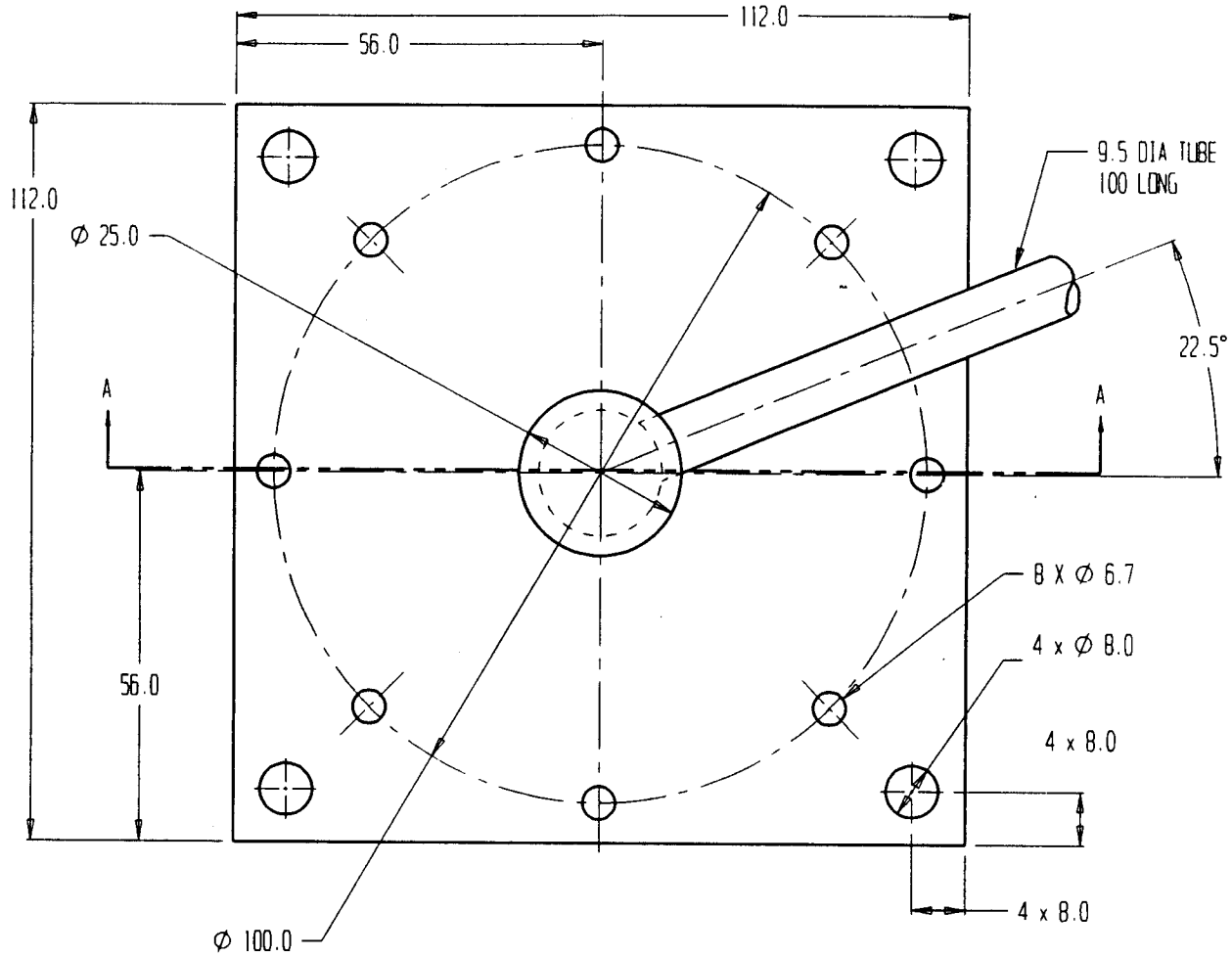

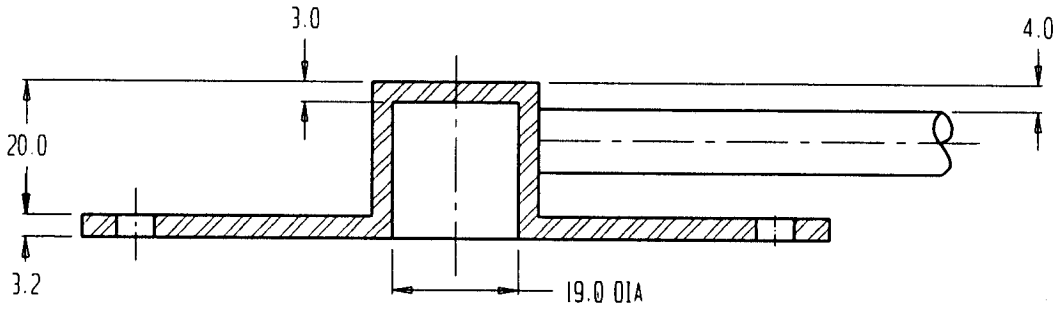

SECTION A-A

BURNER INLET

MAT: SS 304

ASSEMBLE BY WELDING

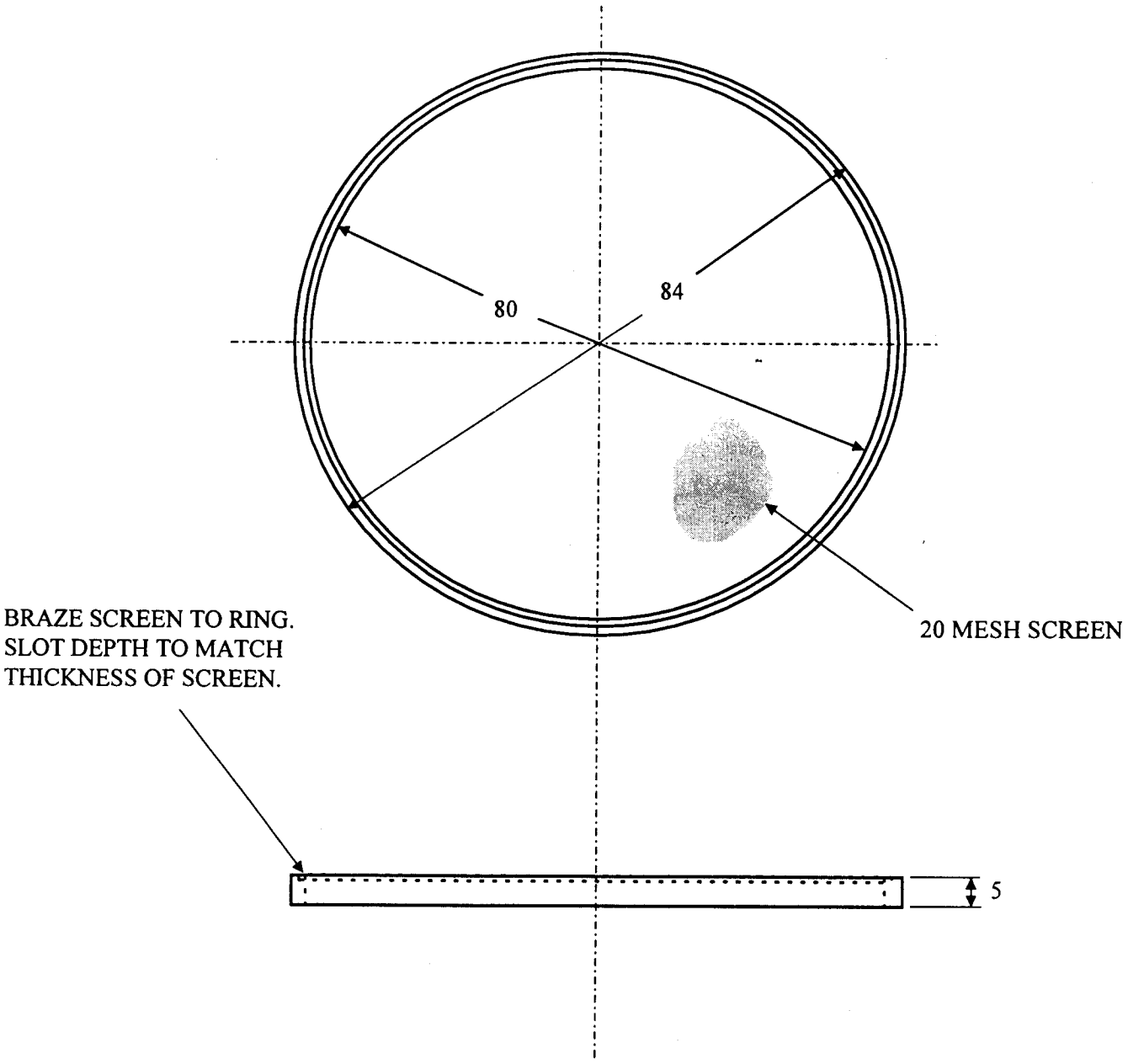

TITLE: MIXING SCREEN, 3 REQRD

MATERIAL: STAINLESS STEEL 304

DIMENSIONS: mm

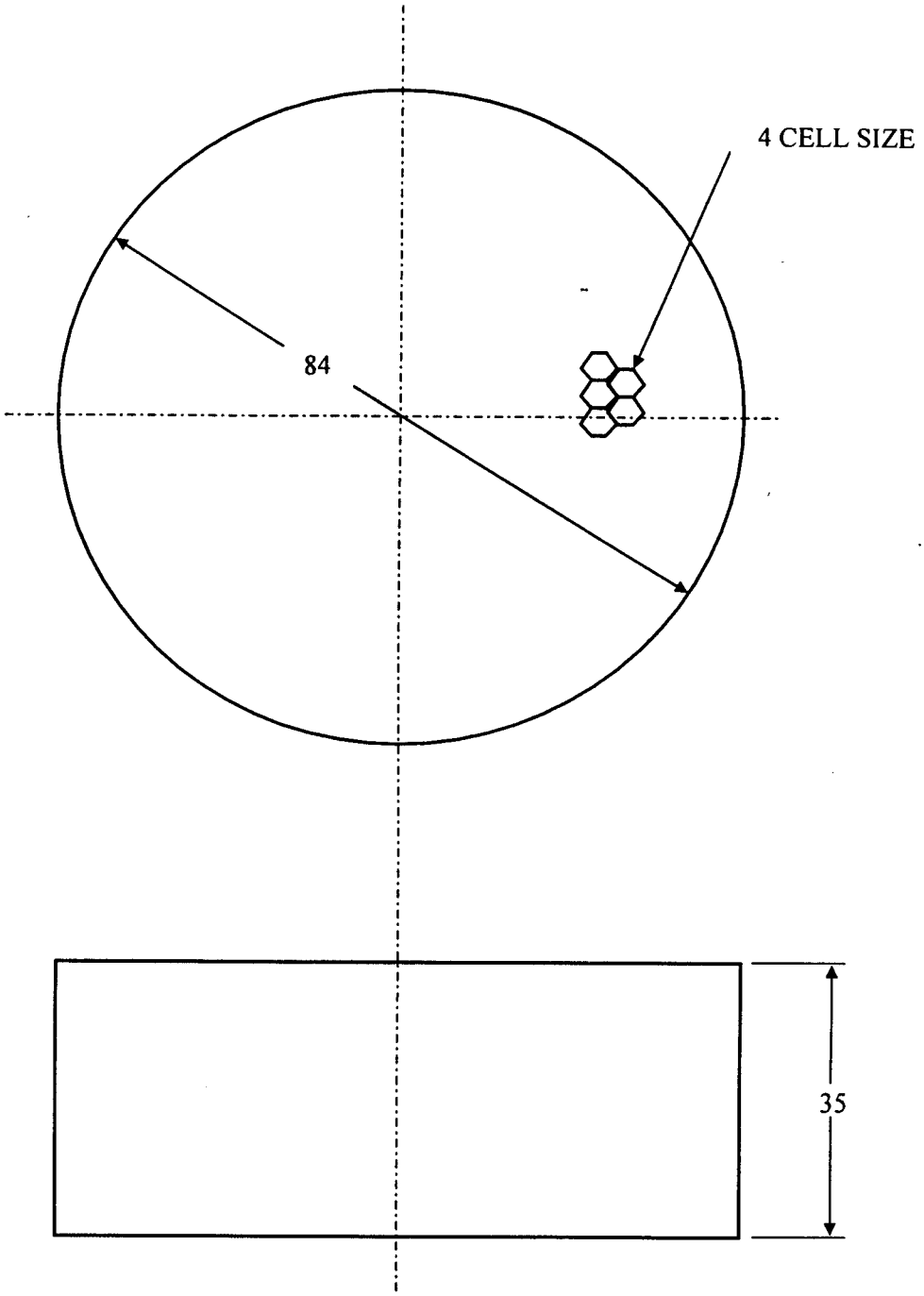

TITLE: FLOW STRAIGHTNER

MATERIAL: STAINLESS STEEL HONEYCOMB

DIMENSIONS: mm

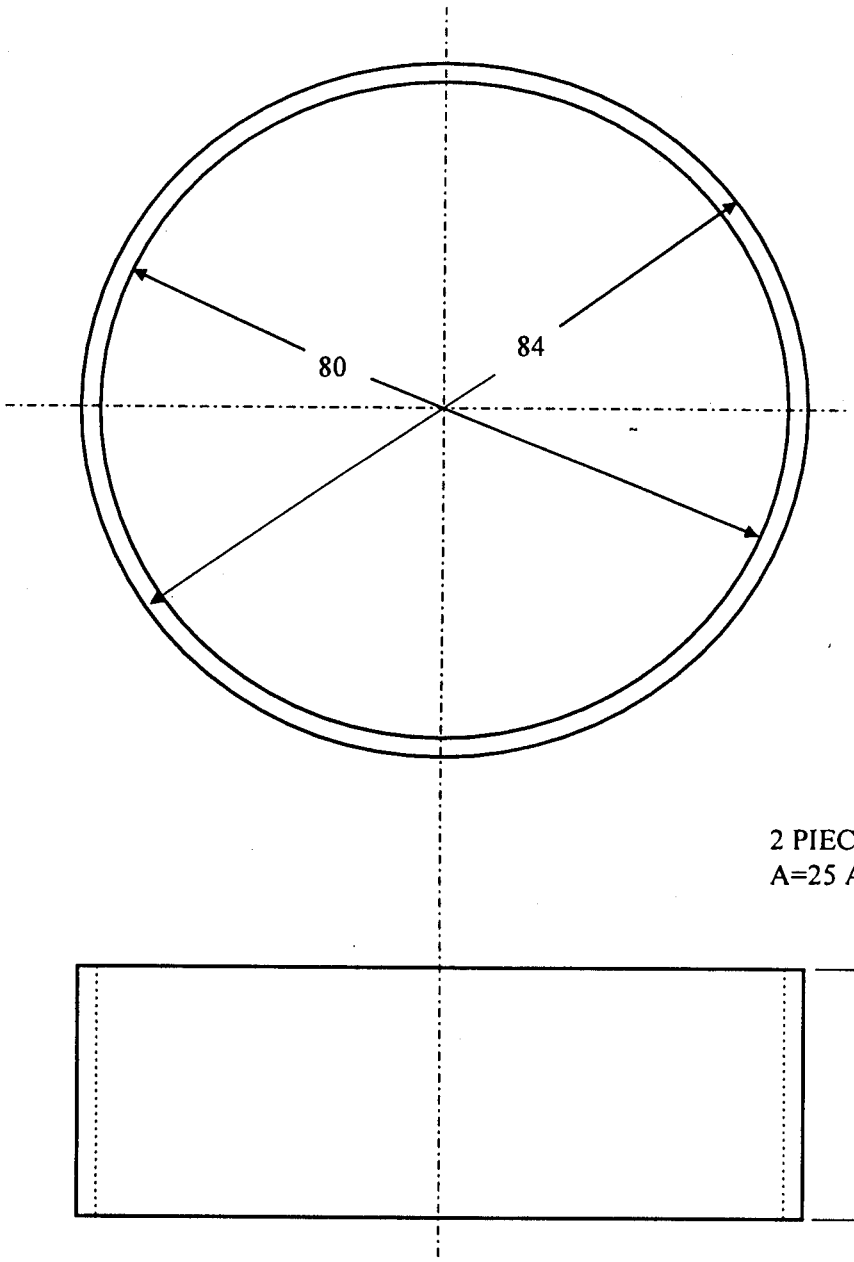

TITLE: SLEEVE

MATERIAL: STAINLESS STEEL 304

DIMENSIONS: mm

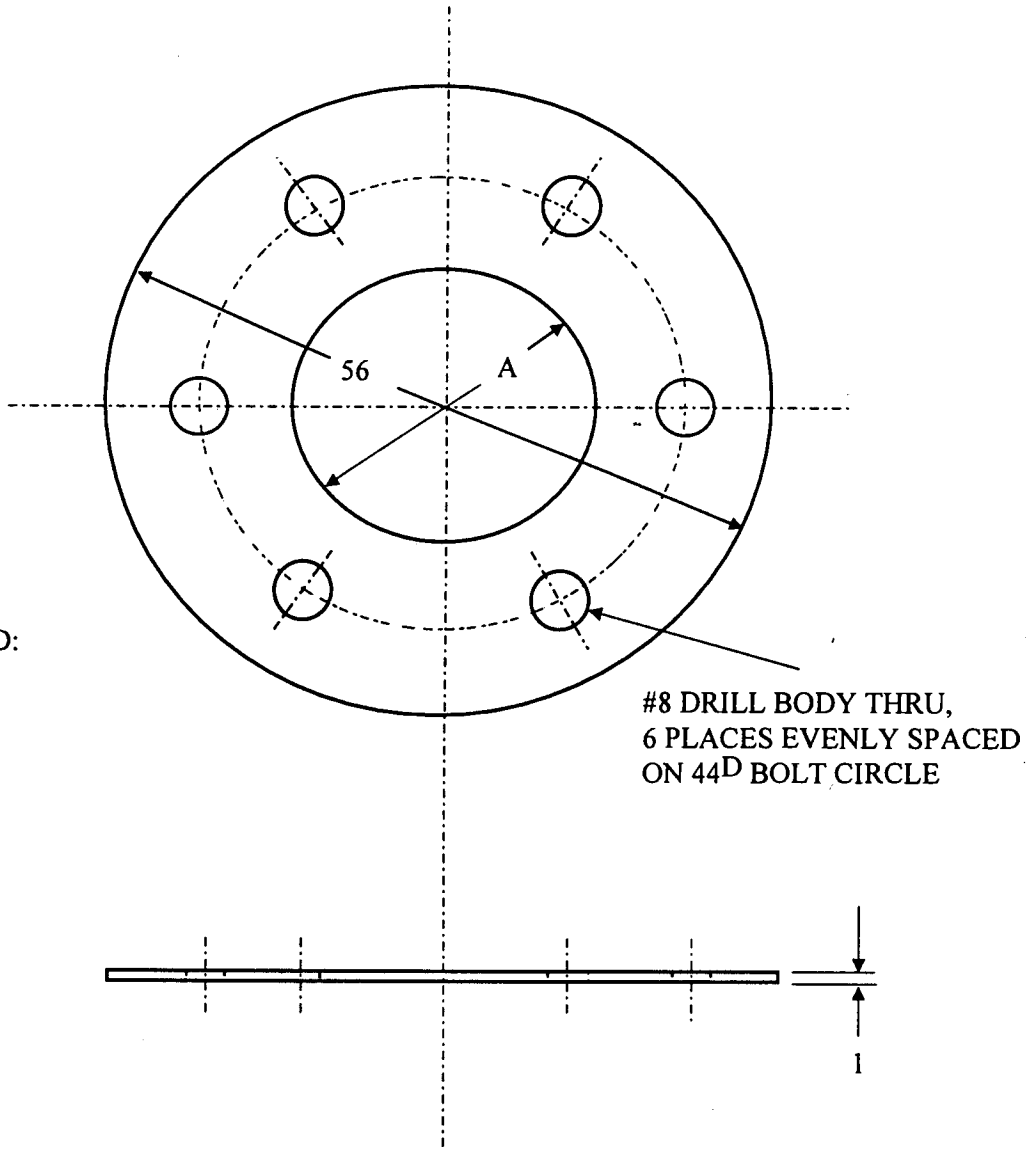

TITLE: GASKET
MATERIAL: COPPER
DIMENSIONS: mm

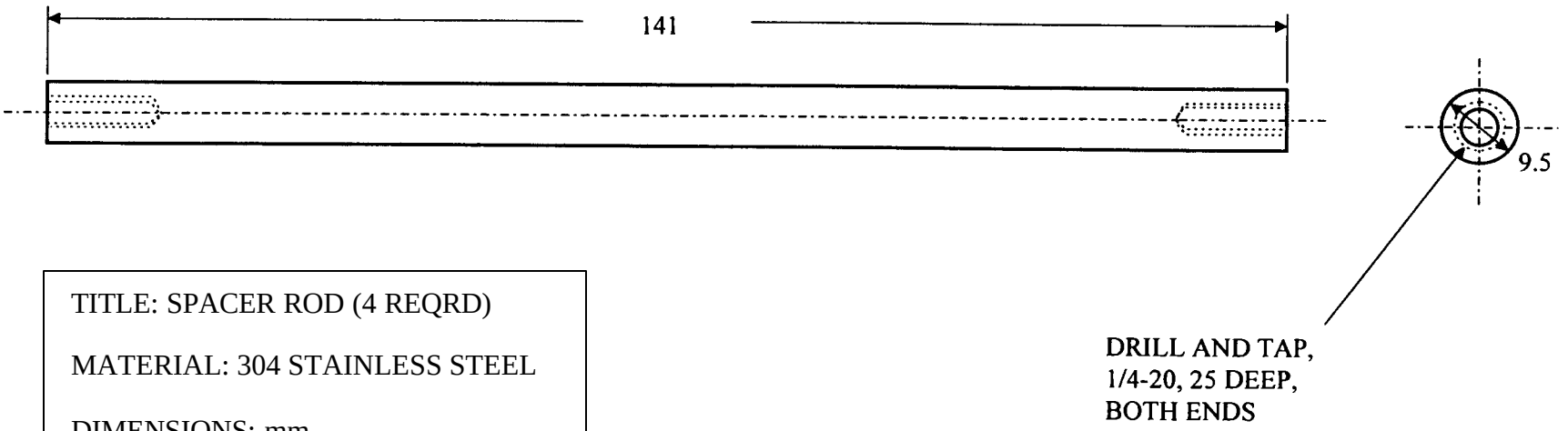

TITLE: SPACER ROD (4 REQRD)

MATERIAL: 304 STAINLESS STEEL

DIMENSIONS: mm